TRW

Advanced Space Communications Architecture Study

Volume 2 — Technical Report

NASA CR 179592

March 1987

TRW

Advanced Space Communications Architecture Study

Volume 2 — Technical Report

NASA CR 179592

March 1987

TRW

Advanced Space Communications Architecture Study

Volume 2 — Technical Report

NASA CR 179592

March 1987

Prepared by

TRW Electronic Systems Group
One Space Park
Redondo Beach, CA 90278

Prepared for

NASA Lewis Research Center
21000 Brookpark Road
Cleveland, OH 44135

Approved:

M. Horstein
Principal Investigator

M.G. Davis, Jr.
Manager, Electronic Development Operation

TABLE OF CONTENTS

LIST OF TABLES

LIST OF FIGURES

LIST OF FIGURES- continued

1. INTRODUCTION

Until recently, it was generally believed that trunking traffic would dominate point-to-point satellite communications. Because of the rapid progress in fiber optics communications, however, it is now clear that trunking traffic will, for the most part, be carried terrestrially rather than by satellite. In the future, therefore, point-to-point satellite communications will be dominated by thin-route applications involving fixed or mobile terminals.

NASA's Advanced Communications Technology Satellite (ACTS) program was conceived during the period when trunking traffic was the dominant point-to-point satellite mode. Accordingly, ACTS is intended to advance technology development in both trunking systems and customer premise service (CPS). The latter service is intended to provide satellite voice and/or data links directly between end users, thereby obviating construction of terrestrial tails between earth station and end user. With the anticipated demise of satellite trunking, the CPS aspect of ACTS is the more relevant to future satellite communications.

This report presents the results of a 12-month study to determine satellite system architectures that are most suitable for CPS communications. As with ACTS, the focus is on 30/20-GHz (Ka-band) technology. However, the system architectures examined are equally applicable to operation at 14/11 GHz (Ku-band). Because large numbers of

users (i.e., 10,000 or more) are intended to be served, emphasis is placed on system designs that permit low user terminal costs.

The satellite links in the type of system under consideration are shown in Figure 1-1. Complete "single-hop" interconnectivity, which is needed for voice communications, is provided between any pair of system users. To establish such a connection, a user requests either a one-way channel or a two-way circuit, as needed, from the master control station. These requests are transmitted over an orderwire channel, typically making use of a random access protocol. When the circuit is no longer needed, it is restored to the pool of circuits available for reassignment.

Minimization of terminal costs generally implies low values of peak EIRP. It is also important to limit the terminal size, since real estate and installation costs might otherwise outweigh terminal equipment costs. The terminal antenna diameter is limited to 1.2m in most of continental United States (CONUS), although 1.8m antennas are permitted in heavier-rainfall areas to maintain system availability. A frequency-division multiple access (FDMA) uplink signal format is selected because it permits narrow-bandwidth transmission, which tends to minimize EIRP requirements.

Single-hop interconnectivity requires that the satellite act like a switchboard in the sky, with accessability to each individual terminal transmission. The accepted means of providing this accessability (and the one employed by ACTS) is use of a time-division multiple access (TDMA) transmission format. The use of FDMA, on the other hand, heretofore

Figure 1-1. Satellite Links

USER TERMINALS

USER TERMINAL

MASTER CONTROL STATION
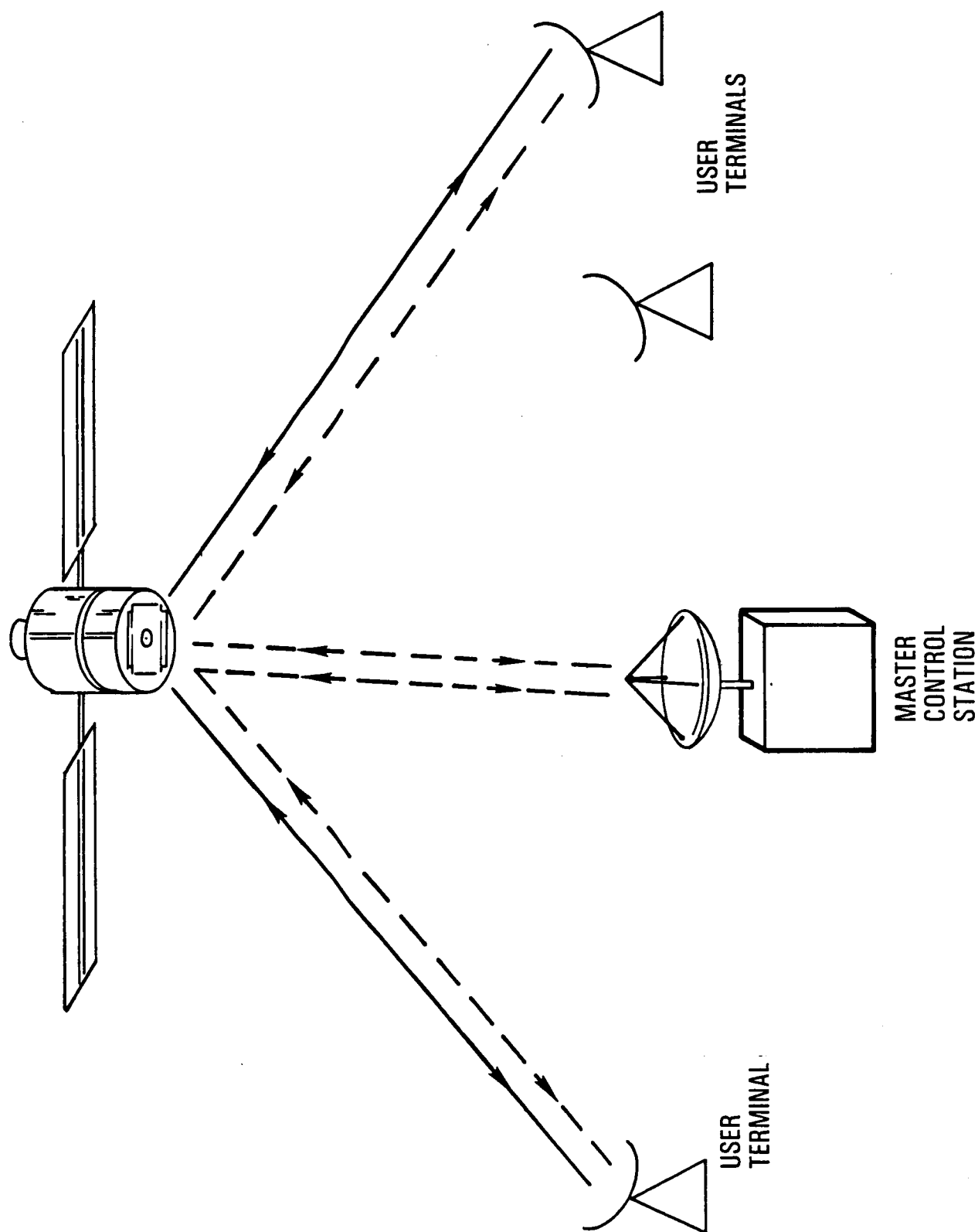
would have required a separate satellite demodulator for each terminal transmission. However, the prospect now exists for the development of "bulk" demodulators of sufficiently low power consumption to be attractive for satellite use. A bulk demodulator accepts as input a composite FDMA signal and provides a time-division multiplexed (TDM) pulse stream in which the demodulated bits of the various input carriers are interleaved. Thus, the demodulator output has a format similar to that of the uplink transmissions in a TDMA system. A single bulk demodulator might simultaneously process 100 FDMA carriers, thereby providing a 100:1 reduction in the number of demodulators that would otherwise be required.

In contrast to the uplink, downlink transmission is accomplished by means of a small number of wideband, TDM carriers. A baseband processor buffers the relatively large number of demodulator outputs and multiplexes them onto the downlink carriers.

The satellite transmit antenna is designed to have a relatively high gain (i.e., small beamwidth), to minimize the transmit power requirements. In addition, the small spot size produced by the antenna permits the introduction of frequency reuse, which expands the effective system bandwidth. A separate antenna beam is generated for each downlink carrier. Each beam is "hopped" among the downlink spots, dwelling on each spot long enough to transmit a predetermined number of bits from each 64-kbps uplink carrier intended for one of the terminals within the spot boundary.

A complete system description and a number of key system tradeoffs are presented in Section 2. Details of the satellite receive and transmit antenna designs are presented in Sections 3 and 4, respectively. The bulk demodulator technology is examined in Section 5, the baseband processor technology in Section 6, and transmitter/receiver technology at 30/20 GHz in Section 7.

Sections 8 to 11 are concerned with the financial aspects of system implementation and operation. The weight of each payload element, together with a satellite subsystem weight budget, is presented in Section 8. Nonrecurring and recurring satellite cost estimates, derived from the weight estimates, are also provided in Section 8. A user terminal design and cost estimate are given in Section 9. Section 10 derives the user service charge needed to provide a specified rate of return on invested capital, based on an assumed traffic profile. The study conclusions are stated in Section 11.

2. SYSTEM DESCRIPTION AND ANALYSIS

Because the ground segment is a major system cost driver, the first step in defining a system concept is to select an appropriate set of user terminal parameters. By means of the link equations, corresponding satellite receive antenna gain and EIRP requirements are then obtained to satisfy the system performance objectives. Subject to the derived satellite requirements, a number of satellite subsystem trades are performed to arrive at a complete system description.

2.1. System Concept

Each terminal is provided the capability to transmit a single narrowband digital carrier. The minimum or standard data rate is taken as 64 kbps. The carriers transmitted by the various terminals are distinguished by frequency and/or polarization. Thus, the uplink signal set comprises a large number of FDMA carriers spread over the 500-MHz Ka-band fixed-satellite allocation not shared with the fixed (terrestrial) service. Since dual polarization is used, the equivalent composite bandwidth is 1000 MHz.

With present-day digital voice representations, the 64-kbps terminal transmission can support two voice channels. With the higher-speed digital circuitry expected by the end of the decade, 16-kbps digital voice should replace the current 32-kbps voice standard. Each terminal will then be capable of transmitting four voice channels. More generally, a terminal could support various combinations of voice and data totaling 64

kbps. The constituents of the 64-kbps transmission need not be directed at the same terminal. With QPSK transmission employed on the uplink (see Section 2.2), the in-phase and quadrature components are readily separated in the satellite and retransmitted to different terminals.

A functional block diagram of the satellite payload is shown in Figure 2-1. The satellite receive antenna produces a number of fixed area beams which provide complete CONUS coverage. The carriers received on a given beam are divided into groups of standard size, each of which is input to a bulk demodulator. The latter converts a set of FDMA signals, contiguous in frequency, to a single TDM pulse stream in which pulses corresponding to an individual input signal are interleaved with those of all other inputs. The demodulator bandwidth is chosen narrow enough so that the traffic handling capability of each beam can be matched to the traffic offered through assignment of an appropriate number of demodulators. Allowing a certain number of demodulators to be switchable between beams leads to accommodation of an *a priori* unknown or time-varying traffic pattern.

The bulk demodulator outputs are fed to a baseband multiplexer which buffers and sorts the data bits according to the downlink beam for which they are intended. The number of downlink beams is considerably smaller than the number of spots (as measured by the antenna beamwidth) needed to cover CONUS. Each downlink beam is therefore programmed to scan over a portion or all of CONUS in a repetitive pattern. The data bits assigned to a beam for transmission during one complete scan are organized according to the downlink spot for which they are intended. In this way, no spot is

Figure 2-1. Satellite Payload Functional Block Diagram
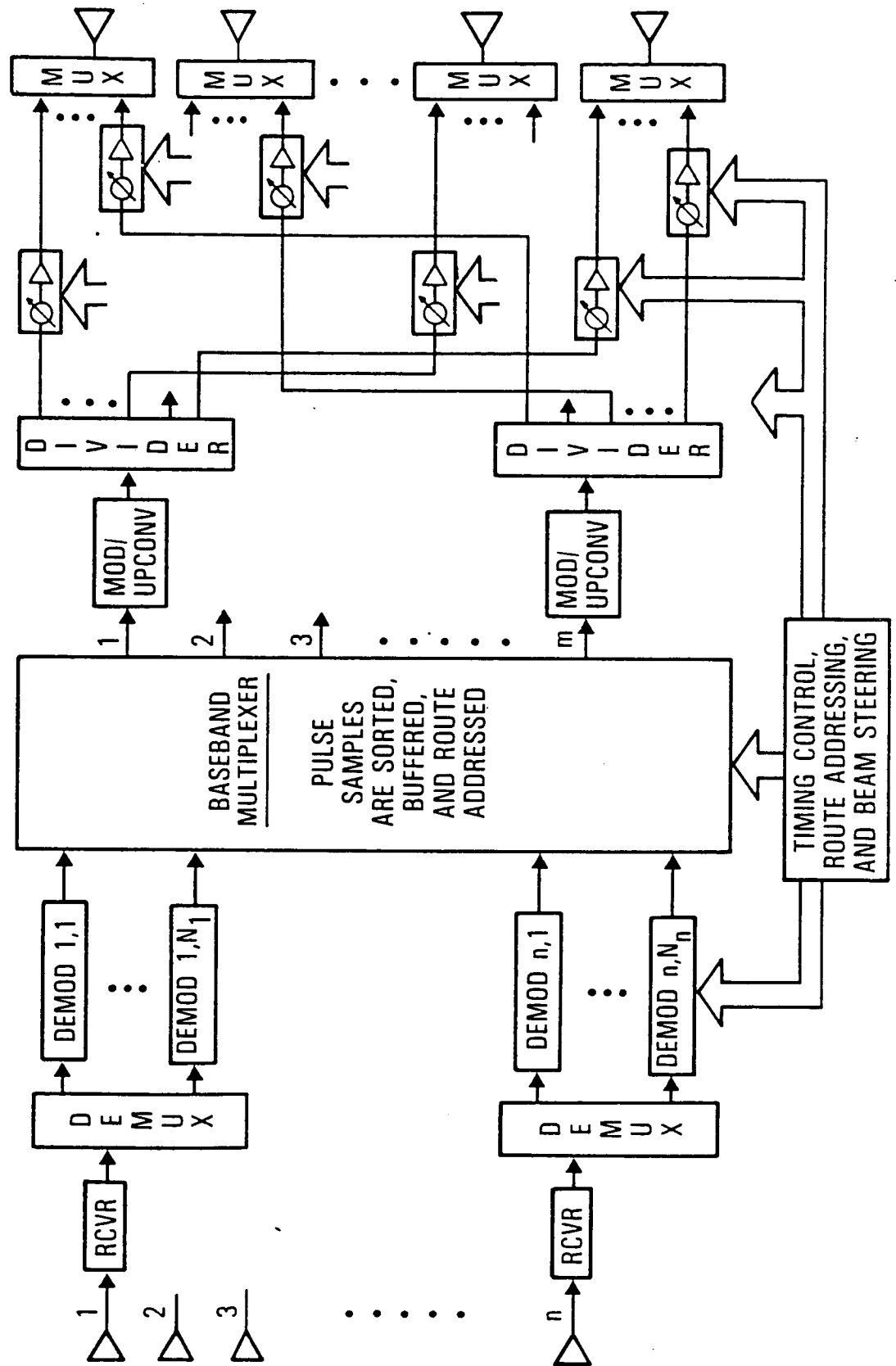
visited more than once per scan by any of the beams.

As depicted in Figure 2-1, each downlink beam is formed by power-dividing the corresponding carrier and feeding the resulting signals to modules associated with the radiating elements. Each module consists of an amplifier and a variable phase shifter. Each radiating element is excited by the combined output of several modules, one for each downlink beam. The set of radiating elements can either form a direct-radiating array or be used as an array feed for a reflector type of antenna.

2.2. Link Design

The user terminals are equipped with 1.2m antennas. This size is typical of very-small-aperture-terminal (VSAT) design. Each terminal that transmits the standard 64-kbps carrier has a 2W transmitter. This power level is about the maximum achievable at reasonable cost. Both the terminal and the satellite are equipped with HEMT LNAs. The corresponding receiver noise figures are projected to be 2.0 dB and 3.0 dB, respectively.

Considerable uncertainty exists concerning the rain margin required to achieve a specified link availability. The margins selected are intended to correspond to an uplink or downlink availability of 0.995 in all but the southeast portion of CONUS (Rain Zone E), as reported in Reference 2-1. Accordingly, no end-to-end transmission path has an availability of less than 0.99. In fact, most composite paths have considerably higher availability. An antenna diameter of 1.8m is required to extend 0.995 link availability to Rain Zone E.

A higher link availability than 0.995 was not selected because of the impact on the satellite design. Improving the link availability to 0.9975 (i.e., halving the link outage) requires uplink and downlink margins of about 15 dB and 6 dB, respectively, compared with 8 dB and 4 dB for a link availability of 0.995.

To maximize system capacity, QPSK transmission is used on the uplink. The data is differentially encoded to simplify the demodulation process on the satellite. On the downlink, the choice of modulation is dictated by the need to minimize the cost, and hence the complexity, of the receive portion of the user terminals. To this end, differential data encoding is essential. BPSK is selected in place of QPSK because of the larger E_b/N_0 requirement associated with differential QPSK. The larger carrier bandwidth associated with BPSK transmission necessitates a degree of spatial frequency reuse, in addition to polarization diversity. This requirement imposes an operational constraint on the downlink-beam scanning patterns, if excessive interbeam interference is to be avoided.

To provide the requisite link quality, assumed to correspond to a BER of 10^{-7}, end-to-end error correction coding is employed. Use of soft-decision decoding on the ground would be largely negated by the demodulation process on the satellite. Therefore, hard-decision decoding is used instead.

Because of the relatively small EIRP and G/T of a 1.2m terminal, it is desirable to obtain as much coding gain as possible. On the other hand, a lower code rate leads to a larger bandwidth per carrier and therefore

smaller system capacity. These opposing factors lead to a choice of rate-3/4 coding.

Uplink and downlink power budgets are given in Tables 2-1 and 2-2. Each link is nominally designed for a decoded BER of 10^{-7} (a fictitious quantity in the case of the uplink). The end-to-end error rate of the undecoded transmissions is twice that of either the uplink or the downlink considered separately. Therefore, the BER of the decoded transmissions will in fact be somewhat greater than 10^{-7}.

The required values of E_b/N_0 in Tables 2-1 and 2-2 include an implementation margin (i.e., departure from theoretical) of 3 dB. In addition, the E_b/N_0 penalty due to differential data encoding is 2.3 dB on the uplink (for QPSK) and 0.6 dB on the downlink (for BPSK).

The required uplink signal quality is achieved by proper design of the satellite receive antenna, while the downlink signal quality depends on proper selection of the satellite EIRP. Accordingly, the receive antenna gain must be at least 33.3 dB throughout CONUS. For the selected downlink data rate of 180 Mbps per beam, the satellite EIRP must be at least 63.1 dBW.

The choice of 180 Mbps for the downlink data rate is governed by the desire to accommodate the downlink data on four carriers. As will be seen in Section 4, this downlink data partitioning leads to use of two identical

TABLE 2-1. UPLINK POWER BUDGET (29.5 GHz)

Transmitter power (2W), dBW	3.0
Line loss, dB	-1.0
Antenna gain (1.2m), dB	49.2
Pointing loss, dB	<u>-1.0</u>
EIRP, dBW	50.2
Path loss, dB	-213.7
Atmospheric loss, dB	-0.6
Rain loss (.995 except Zone E), dB	-8.0
S/C antenna gain (edge of beam) plus line losses, dB	<u>33.3</u>
Received carrier power, dBW	-138.8
System noise temperature, dB-K	27.6
Boltzmann's constant, dB (W/K-Hz)	<u>-228.6</u>
N_0, dB (W/Hz)	-201.0
Bit rate (64 kbps), dB (sec^{-1})	48.1
E_b/N_0, dB	14.1

TABLE 2-2. DOWNLINK POWER BUDGET (19.7 GHz)

EIRP, dBW	63.1
Path loss, dB	-210.2
Atmospheric loss, dB	-0.8
Rain loss, dB	-4.0
E/S antenna gain, dB	45.8
Pointing loss, dB	-0.8
Line loss, dB	<u>-1.0</u>
Received carrier power, dBW	-107.9
System noise temperature, dB-K	25.7
Boltzmann's constant, dB (W/K-Hz)	<u>-228.6</u>
N_o, dB (W/Hz)	-202.9
Bit rate (180 Mbps), dB (sec^{-1})	82.6
E_b/N_o, dB	12.4

transmit antennas, each radiating a pair of carriers on opposite polarization. The downlink data rate is therefore one-fourth of the total satellite throughput.

The satellite throughput is determined by uplink considerations. Each uplink carrier supports a data rate of 64 kbps. With QPSK transmission and rate-3/4 coding, the transmitted symbol rate is 42.67 ksps. For purposes of bulk demodulation, the carrier separation must be twice the transmitted symbol rate, or 85.33 kHz. The effective system bandwidth of 1000 MHz accommodates 11,718 such carriers or, equivalently, a composite data rate of 750 Mbps. Allowing 30 Mbps for system overhead leaves 720 Mbps as the system throughput rate. The downlink data rate is therefore 180 Mbps per beam.

Two 180-Mbps carriers are transmitted on each polarization. With rate-3/4 coding and BPSK modulation, each carrier supports a transmission rate of 240 Msps. With a bandwidth-to-symbol rate ratio of (say) 1.5, each downlink carrier occupies 360 MHz. With a 500-MHz allocation on each polarization, the two carriers clearly have overlapping spectra. As observed earlier, this overlap places constraints on the downlink-beam scanning patterns.

2.3. Satellite Receive Antenna

From Table 2-1, the satellite receive antenna must provide a minimum gain over CONUS of 33.3 dB. This minimum gain determines the required number of uplink beams. For a given angular coverage, the gain at beam edge is maximized if it is chosen 4.3 dB less than the peak gain.

Therefore, the peak gain must be 37.6 dB. This gain provides beam coverage (i.e., 4.3-dB beamwidth) of 2.56 degrees. Approximately eight such beams, forming the pattern shown in Figure 2-2, are needed for CONUS coverage.

The portion of the frequency allocation, and correspondingly the number of bulk demodulators, assigned to each uplink beam is proportional to the traffic offered by user terminals located within the beam coverage area. The frequency band assigned to a given beam may be confined to a single polarization or divided between the two polarizations. The first alternative requires only a single port per feed horn (rather than a separate port for each polarization) and leads to a simpler repeater configuration. For this reason, it has been chosen for the baseline satellite configuration.

It should be pointed out, however, that confining each beam to a single polarization has the effect of dividing the total available bandwidth of 1000 MHz into two distinct 500-MHz allocations. Consequently, the system saturates once the combined traffic in the beams assigned to either polarization requires a bandwidth of 500 MHz. The satellite throughput at which saturation occurs can be increased, however, by taking advantage of the beam overlap in Figure 2-2. Users located in overlap areas can be assigned to either of two satellite beams. If the two beams in a particular case have opposite polarization, proper user/beam assignments can help balance the traffic division between the two polarizations.

Figure 2-2. Uplink Beam Pattern

4.3 dB CONTOUR
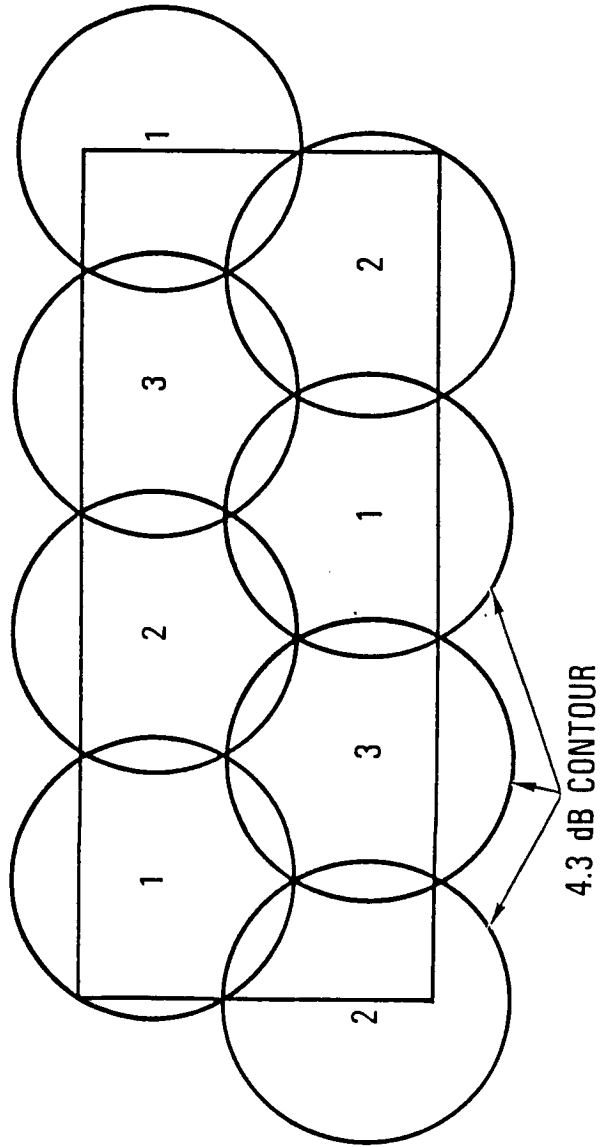
Two possible multiple-beam antennas (MBA) are discussed in Section 3, one based on offset-fed reflectors and the other on multiple lenses. The former has been chosen for the baseline design. The need for multiple reflectors arises from the relationship, in the case of a single reflector, between the feed horn aperture and the separation between feed horn centers needed to generate the beam pattern in Figure 2-2. Proper reflector illumination requires a feed horn aperture which is too large to allow the feed horns to be suitably positioned for the desired beam pattern. Consequently, multiple reflectors are employed. Three reflectors suffice. Two of the reflectors support three beams, while the third reflector supports the remaining two beams. Beams generated by the same reflector are given a common numbering in Figure 2-2. The diameter of each reflector is 14 in.

To achieve an uplink availability of (say) 0.9975, rather than 0.995, between 30 and 40 satellite beams would be required. This would greatly increase the complexity of the satellite payload and therefore was not considered.

2.4. Bulk Demodulators

The power requirements of a set of bulk demodulators spanning a fixed composite bandwidth (1000 MHz in this case) depend on the single-demodulator bandwidth. Based on this relationship, which is developed below, a baseline value of demodulator bandwidth is chosen. Fixing the demodulator bandwidth (and hence the number of demodulators) establishes the connectivity requirements for the baseband processor in Figure 2-1.

The power required by a digital bulk demodulator is shown in Figure 2-3 as a function of the number of 64-kbps channels per demodulator, for different technologies and modes of system operation. A nominal channel spacing of 100 kHz is assumed. Each demodulator consists of an A/D converter followed by an FFT unit. The FFT channel capacity is typically available in blocks which differ by powers of 2. These capacity increments result in FFT power-requirement discontinuities at certain demodulator bandwidths. The preferred operating points, in terms of power consumption, correspond to demodulator bandwidths at which the FFT is fully occupied. A maximum of about 100 channels can be passed through a 128-channel FFT when allowance is made for anti-aliasing filter roll-off. There is no resulting loss of bandwidth utilization, however, as two such FFTs can process a pair of adjacent 100-channel frequency bands.

Two FFT power consumption curves are shown in Figure 2-3, one for synchronous terminal operation and the other for asynchronous terminals. The latter alternative refers to a system in which the terminals are allowed to be time-offset (but frequency synchronous) with respect to each other. This approach would simplify terminal design by eliminating some of the acquisition timing requirements. The impact on FFT power, however, is quite dramatic for large FFTs because of the need for higher sampling rates (2 to 3 times higher) and FFT overlapping and combining operations. In addition, any windowing (for sidelobe reduction) must be performed as a convolution after the transform, increasing total power.

Figure 2-3. Single FFT–Bulk–Demodulator Power Requirements
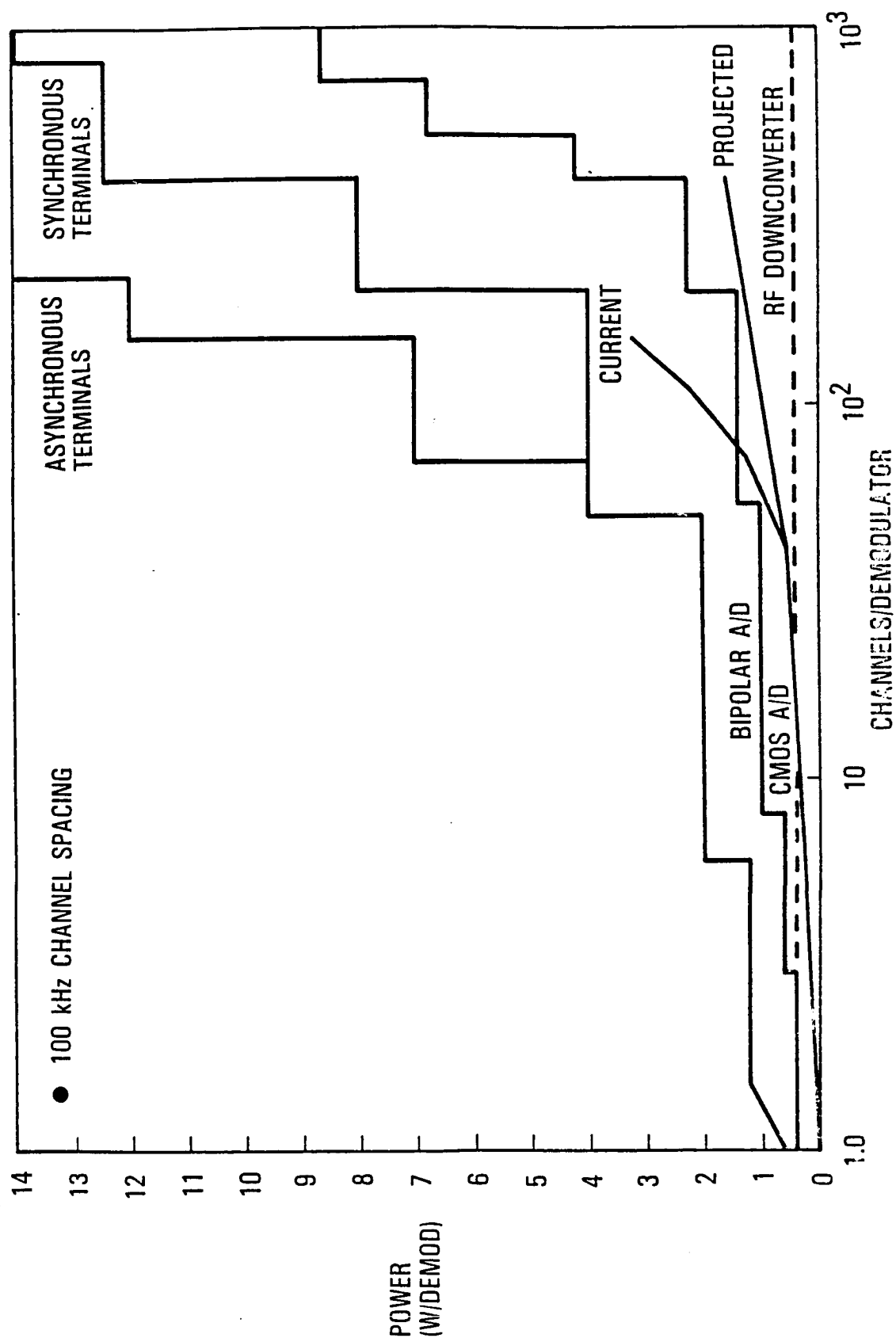
Synchronous time operation, on the other hand, eliminates the need for such high-rate sampling and extra FFTs. Time-synchronous operation also considerably simplifies the multiplexing operation prior to downlink transmission, since data bit-time relations are fixed rather than variable. For these reasons, only synchronous operation of bulk demodulators is considered.

The A/D converter consumes considerably less power than the FFT, the amount depending on the choice between CMOS and bipolar technology. Like the FFT, bipolar A/D devices exhibit discontinuous power consumption as a function of demodulator bandwidth. By contrast, CMOS A/D power consumption increases smoothly with demodulator bandwith.

The total power requirement for a demodulator complement sufficient to span 1000 MHz of bandwidth is shown in Figure 2-4. Curves are drawn for FFT demodulators with both synchronous and asynchronous terminal operation, as well as for SAW demodulators. All three curves incorporate the projected CMOS A/D power requirements from Figure 2-3. Power requirements are based on VLSI and wafer-scale signal processor projections for the next five years. The SAW curve is based on power consumption of 25 watts per 100 channels. This figure is based on experience with the MILSTAR SAW demodulators and represents some power improvement in the A/D area. SAW power requirements tend to be independent of the number of channels, whereas A/D and detector power consumption tend to follow curves similar to the FFT A/D. No significant power reductions due to improvements in SAW technology are expected in the near future.

Figure 2-4. Bulk Demodulator Power Requirements for Composite 1000-MHz Bandwidth
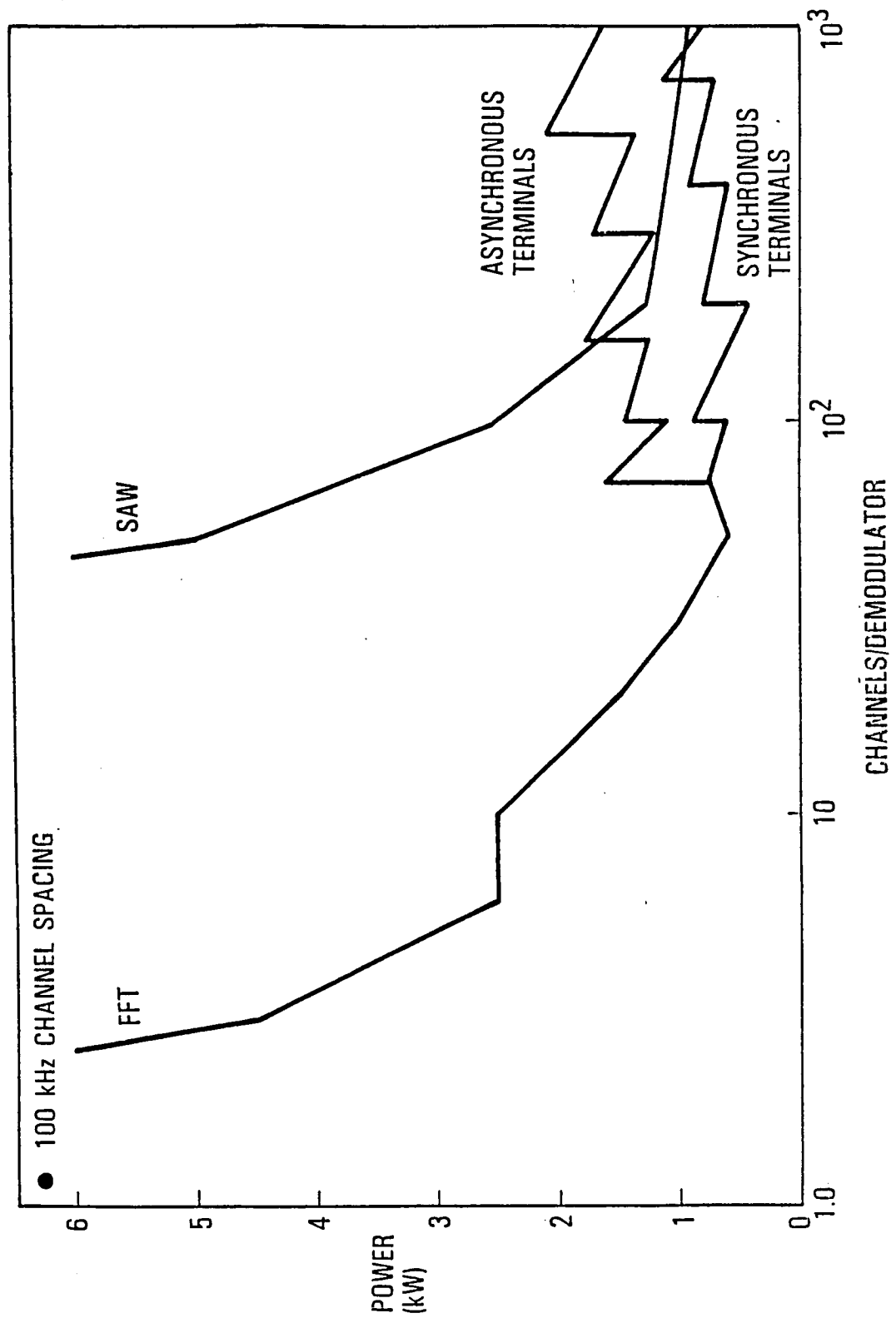
The curves in Figure 2-4 indicate a region, in the neighborhood of 50-200 channels per FFT demodulator for synchronous operation, over which the required power tends to be minimized. The corresponding demodulator bandwidth is 5-20 MHz. A total of 50-200 such demodulators are required for a composite signal bandwidth of 1000 MHz.

A baseline value of 100 bulk demodulators, each of 10-MHz bandwidth and supporting 112 channels, will be adopted for the baseline system. This choice results in a high degree of parallelism (i.e., 112 channels demodulated at a time), while permitting the demodulator capability to be matched to the traffic in each uplink beam to an accuracy of better than 1 percent of satellite capacity.

2.5. Satellite Transmit Antenna

The satellite transmit antenna is required to generate four scanning spot beams, each supporting a 180-Mbps carrier and producing an EIRP of 63.1 dB (at an antenna gain 4.3 dB below the peak value). Three different antenna configurations are considered in Section 4: a paraboloid reflector illuminated by a phased array using a Gregorian subreflector, an active-aperture phased array, and a switched-beam MBA. The latter configuration requires the use of multiple high-power (i.e., 100W) TWTAs. A significant DC power saving results from the high DC/RF conversion efficiency of TWTAs relative to that of solid-state devices. However, the higher reliability of solid-state amplifiers, together with the graceful degradation resulting from amplifier failure in a phased array, makes the array-based configurations more attractive than the MBA for this application. The array-fed reflector antenna, which is depicted in Figure

2-5, is preferred to the direct radiating array because of the reduced array dimension.

The beamwidth of the array-fed reflector antenna is determined by the main reflector dimension, D_1. The array dimension, D_2, is less than D_1 by the magnification factor, M. A larger value of M results in greater maximum scan loss, for a given coverage requirement. A value of M equal to 3 provides a good compromise between the dual objectives of minimizing both array size and scan loss.

An array of given dimension is simplified by a reduction in the number of elements. The maximum permissible spacing between elements is dictated by grating lobe considerations. Generation of grating lobes can produce interbeam interference, as well as a reduction in main lobe gain. An element spacing that avoids generation of grating lobes within the coverage area, without degrading the main beam gain significantly, is identified in Section 4.

For any fixed element spacing, the key tradeoff in the array design is expressed by:

$$EIRP \sim P_{TOT} N_E = P_E N_E^2$$

where N_E is the number of elements, P_E is the RF power per element, and P_{TOT} is the total RF power. The validity of the initial proportionality can be verified by noting that, for a fixed element spacing, N_E is proportional to the array area, and therefore, for fixed M, to the main reflector area and gain.

Figure 2-5. Phased-Array-Fed Gregorian Reflector Antenna

● MAGNIFICATION FACTOR OF 3

$D_1 = 69''$

$D_2 = 23''$
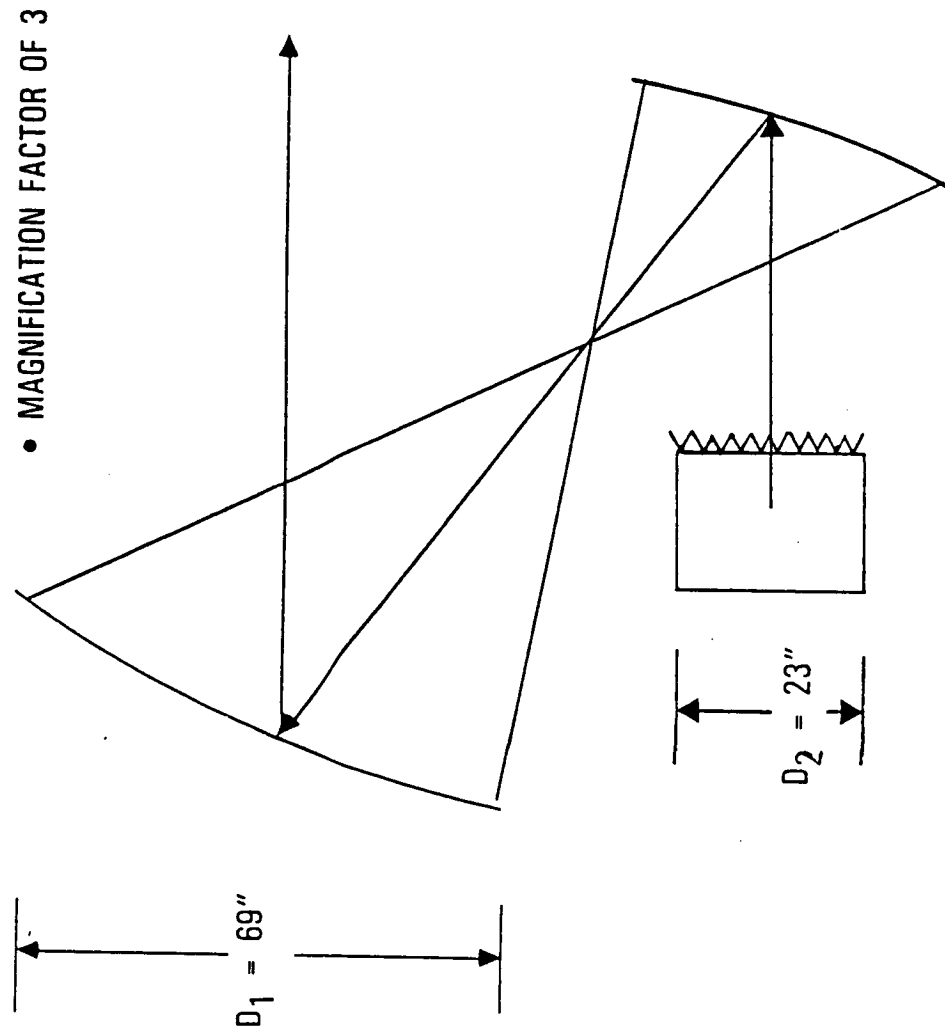
P_E and P_{TOT} are shown as a function of N_E in Figures 2-6 and 2-7, for M equal to 2 and 3, respectively. The curves correspond to transmission of a 180-Mbps carrier with EIRP of 63 dB, and are drawn for an element spacing, d, approximately equal to the wavelength, λ. At this element spacing, there is little loss of power to grating lobes. Complete elimination of grating lobes would require an element spacing of 0.48 λ for M=2, and 0.32 λ for M=3. The main reflector size corresponding to the curves in Figures 2-6 and 2-7 is shown in Figure 2-8.

For M=3, the baseline value, Figure 2-7 shows the RF power per 180-Mbps carrier for a 1000-element antenna to be 105W. The total RF power for four such carriers is 420 W. The latter figure depends only on the 720-Mbps satellite throughput and not on the number of downlink carriers. The corresponding RF power per element for a single carrier is 105 mW. The main reflector diameter is 64 in., according to Figure 2-8.

The selected method of implementing four simultaneously scanning beams is shown in Figure 2-9. Following power division, each carrier is passed through a phase-shifter/amplifier combination for each radiating element. With N elements and four beams, a total of 4N phase shifters and 4N amplifiers are required. Following amplification, the carriers are combined in pairs. The carriers in each pair are given orthogonal circular polarization by passage through an orthomode transducer (OMT) prior to excitation of the radiating element. Two separate antennas are employed, one for each pair of carriers.

Figure 2-6. RF Power Requirements for Magnification Factor of 2
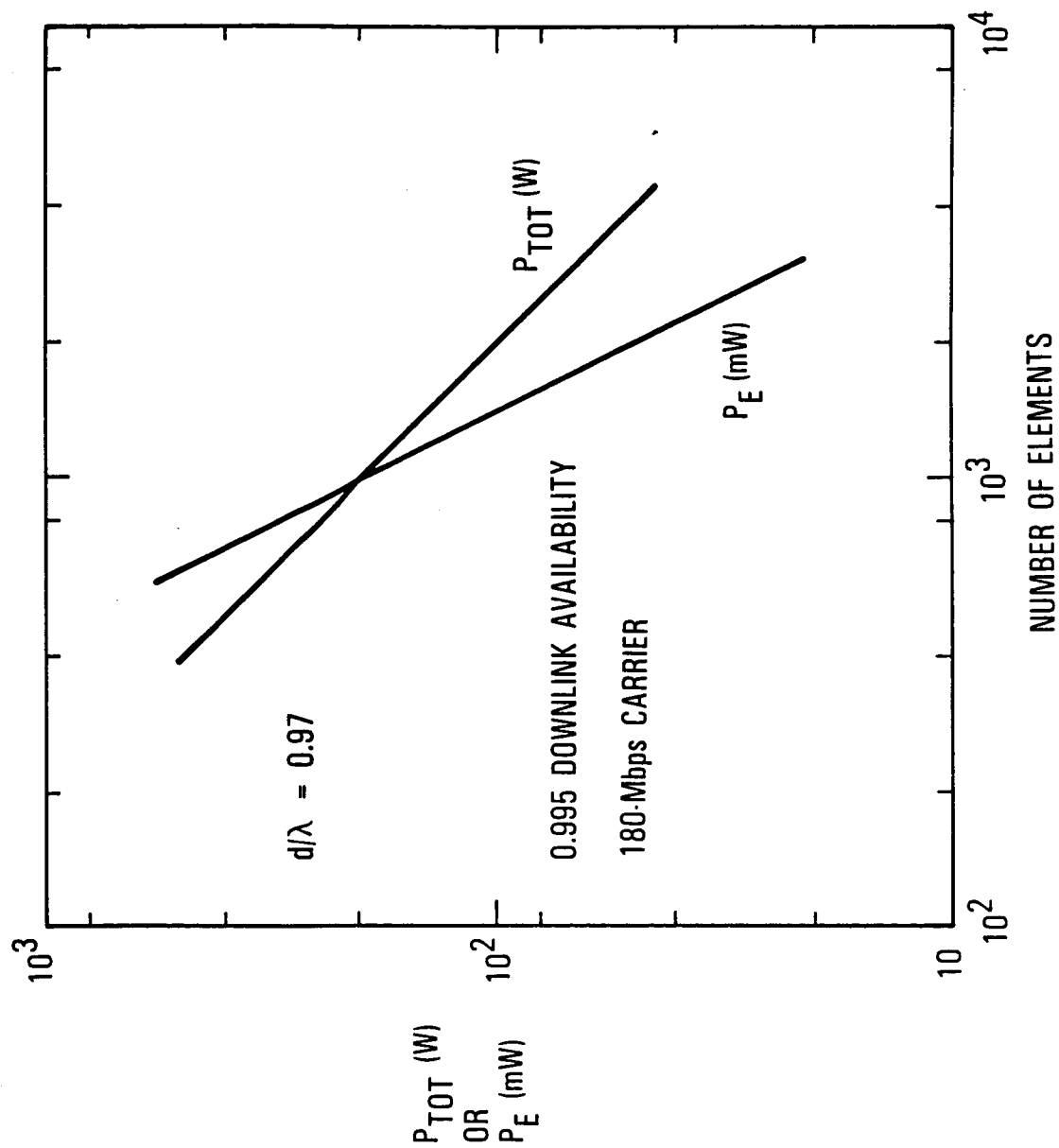
Figure 2-7. RF Power Requirements for Magnification Factor of 3

$d/\lambda = 0.97$

P_E (mW)

P_{TOT} (W)

0.995 LINK AVAILABILITY
180-Mbps CARRIER

P_{TOT} (W)
OR
P_E (mW)

NUMBER OF ELEMENTS
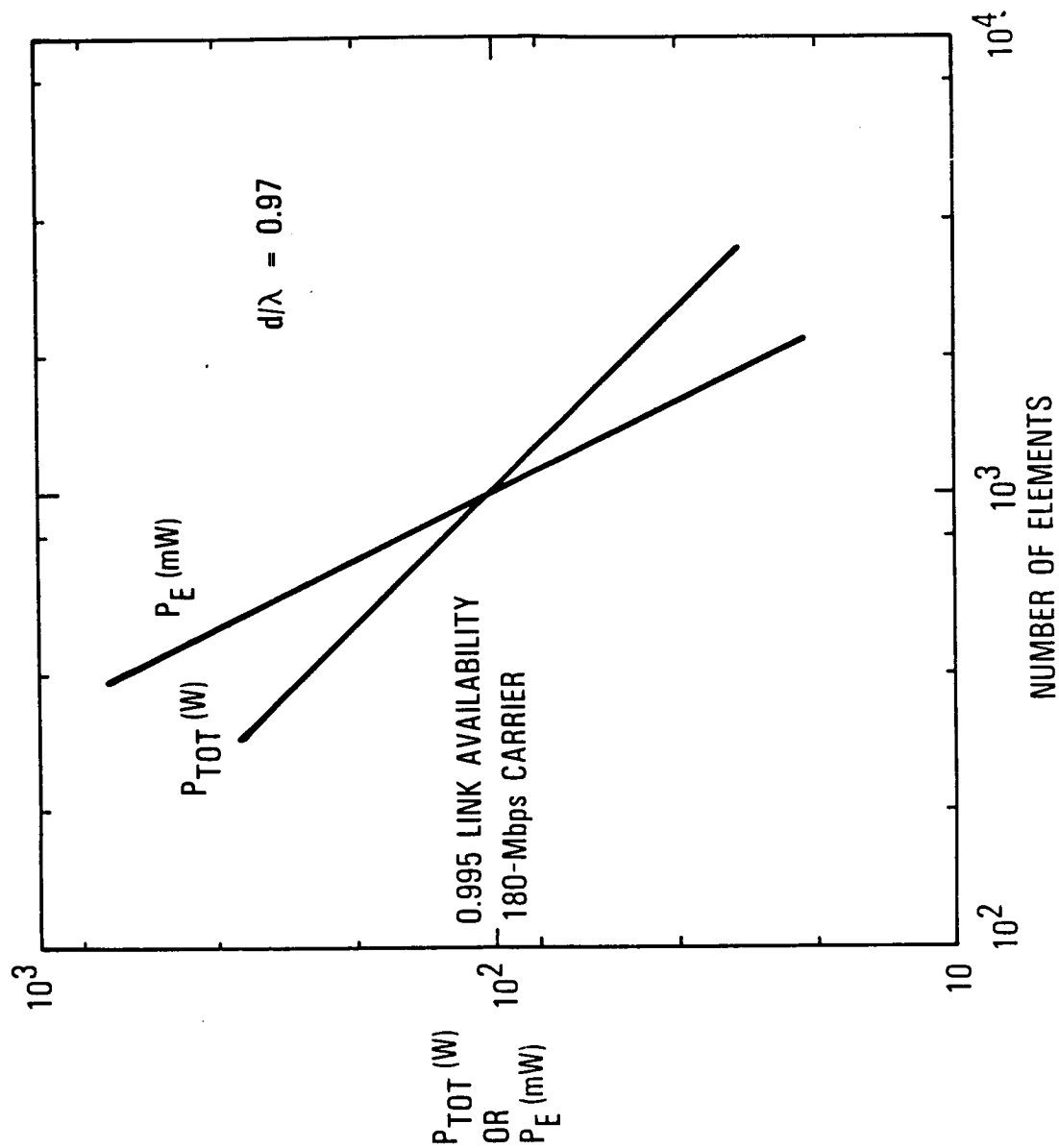
Figure 2-8. Main Reflector Diameter for Array-Fed Dual Reflector Antenna
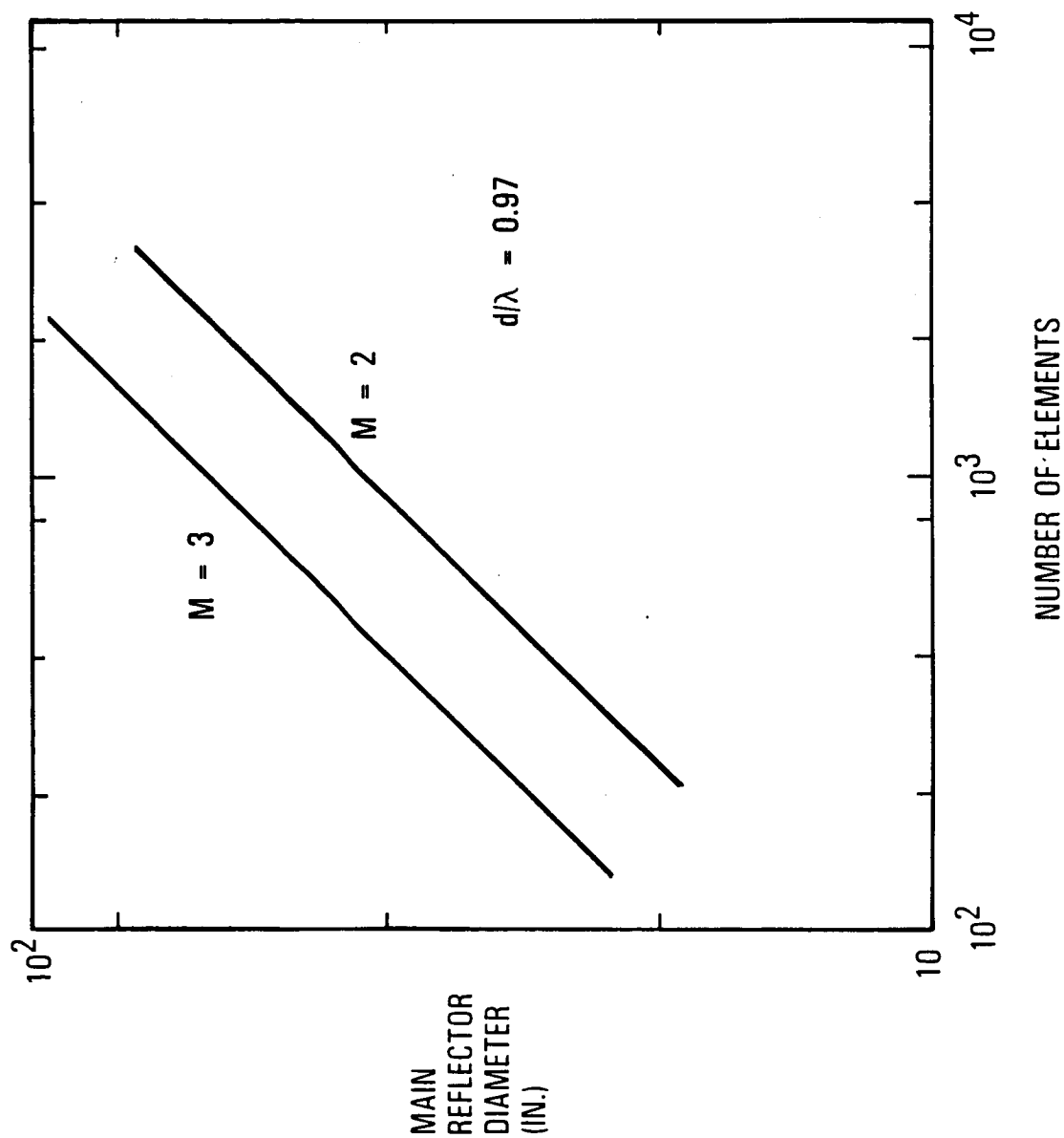
Figure 2-9. Two-Antenna Transmit Configuration
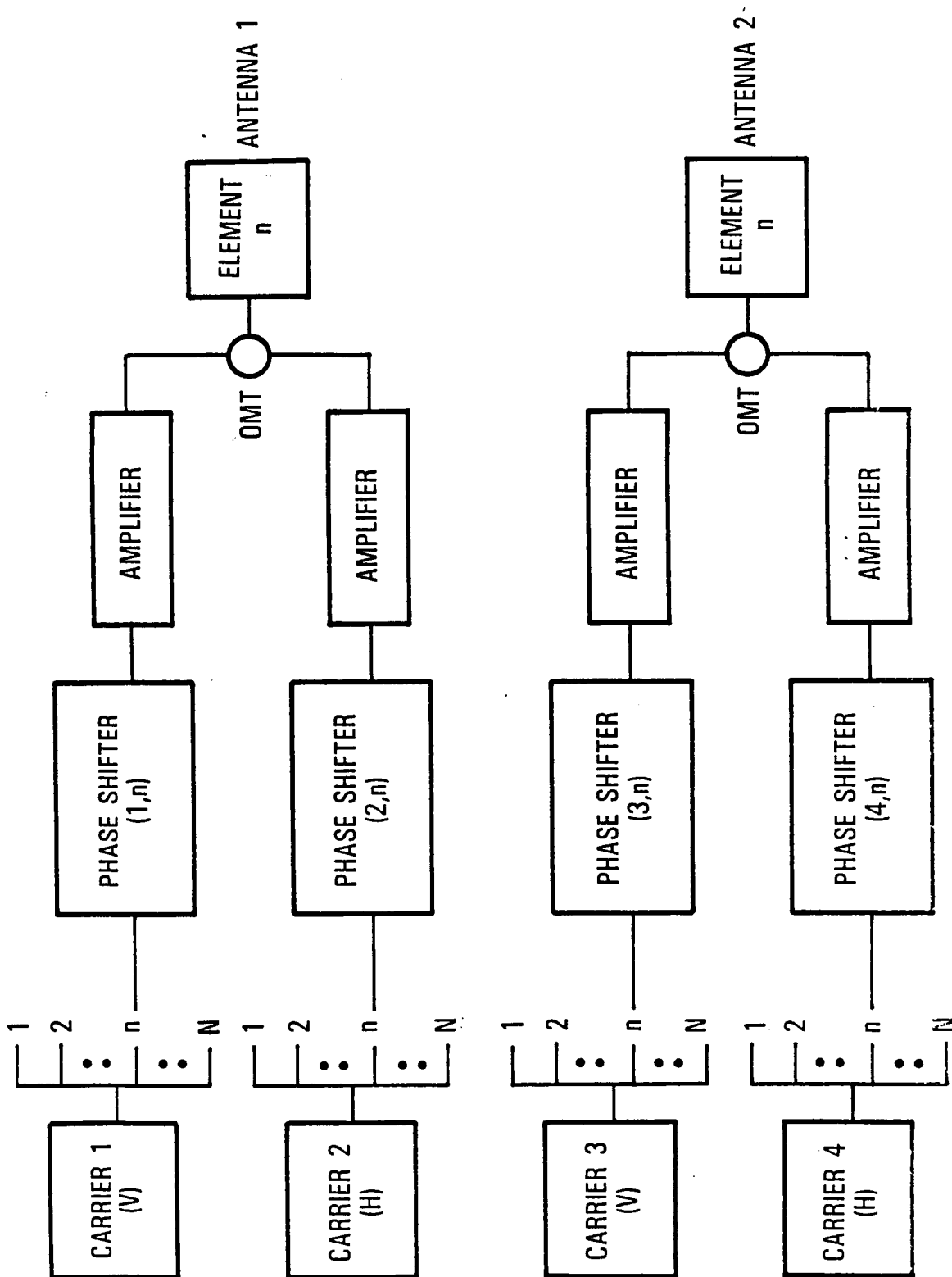
Use of a separate amplifier for each carrier element avoids generation of intermodulation products, which reduce useful output power and generally add to the overall background noise level. In addition, the OMT results in essentially lossless carrier combining following amplification. Therefore, this configuration minimizes the DC power requirement for a given configuration of radiating elements. The obvious disadvantage is the need for two distinct antennas.

The data in Section 4 can be used to derive an appropriate antenna configuration, under the condition that the absence of grating lobes is required only within the coverage area (i.e., over CONUS). For an array of hexagonal shape, a minimum element spacing of 1.84 λ suffices. Each array has 331 radiating elements, and the main reflector diameter is 69 in. The half-power beamwidth is 0.75 degree. Beam coverage, however, is defined by the 4.3-dB beamwidth. About 60 spots are required for complete CONUS coverage.

The RF power per carrier with this configuration is 97W. Of equal importance, the RF power per carrier element (i.e., per amplifier) is 300 mW. This is a modest power level, even for current 20-GHz technology.

The DC/RF efficiency of a single-stage, 20-GHz GaAs amplifier operated at saturation is projected to be in the neighborhood of 35 percent in 1990. The achievable efficiency of a multistage amplifier, including the effect of power conversion, will probably be no greater than 25 percent. The latter figure implies a DC power requirement on the order of 1600W for the amplifiers associated with the four downlink carriers.

A reduction in DC power can be achieved through an increase in antenna gain (i.e., larger main reflector), which, for fixed values of M and minimum element spacing, implies a larger number of radiating elements. Doubling the number of elements, for example, would halve the DC power requirement. An assessment of this tradeoff depends on the resulting satellite weight and cost, and is therefore deferred until Section 8, where these topics are discussed.

The above results are valid for a downlink availability of 0.995. For a fixed number of elements, a downlink availability of 0.9975 would increase the DC power requirement by 2.3 dB. Alternatively, if the DC power is held fixed, the number of elements must be increased by the same factor. If either of these alternatives were chosen, the minimum end-to-end link availability would only be increased from 0.99 to 0.9925, because the uplink availability is only guaranteed to be 0.995.

2.6. Baseband Multiplexer

The baseband multiplexer combines the 100 bulk-demodulator outputs into four downlink data-streams. Three different multiplexer configurations are discussed in Section 6. The preferred candidate is termed a memory-based multiplexer; associated with each demodulator is a memory that can hold up to 2×10^4 data bits. The total memory requirement is therefore 2×10^6 bits for the 100-demodulator complement.

From a system standpoint, a key parameter is the number of bits from

each 64-kbps uplink channel that are stored by the multiplexer and subsequently transmitted as a unit on the downlink. At one extreme, each uplink quadriphase symbol could be treated as an independent entity. However, this would require unreasonably rapid hopping of the downlink beams. The transmission time for each uplink symbol is 23.44 μs. Suppose that each of the four downlink beams is required to transmit to 30 of the 60 spots covering CONUS during this interval. In addition, assume that the time allowed to switch between beam positions is 2 percent of the average dwell time. The required beam switching time for separate transmission of each downlink symbol would then be only 16 ns.

The time allowed for beam switching increases in proportion to the number of uplink symbols per channel stored prior to downlink transmission. This relationship is displayed in Figure 2-10 for different numbers of spots/beam covered during a single scan. Beam switching times of 100 μs or greater are quite feasible. Therefore, at least five bits/channel should be stored and transmitted as a unit on the downlink, for the 30 spots/beam case. This minimum number implies that 112 kbits of data are buffered by the multiplexer at any time. The permissible beam switching time can be increased to 400 ns by increasing the onboard data storage to 560 kbits.

The minimum number of spots/beam is influenced by the uplink and downlink signal characteristics. Suppose that the user terminals are required to transmit and receive on opposite polarization. If only a single polarization is used in each uplink beam, roughly half the downlink spots will contain terminals that transmit on one polarization, and the other

Figure 2-10. Onboard Data Storage Versus Downlink-Beam Switch Time

Symbols Stored per U/L Channel	Total Data Storage (Kbits)	Switch Time (nsec) Spots/Beam		
		15	30	60
1	22.5	32	16	8
5	112.5	160	80	40
25	562.5	800	400	200

half will contain terminals that transmit on the opposite polarization. In this case, the two downlink beams with the same polarization need only cover half the 60 spots between them; a single beam must therefore cover 15 spots. On the other hand, if both polarizations are permitted in each uplink beam, each downlink spot must be visited by at least one of the beams on each polarization. In this situation, each downlink beam must cover 30 spots.

Reference:

2-1. "30/20 GHz Demonstration System", TRW Final Report - Volume II, Documentation No. 36565-018, 29 May 1981

3. SATELLITE RECEIVE ANTENNA DESIGN

As derived in the uplink power budget of Table 2-1, the satellite receive antenna must provide a gain of 33.3 dB as measured at the receiver input. For a beam of given angular coverage, the gain at the beam edge is maximized if it is chosen to be 4.3 dB less than the peak gain. Therefore, the required peak gain is $37.6 + L_S$ dB, where L_S is the loss between the feed horn output port and the LNA input port. A value of $L_S = 0.2$ dB will be assumed; therefore, the peak gain must be 37.8 dB.

The corresponding antenna diameter is given by

$$D = (\lambda/\pi)\sqrt{G/\eta} \qquad (3-1)$$

where λ is the wavelength, G is the peak gain, and η is the antenna efficiency. For $\eta = 0.5$, $D = 34.9\lambda = 13.9$ in. The half-power beamwidth, θ_3, for a horn-fed reflector can be approximated by

$$\theta_3 = 75\,\lambda/D \qquad (3-2)$$

The 4.3-dB beamwidth, $\theta_{4.3}$, is given by

$$\theta_{4.3} = 1.2\,\theta_3 \qquad (3-3)$$

and, finally, the angle between neighboring beam centers (Figure 3-1), θ_b,

Figure 3-1. Uplink Beam Pattern

Typical minimum gain point

4.3 dB contour

Eight beam MBA

$3.5\theta_b$

θ_b

$.58\theta_b$
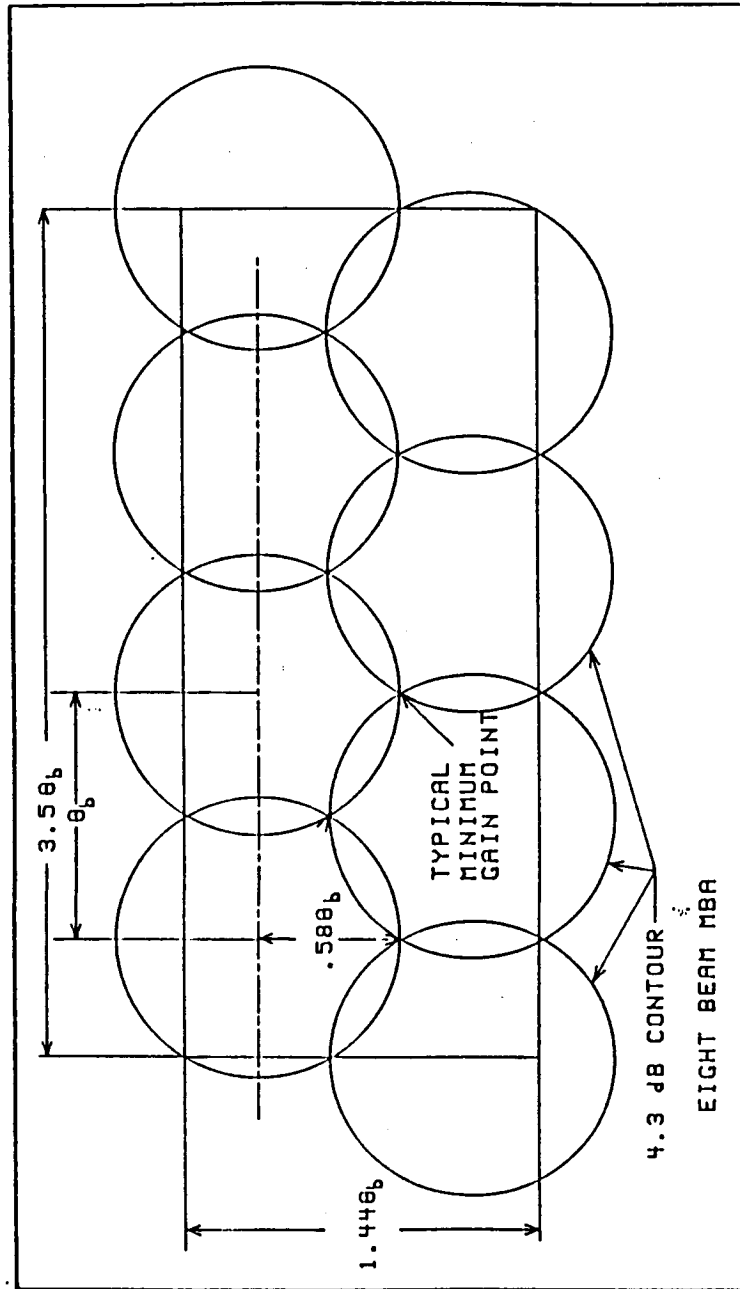
$1.44\theta_b$

is given by

$$\theta_b = 0.86\, \theta_{4.3} \qquad\qquad (3\text{-}4)$$

It follows that $\theta_3 = 2.15°$, $\theta_{4.3} = 2.56°$, and $\theta_b = 2.22°$.

The eight-beam configuration in Figure 3-1 includes a rectangular area measuring $3.5\,\theta_b \times 1.44\,\theta_b$. With $\theta_b = 2.22°$, this rectangle is $7.8° \times 3.2°$ and therefore includes the boundaries of CONUS, which measures approximately $7° \times 3°$. This eight-beam configuration will be taken as the baseline uplink antenna pattern.

Two candidate multiple-beam antennas (MBA) are considered, one based on offset-fed reflectors and the other on multiple lenses. From a system viewpoint, the frequency band allocated to each beam may be confined to a single polarization or it may be divided between the two polarizations. In the first case, the feed horns (for either antenna configuration) have only a single port; in the latter case, a separate port is required for each polarization. If both polarizations are used in a single beam, the lens antenna may be preferred because of its superior polarization properties.

3.1. MBA with Multiple Reflectors

This antenna consists of three offset-fed paraboloid reflectors. The geometry for each reflector is shown in Figure 3-2. The angle, θ_f,

Figure 3-2. Offset-Fed Reflector Antenna Geometry

subtended by the reflector is given by

$$\theta_f = \tan^{-1}[4\xi/(4-\xi^2)] \qquad (3-5)$$

where ξ is the ratio of the reflector diameter, D, to the focal length, f. A conventional design will be assumed, in the sense that f = D. This leads to a value of θ_f equal to 53°.

Two of the reflectors are fed by three horns, and the third by a pair of horns. Beam assignments for the three reflectors are shown in Figure 2-2. Beams generated by the same reflector have an angular separation of $1.5\,\theta_b$.

The need for three reflectors arises from the relationship between the feed horn aperture (d_1), the spacing between feed horns (S_f), and the angular separation between beams generated by a common aperture. The parameter d_1 is chosen equal to the smaller of S_f or the aperture size that provides the desired reflector illumination. It can be shown that a radiation pattern with a -10 dB intensity (I_e) at the edge of the reflector (referred to the illumination intensity at the center of the reflector) maximizes the aperture efficiency. The reason is that a -10 dB taper produces the best compromise between spillover loss and underillumination of the reflector. (This optimization is a "broad" function of I_e because, for $I_e = -6$ dB or -20 dB, the aperture efficiency is only reduced by 0.5 dB.) The 10-dB beamwidth of a circular-aperture horn

antenna is given approximately by

$$\theta_{10} \approx 120 \, \lambda/d_1 \qquad\qquad (3\text{-}6)$$

Substituting $\theta_{10} = \theta_f = 53°$ in (3-6) and solving for d_1/λ results in

$$d_1/\lambda \leq 2.26 \qquad\qquad (3\text{-}7)$$

The value of S_f required to produce a pair of beams with angular separation θ is given by

$$S_f = f[\tan (F_{bd}\theta)] \qquad\qquad (3\text{-}8)$$

where F_{bd} is the beam deviation factor, which typically has a value of 1.1. If the eight-beam antenna pattern were produced by a single reflector, θ would be equal to $\theta_b = 2.22°$ and S_f would be equal to 0.59 in. or 1.48 λ. The feed horn aperture would be limited to the latter value, rather than 2.26 λ as expressed by (3-7). The resulting spillover loss, with D = 34.9 λ = 13.9 in., would reduce the antenna gain by 1.7 dB relative to the assumed 50-percent efficiency.

With the three-reflector configuration, on the other hand, the beam separation for each reflector considered separately is 1.5 θ_b = 3.33°. From (3-8), the corresponding feed horn separation is 2.22 λ = 0.89 in. Thus, d_1, as well as S_f, can be chosen equal to 2.22 λ. This results in a 10-dB

illumination taper and the previously assumed 50-percent antenna efficiency.

The polarization isolation that must be maintained when both polarizations are used in a single beam depends on the disparity in received signal strength from different terminals. For signals of equal magnitude, polarization isolation of 20 dB would result in a 1-dB reduction in overall carrier-to-noise ratio. (A 14-dB carrier power-to-thermal noise ratio is assumed.) However, the combination of EIRP variations and rain attenuation can lead to a 10-dB disparity in received signal strength. Therefore, 30-dB polarization isolation is required.

An antenna such as the multiple-reflector configuration, or the multiple-lens configuration described in the next section, has crosspolarized sidelobes that attain their maximum value at an angle θ_C from the copolarized beam axis. Usually, $\theta_C \approx \theta_3/2$. For linearly polarized transmission, the crosspolarized sidelobes comprise four "beams" equally spaced on a circle of radius θ_C and displaced from the direction of polarization by 45°. With a center-fed antenna, the crosspolarized lobes are approximately equal in magnitude. With an offset-fed reflector, two lobes are stronger than the other two and are usually stronger than those produced by a center-fed antenna. With $f/D \approx 1$, the crosspolarized lobes are about 25 dB below the copolarized beam peak. With careful design and fabrication, it may be possible to reduce the crosspolarized lobes to -30 dB with respect to the peak of the copolarized beam. With circular

polarization, the four distinct lobes become a continuous circular lobe at an angle $\theta_3/2$ from the copolarized beam axis.

Note that, even if each beam is restricted to a single polarization, the crosspolarized sidelobes, which are at an angle $\theta_3/2$ from the copolarized beam axis, may interfere with transmissions in an adjacent beam. To avoid this possibility, it is necessary to impose an operational constraint that precludes frequency reuse in adjacent beams.

3.2. MBA with Multiple Lenses

The rationale that led to the need for multiple reflectors applies to the lens configuration as well. Consequently, an antenna efficiency of 50 percent may be assumed with a three-lens system. Such an antenna is shown schematically in Figure 3.3. The lens diameter, D, and the focal length, f, are again both equal to 13.9 in. The feed-horn spacing and the diameter of the horn aperture are both 0.89 in.

The lens is designed to convert spherical waves radiated by the feed horn into plane waves propagating away from the lens aperture. A first-order design is obtained by choosing the lens thickness so that all rays, emanating from the focal point and terminating in the aperture plane, have the same electrical length; the lens thickness, t, is given by

$$t = [1-(\cos \phi/\cos \phi_m)]/(1-\sqrt{\varepsilon}\cos \phi) \qquad (3-9)$$

where ϕ is the angle indicated in Figure 3-3, $2\phi_m$ is the angle subtended by

Figure 3-3.   Multiple-Lens Antenna Geometry
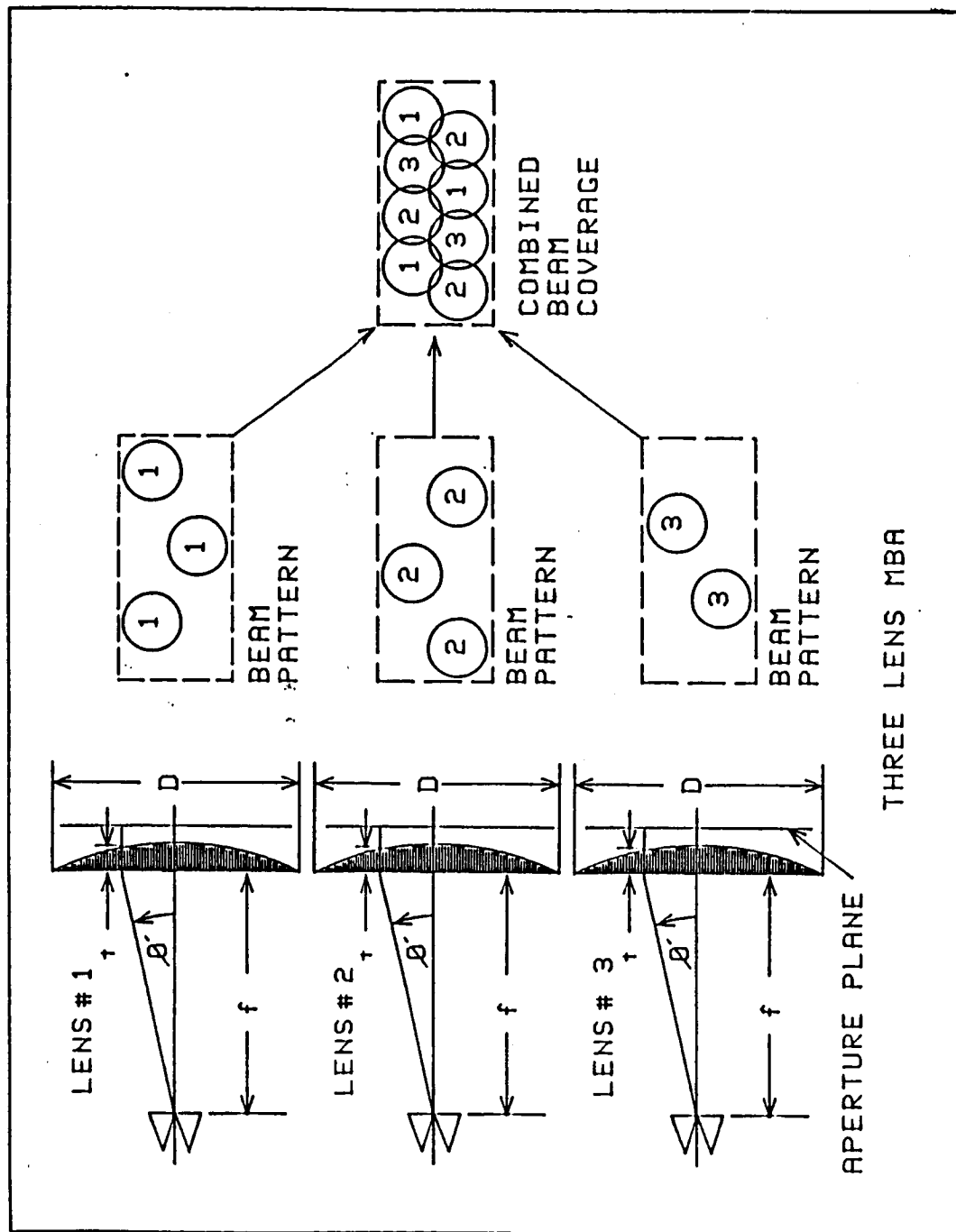
the lens, and ε is the dielectric constant of the lens. Using D = f = 13.9 in., the thickness of a rexolite lens (ε = 2.4) varies from 3.0 in. at the center to zero at its outer edge.

Lens antennas must use a slow-wave medium to convert the incident spherical wave to a plane wave. The slow-wave medium has a characteristic impedance different from that of air or free space. This impedance mismatch introduces reflected waves and reduces the antenna gain. If a quarter-wave matching layer is placed over the entrance and exit surfaces of the lens, this mismatch loss can be reduced from about 1.0 dB to less than 0.1 dB. Assuming that a matching surface is used, the lens antenna gain, half-power beamwidth, and scan properties will be essentially the same as those of the reflector system described previously.

Crosspolarized radiation of a lens antenna, as well as for a paraboloid reflector, depends strongly on the f/D ratio. Larger f/D and center-fed antenna systems have lower response to crosspolarized incident fields. With the lens being center-fed and the reflector offset-fed, the lens antenna will have less coupling between orthogonally polarized ports.

The weight of the lens antenna combination is about four times that of the reflector configuration. In absolute terms, however, the lens antennas weigh a total of only 25 lb.

4. SATELLITE TRANSMIT ANTENNA DESIGN

The satellite transmit antenna is required to generate four scanning spot beams, each supporting a data rate of 180 Mbps and providing an EIRP of 63.1 dBW. Three different antenna configurations are considered for this purpose: a paraboloid reflector illuminated by a phased array using a Gregorian subreflector, an active-aperture phased array, and a switched-beam MBA. Performance characteristics and estimated size of these candidate systems are presented below.

4.1. Phased-Array-Fed Reflector Antenna

A single scanning beam can be produced by a phased array illuminating a Gregorian configuration of dual confocal paraboloid reflectors as shown in Figure 4-1. Conceptually, the phased array launches a plane wave toward the smaller paraboloid subreflector. The subreflector intercepts this energy and converges it to a "point" near, or on, its focal point. This energy, in turn, is intercepted by the larger (main) paraboloid, which transforms it into a narrow beam. If the phased array is excited with a uniform phase distribution, the subreflector converges the intercepted energy at its focus. Since both reflectors have the same focal point, the axis of the secondary beam produced by the main paraboloid is coincident with the common focal axis of the paraboloids. If, instead, the phase distribution varies linearly with distance from a point on the edge of the array, the beam axis is scanned off the focal axis.

The array is shown schematically in Figure 4-2a. An input carrier

Figure 4-1. Array-Fed Dual Reflector Antenna System
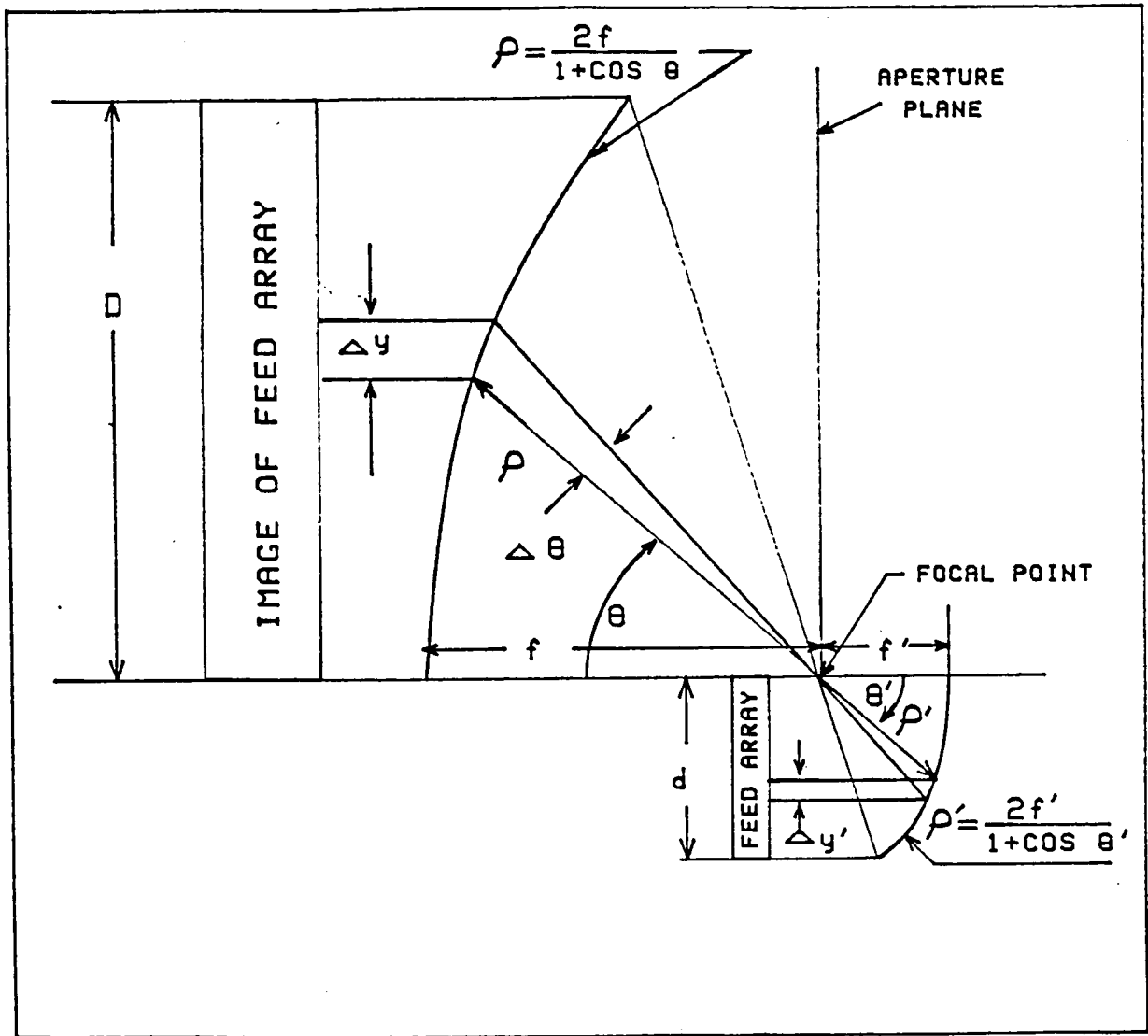
Figure 4-2. Phased Array Transmit Modules

a) SINGLE BEAM ARRAY

b) TWO BEAM ARRAY

c) TWO BEAM ARRAY
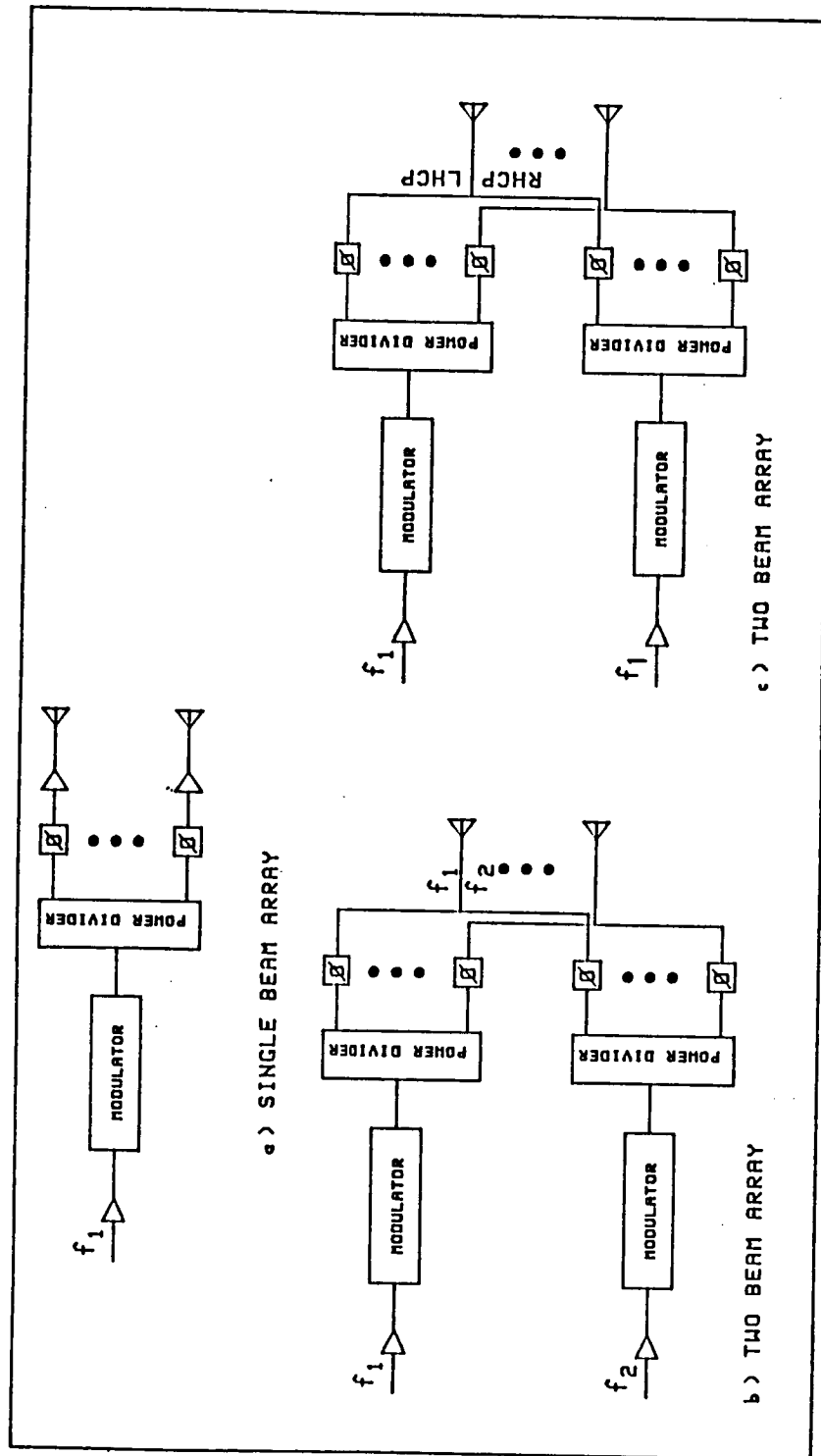
signal at frequency f_1 is modulated and divided equally among N phase shifters which, in turn, excite N modules. Each module consists of an SSPA, a horn radiator, and associated circuitry. The N modules are assembled to form an N-element array antenna.

The circuit shown in Figure 4-2b has two input carrier signals, f_1 and f_2. Each carrier signal is divided equally among its own set of phase shifters. The output of each set of phase shifters drives an associated set of SSPAs to produce two independent excitation phase distributions, ϕ_1 and ϕ_2, across the array aperture. This, in turn, produces two separate beams, one for f_1 and a second for f_2.

Antenna Dimensions. The antenna gain is determined by the dimension of the main reflector. For a fixed EIRP, therefore, the antenna size (and, as will be seen, the size of the array) can be traded off against RF power. For purposes of illustration, the RF power per carrier is assumed to be 100W. It can be shown that the antenna gain at the edge of a beam of specified angular coverage is maximized when the peak gain is 4.3 dB greater than the edge gain. Allowing 0.5 dB for scan loss, the required peak gain, G, is equal to 63.1 - 20 + 4.3 + 0.5 = 48 dBi.

The required half-power beamwidth, θ_3, can be estimated using the approximate relationship,

$$\theta_3 = \sqrt{35000/G} \qquad (4-1)$$

Substituting G = 63096 (i.e., 48 dBi) leads to the result that θ_3 must be 0.75°. The antenna gain at an angle θ from boresight is given by

$$G(\theta) \approx -12(\theta/\theta_3)^2 \quad \text{dB} \qquad (4\text{-}2)$$

Setting G(θ) = -4.3 dB and solving (4-2) for θ indicates that the 4.3-dB beamwidth is $1.2\theta_3 = 0.9°$. Consequently, the beam coverage area is 0.9° in diameter. The 0.9-deg beams are overlapping, such that all points of interest lie within either one or two beams.

The half-power beamwidth of a circular aperture can be estimated from

$$\theta_3 = k\lambda/D \qquad (4\text{-}3)$$

where D is the aperture diameter, λ is the wavelength, and k is approximately 70 for the nearly uniform array illumination with sharp edge taper. Solving for D/λ gives

$$D/\lambda = 70/\theta_3 \qquad (4\text{-}4)$$

At f = 19.7 GHz, λ = 0.598 in. and, from (4-4), D = 56 in. when θ_3 = 0.75°. Hence, the area of the reflector projected parallel to the focal axis will be 56 in. in diameter. The focal length of the paraboloid can vary over a wide range; however, choosing f = D = 56 in. represents a reasonable compromise between physical size and scan loss.

The subreflector is also an offset section of a paraboloid. Its focal axis and focal point must coincide with the focal axis and focal point of the main reflector. The projection of the subreflector parallel to the focal axis is a circle with diameter d. The focal length f' of the subreflector will be assumed equal to d. The focal length f' can be less than d; however, it cannot be larger than d. Referring to Figure 4-1, the surface of the reflectors is given by

$$\rho = 2f/(1 + \cos \theta) \qquad (4\text{-}5)$$

for the main reflector and

$$\rho' = 2f'(1 + \cos \theta') \qquad (4\text{-}6)$$

for the subreflector.

Magnification of the feed array by the Gregorian optics is the primary advantage of using the array-fed, dual-reflector system instead of a planar phased array. Assume that the feed array diameter equals d, although it can be smaller. The dual-reflector system produces an image of the feed array as indicated. The image has a diameter equal to D, as long as the feed array diameter is ≥d. (If the array diameter is less than d, the image diameter will, for main beam analysis, be less than D.) The array diameter is decreased by the magnification factor, M, where

$$M = D/d \qquad (4\text{-}7)$$

The array diameter is also a function of the number of elements, N, in the array and the element aperture diameter, d_0. It is important to note that radiation patterns and gain can be analytically determined using the image of the feed array instead of integrating currents on the reflector surface.

Number of Elements. The feed array should be filled, rather not thinned, to cause the angle θ_g between a grating lobe and the beam axis to be as large as possible. Choosing a smaller value of d_0 will also cause θ_g to be larger. Distributing the elements on a hexagonal grid minimizes the maximum spacing between adjacent elements and also maximizes θ_g. It is important to maximize θ_g because this reduces the gain of the grating lobe, thereby increasing the main lobe gain. (This aspect of array design, which is the same for an active-aperture phased array, is discussed in Section 4-2.) Consequently, the feed array is assumed to consist of N elements on a hexagonal grid. Each element has a circular aperture with diameter d_0. Adjacent element spacing is uniformly equal to d_0.

The radiation patterns and gain of the array-fed reflector system will be established by reference to the corresponding properties of the image array shown in Figure 4-1. The gain of an array antenna, G_a, is approximated by

$$G_a = NG_{el} \qquad (4-8)$$

where G_{el} is the gain of an array element. Assuming the element has a uniformly illuminated circular aperture (a good approximation for a horn

antenna), G_{e1} is given by

$$G_{e1}(\phi) = 4(\pi d_0 M/\lambda)^2 [J_1(u)/u]^2 \qquad (4\text{-}9)$$

where

$$u = \pi M d_0 \sin \phi/\lambda \qquad (4\text{-}10)$$

and ϕ is the angle between a ray to the far-zone observation point and the focal axis. $J_1(u)$ is the Bessel function of order 1 with argument u. The magnification factor, M, converts the diameter of the array element to the diameter of its image in the image array.

G_a, as given by (4-8) to (4-10), is the gain at the peak of a beam; the gain G_e at the edge of beam coverage is 4.3 dB less. Hence,

$$G_e(\phi) = 1.49 N(\pi M d_0/\lambda)^2 [J_1(u)/u]^2 \qquad (4\text{-}11)$$

The factor $J_1(u)/u$ reduces $G_e(\phi)$ as ϕ is increased. The maximum reduction, ΔG_e, occurs when the beam is scanned to the edge of CONUS. From geosynchronous orbit, CONUS subtends an approximately rectangular area measuring 7° x 3°. Increasing N reduces ΔG_e and, as stated before, increases θ_g.

The satellite EIRP in each of the four scanning beams is given by

$$EIRP = 1.49N^2P_e(\pi Md_0/\lambda)^2[J_1(u)/u]^2 \qquad (4\text{-}12)$$

where P_e is the RF power per element. To use (4-12) to relate EIRP, N, and P_e, it is first necessary to express d_0 in terms of N. The number of elements in a hexagonal array varies in accordance with

$$N = 1 + \sum_{i=1}^{J} 6i = 1 + 3J(J+1) \qquad (4\text{-}13)$$

where $N_0 = 2J + 1$ is the number of elements along a major diagonal of the array. However, N_0 is also equal to D/Md_0. Equating the two expressions for N_0, solving for J, and substituting the result into (4-13) yields

$$N = 1 + \frac{3}{4}\left[\left(\frac{D}{Md_0}\right)^2 - 1\right] \qquad (4\text{-}14)$$

Practical values of M are limited by the associated scan loss. It can be shown that the scan loss, L_s, is given approximately by

$$L_s = 10 \log[1 - 4(M+1)(f'/d)(\phi/\pi)] \quad dB \qquad (4\text{-}15)$$

where ϕ is in radians. With $f'/d = 1$ and $\phi = 0.06$ radian (i.e., $\phi = 3.5°$), $L_s = 10 \log[1 - .078(M + 1)]$ dB. A value of M equal to 3, for example,

produces a scan loss of 1.6 dB. For a selected value of M, the associated scan loss must be subtracted from the EIRP computed from (4-12) to obtain the EIRP actually realized.

The EIRP resulting from various combinations of M, P_e, and N is shown in Table 4-1 for a main reflector diameter of 56 in. For a hexagonal array, N varies in discrete steps according to the selected value of J in (4-13). It is seen, for example, that for M = 3 and P_e = 0.5W, a 331-element array is needed to produce the required EIRP of 63.1 dBW.

The required RF power per beam (165W in this case) can be reduced by choosing a larger main reflector, with a corresponding increase in the size of the array. If the element size is held fixed (thereby maintaining the grating lobe properties), the number of elements, N, increases as the square of the reflector diameter. The RF power per beam varies inversely with N, while P_e varies inversely with N^2. The larger reflector implies a larger number of downlink beam positions (i.e., spots) for CONUS coverage.

Increasing M decreases the dimension of the subreflector proportionately. It also increases the scan loss. For M = 5, D = 56 in., and N = 331, the element size and the interelement spacing approach the width of a standard section of rectangular waveguide. Smaller interelement spacing could lead to difficulty in packaging the amplifiers, phase shifters, connecting waveguide, etc. Review of the data in Table 4-1 indicates that M = 3 is probably the best choice. Similarity between the array-fed reflector system and the active-aperture array permits other

Table 4-1. EIRP for Array-Fed Dual Reflector Antenna

Frequency = 19.7 GHz   Wavelength= .598 Inches
Diameter of Main Reflector= 56 Inches   Focal Length = 56 Inches
Maximum Scan Angle= 3.5 Degrees

Magnification Factor= 3   Scan Loss=-1.619 dB   Power Per Element= .5 Watt

Number of Elements	Diameter of Element (Inches)	Loss Due To Element Factor(dB)	EIRP (Including all) Losses) (dBW)
91	1.697	-3.065	55.711
127	1.436	-2.155	58.066
169	1.244	-1.601	59.859
217	1.098	-1.237	61.306
271	0.982	-0.986	62.522
331	0.889	-0.804	63.572
397	0.812	-0.668	64.496

Magnification Factor= 3   Scan Loss=-1.619 dB   Power Per Element= 1 Watt

Number of Elements	Diameter of Element (Inches)	Loss Due To Element Factor(dB)	EIRP (Including all) Losses) (dBW)
91	1.697	-3.065	58.722
127	1.436	-2.155	61.076
169	1.244	-1.601	62.869
217	1.098	-1.237	64.317
271	0.982	-0.986	65.532
331	0.889	-0.804	66.582
397	0.812	-0.668	67.506

Magnification Factor= 4   Scan Loss=-2.139 dB   Power Per Element= .5 Watt

Number of Elements	Diameter of Element (Inches)	Loss Due To Element Factor(dB)	EIRP (Including all) Losses) (dBW)
91	1.273	-3.065	55.191
127	1.077	-2.155	57.546
169	0.933	-1.601	59.338
217	0.824	-1.237	60.786
271	0.737	-0.986	62.002
331	0.667	-0.804	63.051
397	0.609	-0.668	63.976

Magnification Factor= 4   Scan Loss=-2.139 dB   Power Per Element= 1 Watt

Number of Elements	Diameter of Element (Inches)	Loss Due To Element Factor(dB)	EIRP (Including all) Losses) (dBW)
91	1.273	-3.065	58.201
127	1.077	-2.155	60.556
169	0.933	-1.601	62.349
217	0.824	-1.237	63.796
271	0.737	-0.986	65.012
331	0.667	-0.804	66.062
397	0.609	-0.668	66.986

Table 4-1. EIRP for Array-Fed Dual Reflector Antenna (continued)

Frequency = 19.7 GHz   Wavelength= .598 Inches
Diameter of Main Reflector= 56 Inches   Focal Length = 56 Inches
Maximum Scan Angle= 3.5 Degrees

Magnification Factor= 5   Scan Loss=-2.731 dB   Power Per Element= .5 Watt

Number of Elements	Diameter of Element (Inches)	Loss Due To Element Factor(dB)	EIRP (Including all) Losses) (dBW)
91	1.018	-3.065	54.600
127	0.862	-2.155	56.954
169	0.747	-1.601	58.747
217	0.659	-1.237	60.195
271	0.589	-0.986	61.411
331	0.533	-0.804	62.460
397	0.487	-0.668	63.385

Magnification Factor= 5   Scan Loss=-2.731 dB   Power Per Element= 1 Watt

Number of Elements	Diameter of Element (Inches)	Loss Due To Element Factor(dB)	EIRP (Including all) Losses) (dBW)
91	1.018	-3.065	57.610
127	0.862	-2.155	59.965
169	0.747	-1.601	61.757
217	0.659	-1.237	63.205
271	0.589	-0.986	64.421
331	0.533	-0.804	65.470
397	0.487	-0.668	66.395

characteristics of the former to be discussed in greater detail in the next section, where the active aperture antenna design and its performance characteristics are addressed.

Dual Polarization. Two data streams operating at the same carrier frequency can be multiplexed on the same dual-polarized feed horn. The circuit shown in Figure 4-2c schematically represents the use of circularly polarized horns in the feed array. One data stream excites the left-hand circularly polarized (LHCP) port of the horns; the other data stream excites the right-hand circularly polarized (RHCP) port. Both data streams modulate the same carrier frequency f_1 and use a different set of phase shifters. Therefore, two independent beams are produced, operating at the same frequency and each carrying its own data stream.

The feed horns used in a planar array inherently radiate a wave whose polarization is very well-defined. The dual-reflector system tends to degrade the polarization purity of the feed array. The degree of degradation depends on f/D, surface accuracy, and beam scan angle. The dual-reflector system may increase the amount of energy radiated in the cross-polarized fields from less than -25 dB (with respect to the copolarized maximum) at the feed array to as much as -15 dB in the radiated beam. Generally, the cross-polarized energy in the main beam (i.e., within the 4.3-dB beamwidth) will be less than -20 dB with respect to the copolarized energy.

4.2. Active-Aperture Phased Array

An active-aperture phased array consists of a contiguous array of antenna modules, each containing a radiating element excited by an SSPA. Each SSPA is driven by a modulator/driver through a diode phase shifter; the latter is part of the antenna module. The phase of the signal fed to each SSPA is adjusted by the phase shifter so that the radiated signals add coherently to form a beam pointed in the desired direction. The diode phase shifters can be programed to insert any phase shift, modulo 2π, in less than a 0.1 μsec. The active-aperture array is, except for overall size, similar to the feed array described in the previous section.

· <u>Antenna Dimensions and Number of Elements</u>. Consider a planar array of horn antennas. Since the antenna beam has a circular cross section, the array configuration should also tend to be circular. The elements of the array are identical. Each element has a radiation pattern with an approximately circular cross section and a half-power beamwidth, θ_3, equal to or greater than the largest angle subtended by CONUS when viewed from geosynchronous altitude. The elements are arranged on an equilateral triangular, or hexagonal, grid and spaced to preclude the occurrence of grating lobes pointing toward CONUS. Each horn has a circular aperture, d_0, equal to the spacing between horns.

The approximate gain of the horn is given by (4-9) with M=1. The maximum element gain at the edge of CONUS (ϕ = 3.5°) is plotted in Figure

4-3. This gain reaches a maximum value of 28.4 dBi for $d_0/\lambda \approx 12$. This maximum is 4.3 dB below the element gain at the center of CONUS. For $d_0/\lambda > 12$, element gain decreases. The ratio d_0/λ must be greater than 0.5 to support propagation. Therefore, $0.5 < d_0/\lambda < 12$ and the corresponding minimum element gain over CONUS varies from 10 to about 29 dBi.

The minimum gain of the array, G_e, occurs at the edge of a beam coverage area and is given by (4-11) with $M = 1$, i.e.,

$$G_e(\phi) = 1.49N(\pi d_0/\lambda)^2[J_1(u)/u]^2 \qquad (4\text{-}16)$$

Equation 4-16 assumes that the antenna aperture is chosen so that the 4.3-dB beamwidth is equal to the angular diameter of the desired beam coverage area. The 4.3-dB beamwidth and a major diagonal D of the hexagonal array are related by

$$D/\lambda = 70/\theta_{4.3} \qquad (4\text{-}17)$$

To find the value of N required to produce a given value of G_e in (4-16), it is necessary to express d_0 in terms of N through use of (4-13), (4-14), and (4-17).

The EIRP of the active aperture array is given by

$$EIRP = 1.49P_e N^2(\pi d_0/\lambda)^2[J_1(u)/u]^2 \qquad (4\text{-}18)$$

Figure 4-3. Radiating Horn Edge-of-Coverage Gain
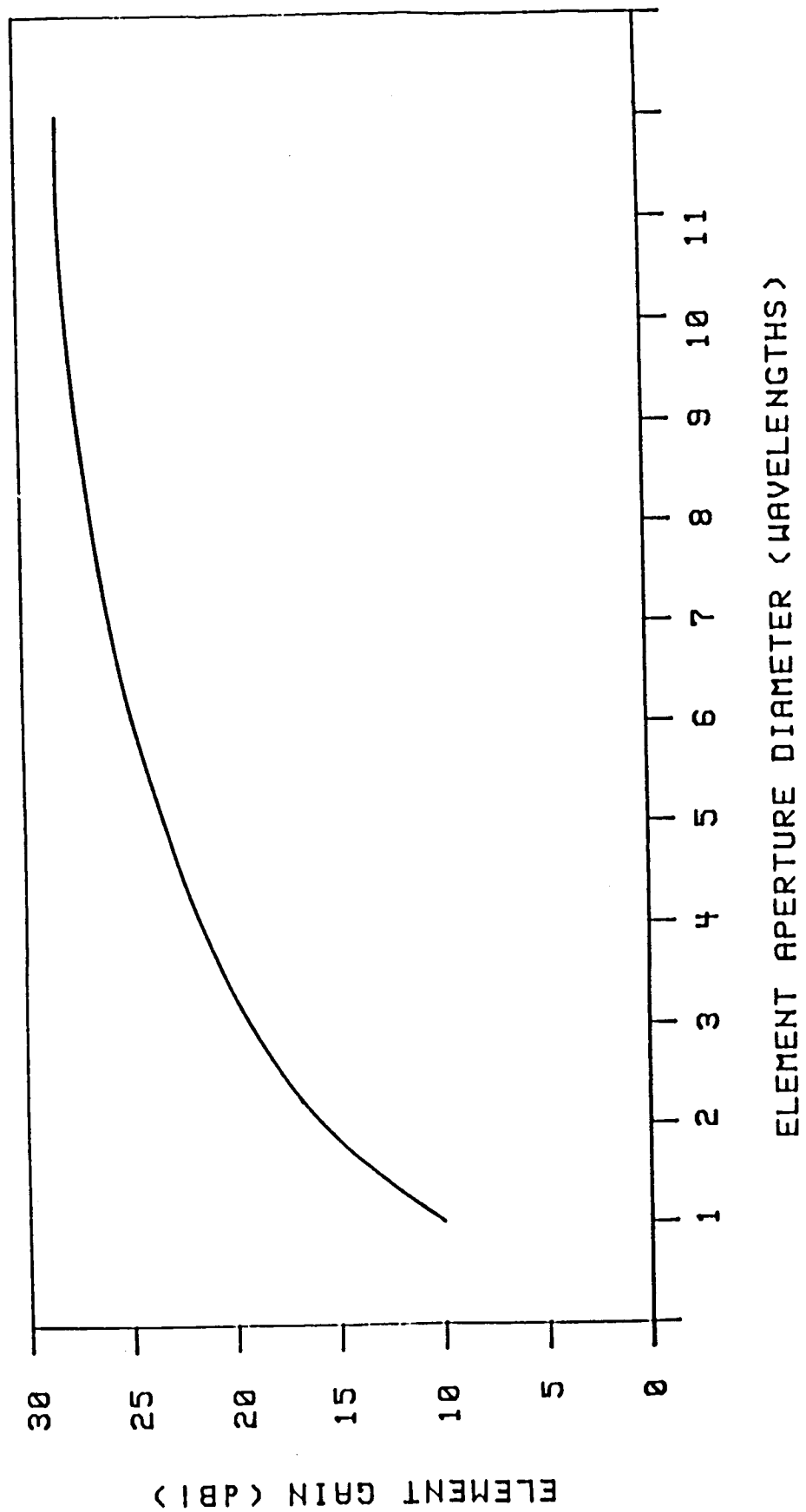
Using (4-18), EIRP was calculated for different values of N, P_e, and D, with maximum scan angle $\phi = 3.5°$. The results are shown in Table 4-2. Note that the desired 0.9-deg beam coverage (i.e., 4.3-dB beamwidth) is obtained with D $\doteq$ 46.4 in. instead of 56 in. as required by the array-fed dual-reflector antenna. The difference in aperture size results principally from the scan loss introduced by the dual-reflector system. The results shown in Table 4-2 are plotted in Figure 4-4.

Radiation Patterns and Grating Lobes. The hexagonal active-aperture array with 217 elements is shown in Figure 4-5. The diagram shows the relative positions of the element centers; the element diameter is the largest value permitted by the element spacing. Radiation patterns in the plane of a major diagonal and in a plane bisecting an opposite pair of sides can be calculated by reference to a linear array representing the hexagonal array. In the first case, the off-diagonal elements in a direction normal to the plane of the diagonal can be represented by a single-element radiator with the appropriate excitation, as shown in Figure 4-5. The hexagonal array can be represented by a different linear array to compute the radiation pattern in a plane perpendicular to a pair of opposite sides.

An expression for the pattern $E(\theta)$ in these planes is the product of two terms, an element factor $G_{eh}(\theta)$ and an array factor $A(\theta)$. Exciting all elements in the array with equal amplitude and a linear phase gradient to scan the beam to the angle θ_1, the radiation pattern in the diagonal plane

Table 4-2. EIRP for Active-Aperture Phased Array

Frequency = 19.7 GHz   Wavelength= .598 Inches
Maximum Scan Angle= 3.5 Degrees

Array Diameter = 58 inches   Power per Element= .5 Watt
****************4.3dB Beamwidth= .72 degrees****************

Number of Elements	Diameter of Element (Inches)	Loss Due To Element Factor(dB)	EIRP (Including all) Losses) (dBW)
91	5.273	-3.304	57.396
127	4.462	-2.319	59.825
169	3.867	-1.721	61.662
217	3.412	-1.330	63.137
271	3.053	-1.059	64.372
331	2.762	-0.863	65.435
397	2.522	-0.718	66.370

Array Diameter = 58 inches   Power per Element= 1 Watt
****************4.3dB Beamwidth= .72 degrees****************

Number of Elements	Diameter of Element (Inches)	Loss Due To Element Factor(dB)	EIRP (Including all) Losses) (dBW)
91	5.273	-3.304	60.406
127	4.462	-2.319	62.835
169	3.867	-1.721	64.672
217	3.412	-1.330	66.148
271	3.053	-1.059	67.383
331	2.762	-0.863	68.446
397	2.522	-0.718	69.380

Array Diameter = 52.2 inches   Power per Element= .5 Watt
****************4.3dB Beamwidth= .8 degrees****************

Number of Elements	Diameter of Element (Inches)	Loss Due To Element Factor(dB)	EIRP (Including all) Losses) (dBW)
91	4.745	-2.640	57.144
127	4.015	-1.861	59.368
169	3.480	-1.385	61.083
217	3.071	-1.072	62.480
271	2.747	-0.854	63.662
331	2.486	-0.697	64.687
397	2.270	-0.580	65.593

Array Diameter = 52.2 inches   Power per Element= 1 Watt
****************4.3dB Beamwidth= .8 degrees****************

Number of Elements	Diameter of Element (Inches)	Loss Due To Element Factor(dB)	EIRP (Including all) Losses) (dBW)
91	4.745	-2.640	60.154
127	4.015	-1.861	62.378
169	3.480	-1.385	64.093
217	3.071	-1.072	65.491
271	2.747	-0.854	66.672
331	2.486	-0.697	67.697
397	2.270	-0.580	68.603

Table 4-2. EIRP for Active-Aperture Phased Array (continued)

Frequency = 19.7 GHz   Wavelength= .598 Inches
Maximum Scan Angle= 3.5 Degrees

Array Diameter = 46.4 inches   Power per Element= .5 Watt
****************4.3dB Beamwidth= .9 degrees****************

Number of Elements	Diameter of Element (Inches)	Loss Due To Element Factor(dB)	EIRP (Including all) Losses) (dBW)
91	4.218	-2.062	56.699
127	3.569	-1.459	58.747
169	3.093	-1.088	60.357
217	2.729	-0.843	61.686
271	2.442	-0.673	62.820
331	2.210	-0.549	63.811
397	2.017	-0.457	64.693

Array Diameter = 46.4 inches   Power per Element= 1 Watt
****************4.3dB Beamwidth= .9 degrees****************

Number of Elements	Diameter of Element (Inches)	Loss Due To Element Factor(dB)	EIRP (Including all) Losses) (dBW)
91	4.218	-2.062	59.710
127	3.569	-1.459	61.757
169	3.093	-1.088	63.367
217	2.729	-0.843	64.696
271	2.442	-0.673	65.831
331	2.210	-0.549	66.822
397	2.017	-0.457	67.703

Array Diameter = 40.6 inches   Power per Element= .5 Watt
****************4.3dB Beamwidth= 1.03 degrees****************

Number of Elements	Diameter of Element (Inches)	Loss Due To Element Factor(dB)	EIRP (Including all) Losses) (dBW)
91	3.691	-1.563	56.038
127	3.123	-1.109	57.937
169	2.707	-0.829	59.456
217	2.388	-0.643	60.726
271	2.137	-0.513	61.820
331	1.933	-0.419	62.781
397	1.765	-0.349	63.641

Array Diameter = 40.6 inches   Power per Element= 1 Watt
****************4.3dB Beamwidth= 1.03 degrees****************

Number of Elements	Diameter of Element (Inches)	Loss Due To Element Factor(dB)	EIRP (Including all) Losses) (dBW)
91	3.691	-1.563	59.049
127	3.123	-1.109	60.947
169	2.707	-0.829	62.466
217	2.388	-0.643	63.736
271	2.137	-0.513	64.830
331	1.933	-0.419	65.792
397	1.765	-0.349	66.651

Table 4-2. EIRP for Active-Aperture Phased Array (continued)

Frequency = 19.7 GHz   Wavelength= .598 Inches
Maximum Scan Angle= 3.5 Degrees

Array Diameter = 34.8 inches   Power per Element= .5 Watt
****************4.3dB Beamwidth= 1.2 degrees****************

Number of Elements	Diameter of Element (Inches)	Loss Due To Element Factor(dB)	EIRP (Including all) Losses) (dBW)
91	3.164	-1.139	55.124
127	2.677	-0.810	56.897
169	2.320	-0.606	58.339
217	2.047	-0.471	59.559
271	1.832	-0.376	60.618
331	1.657	-0.307	61.554
397	1.513	-0.256	62.395

Array Diameter = 34.8 inches   Power per Element= 1 Watt
****************4.3dB Beamwidth= 1.2 degrees****************

Number of Elements	Diameter of Element (Inches)	Loss Due To Element Factor(dB)	EIRP (Including all) Losses) (dBW)
91	3.164	-1.139	58.134
127	2.677	-0.810	59.907
169	2.320	-0.606	61.350
217	2.047	-0.471	62.570
271	1.832	-0.376	63.628
331	1.657	-0.307	64.565
397	1.513	-0.256	65.405

Array Diameter = 29 inches   Power per Element= .5 Watt
****************4.3dB Beamwidth= 1.44 degrees****************

Number of Elements	Diameter of Element (Inches)	Loss Due To Element Factor(dB)	EIRP (Including all) Losses) (dBW)
91	2.636	-0.786	53.894
127	2.231	-0.560	55.563
169	1.933	-0.419	56.943
217	1.706	-0.326	58.120
271	1.526	-0.261	59.150
331	1.381	-0.213	60.065
397	1.261	-0.178	60.890

Array Diameter = 29 inches   Power per Element= 1 Watt
****************4.3dB Beamwidth= 1.44 degrees****************

Number of Elements	Diameter of Element (Inches)	Loss Due To Element Factor(dB)	EIRP (Including all) Losses) (dBW)
91	2.636	-0.786	56.904
127	2.231	-0.560	58.574
169	1.933	-0.419	59.953
217	1.706	-0.326	61.131
271	1.526	-0.261	62.160
331	1.381	-0.213	63.075
397	1.261	-0.178	63.900

Figure 4-4. Hexagonal Array EIRP

ANGULAR WIDTH OF SPOT (degrees)

ARRAY DIAMETER

N=397
N=331
N=271
N=217
N=169
N=127
N=91

EIRP per WATT (dBW)

ARRAY DIAMETER (WAVELENGTHS)
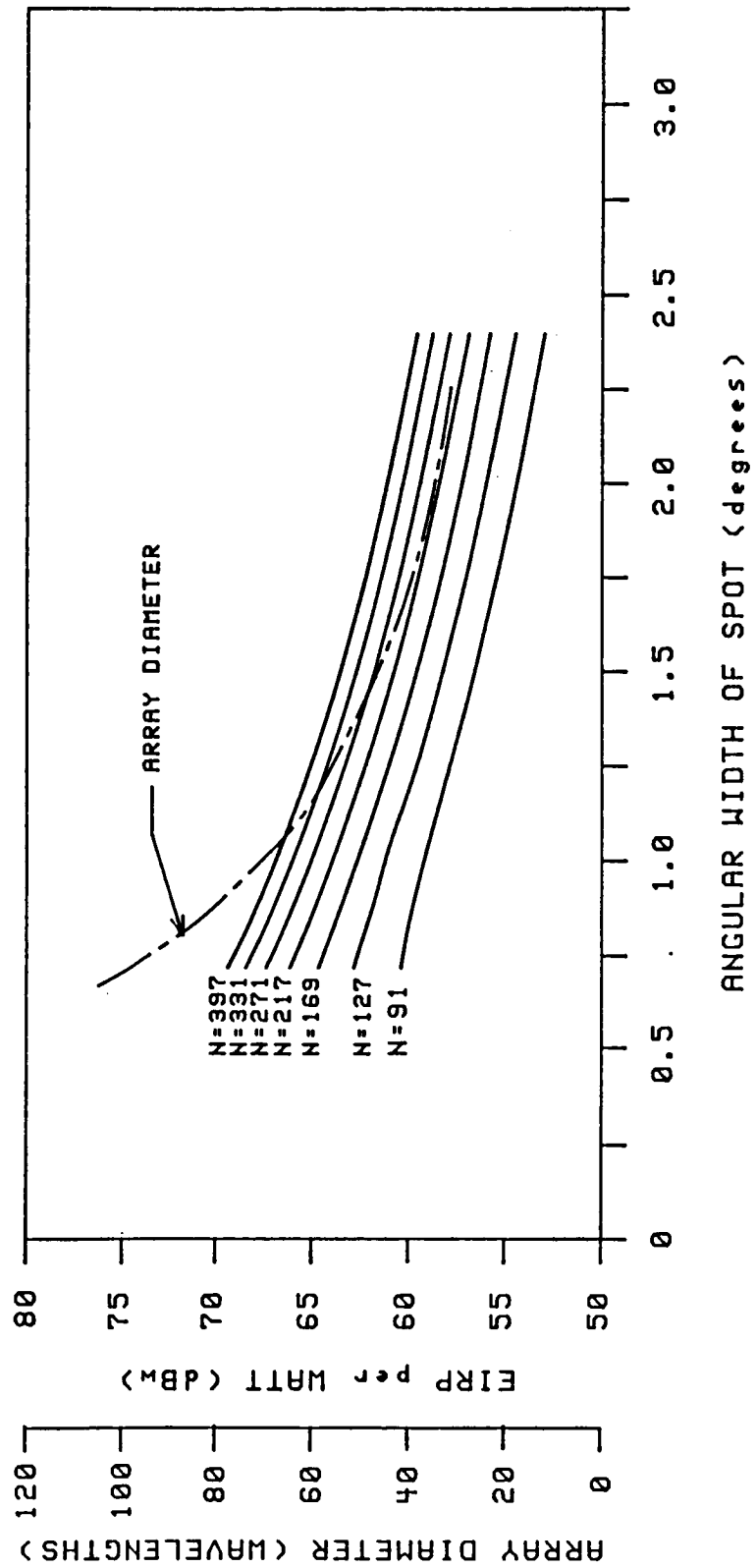
Figure 4-5. Linear Array Equivalents to Hexagonal Array
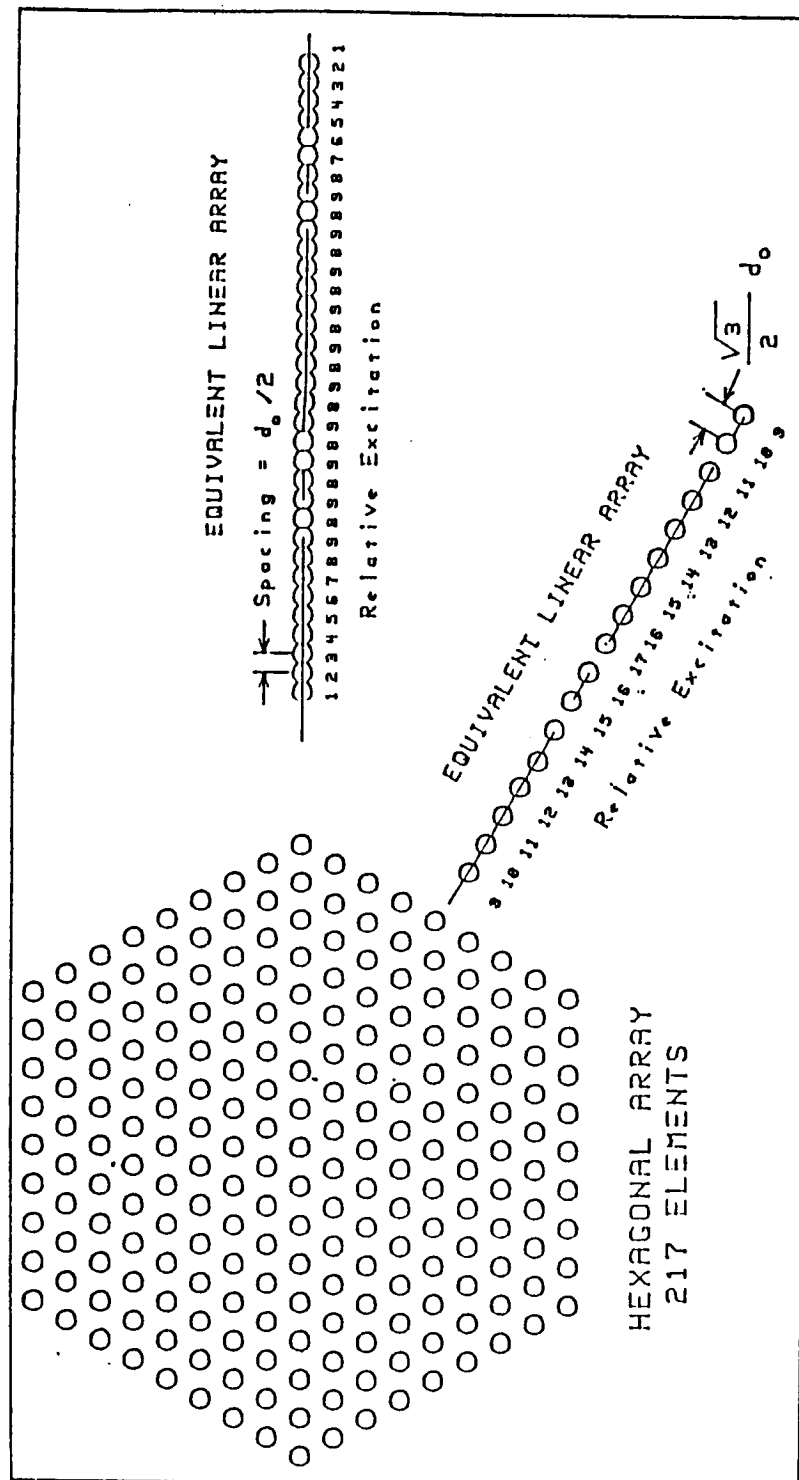
is given by

$$E_d(\theta) = G_{eh}(\theta)A_d(\theta) \qquad (4\text{-}19)$$

where $G_{eh}(\theta)$ is given by (4-9) with $M = 1$ and $\phi = \theta$, and

$$A_d(\theta) = 9 + \sum^{9} a_i\cos\left[i\pi(d_0/\lambda)(\sin\theta - \sin\theta_1)\right]$$

$$+ \sum_{i=1}^{17}(18-i)\cos\left[i\pi(d_0/\lambda)(\sin\theta - \sin\theta_1)\right] \qquad (4\text{-}20)$$

where

$$a_i = 8, \quad i \text{ odd}$$
$$a_i = 9, \quad i \text{ even}$$

Note that a grating lobe occurs at θ_g when

$$\pi(d_0/\lambda)(\sin\theta_g - \sin\theta_1) = \pm 2\pi \qquad (4\text{-}21)$$

Solving for θ_g gives

$$\sin\theta_g = \pm(2\lambda/d_0) + \sin\theta_1 \qquad (4\text{-}22)$$

The minus sign in (4-22) will be chosen, and θ_1 will be assumed positive. This combination, which places the grating lobe closest to the region of interest (i.e., CONUS), yields

$$\sin \theta_g = -[(2\lambda/d_0) - \sin \theta_1] \qquad (4\text{-}23)$$

For the 217-element active-aperture array, $d_0/\lambda = 4.66$. With $\theta_1 = 3.5°$, $\theta_g = -21.7°$. The element pattern [see (4-9) with M=1] suppresses the grating lobe 18 dB below the main-beam peak.

In the plane perpendicular to opposite sides of the hexagon,

$$E_1(\theta) = G_{eh}(\theta)A_p(\theta) \qquad (4\text{-}24)$$

where

$$A_p(\theta) = 17 + \sum_{i=1}^{8} (17-i)\cos[i\pi\sqrt{3}(d_0/\lambda)(\sin \theta - \sin \theta_1)] \qquad (4\text{-}25)$$

Note that a grating lobe occurs when

$$\pi\sqrt{3}(d_0/\lambda)(\sin \theta_g - \sin \theta_1) = \pm 2\pi \qquad (4\text{-}26)$$

Again choosing the minus sign,

$$\sin \theta_g = -[(2\lambda/\sqrt{3}d_0) - \sin \theta_1] \qquad (4\text{-}27)$$

If the major diagonal is oriented to coincide with the maximum dimension of CONUS, the maximum scan angle θ_1 in this case will be somewhat smaller than 3.5°, say 3.0°. The corresponding value of θ_g is -11.3°. The grating lobe at this location is suppressed 13.8 dB.

4.3. MBA With Beam Switching Matrix

Several traveling wave tube amplifiers (TWTA) operating at 20 GHz have been developed for communication satellite systems. Of prime interest are a series that have been space qualified, have 25-30W average power output, and operate at approximately 33-percent efficiency. Manufacturers of these TWTAs claim that 50-60W devices are within the state-of-the-art. Use of these tubes in redundant systems, with switched beam antennas, has forced development of ferrite latching isolator switches that have less than 0.1 dB insertion loss and handle up to 100W average power. Existence of these devices stimulates consideration of the transmit antenna subsystem schematically shown in Figure 4-6.

Signals from the payload signal router are fed to four modulators which are connected to any four of eight TWTAs. A redundancy switch connects the selected four TWTAs to four MBAs. Each MBA has a beam switching network that connects a single input port to any beam port. The latter ports are connected to feed horns, each of which produces a beam pointing to a different 0.9-deg spot within CONUS. Beams radiated by the four MBAs provide contiguous coverage over a 7° x 3° field of view that spans CONUS. Dual polarization characteristics of the horns and operation at either of two frequency bands permit simultaneous excitation of four beams on a noninterfering basis.

Antenna Configuration. The beams from the MBA provide coverage over a 0.9-deg-diameter area, with the coverage areas forming the triangular lattice structure illustrated in Figure 4-7. Minimum gain over

ORIGINAL PAGE IS
OF POOR QUALITY

Figure 4-6. MBA with Beam Switching Matrix

LENS #1
LENS #2
LENS #3
LENS #4

9 HORN FEED
12 HORN FEED
12 HORN FEED
9 HORN FEED

9 PORT SWITCH NETWORK
12 PORT SWITCH NETWORK
12 PORT SWITCH NETWORK
9 PORT SWITCH NETWORK

8X4 REDUNDANCY SWITCH

TWTA TWTA TWTA TWTA TWTA TWTA TWTA TWTA

4X8 DIST. SWITCH

MOD. #1
MOD. #1
MOD. #1
MOD. #1

TO SIGNAL ROUTER

NOTE: EACH TWTA IS A 100 WATT DEVICE OR
A PAIR OF 50 WATT DEVICES
OPERATED IN PARALLEL
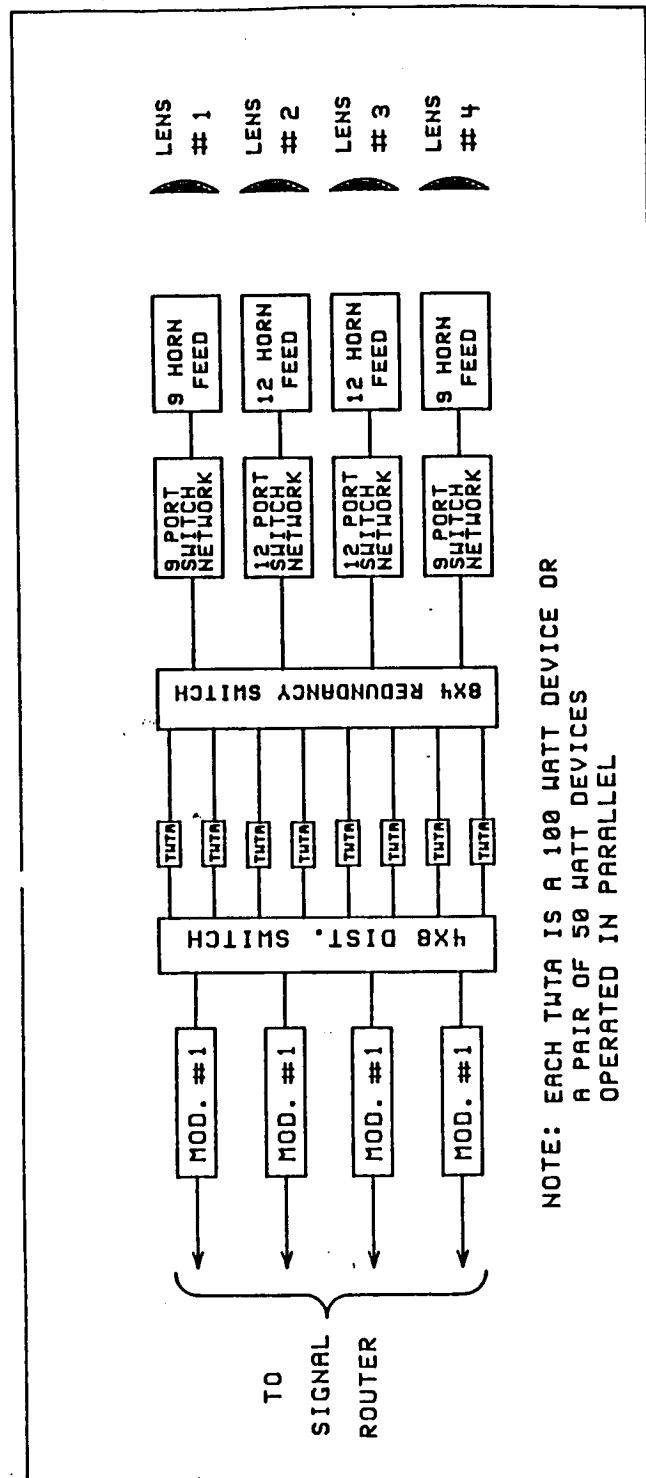
Figure 4-7. Triangular Beam Pattern
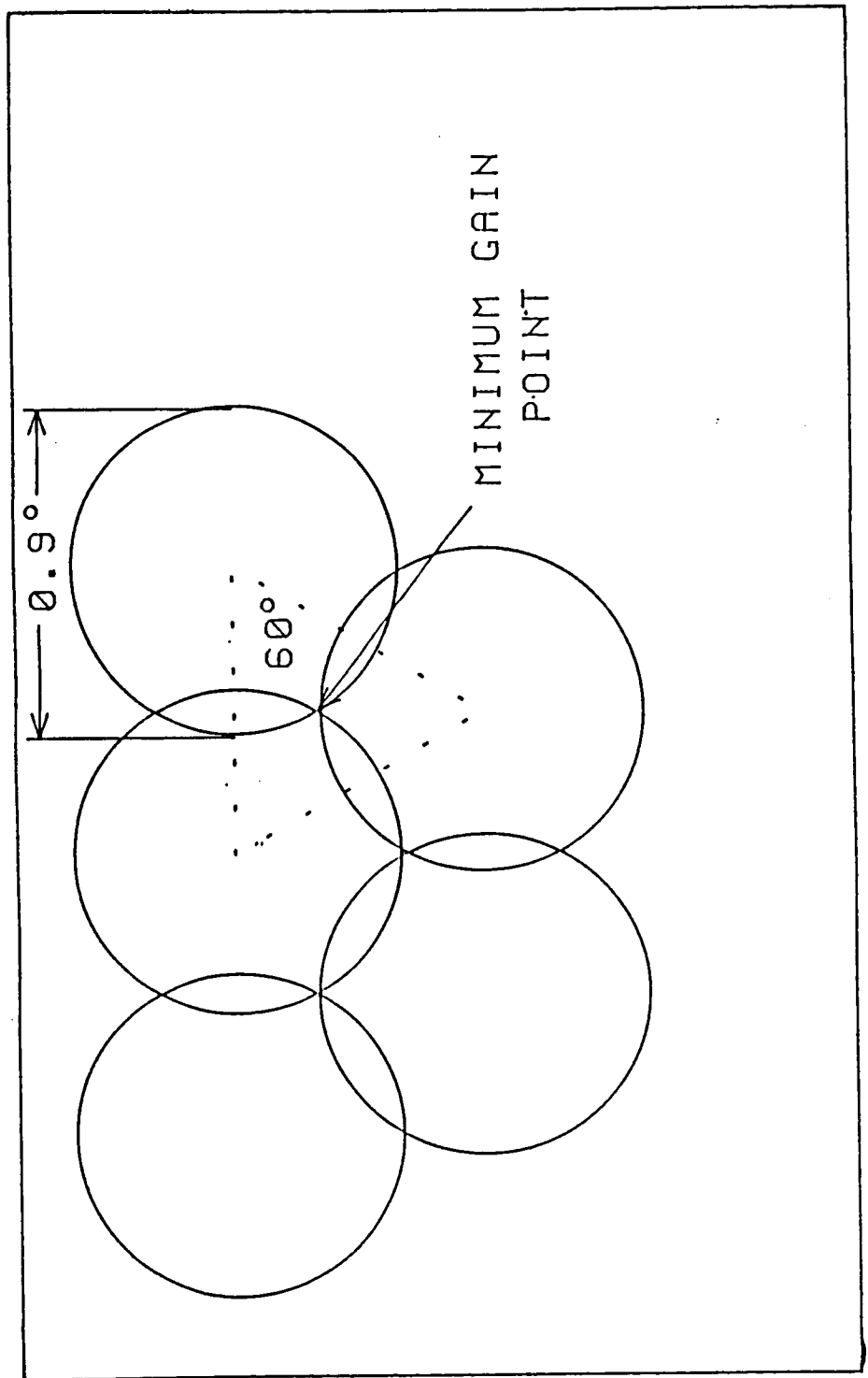
the coverage area occurs at points equidistant from three adjacent beam peaks. The beam-to-beam spacing is $\sqrt{3} \times 0.45° = 0.78°$. A total of about 60 beams is required to cover the 7° x 3° area spanned by CONUS. A representative 42-beam configuration is shown in Figure 4-8.

To maximize the gain of the MBA and minimize feed spillover losses, four MBAs producing an interlaced set of beams are used. Each MBA produces beams arranged in a hexagonal lattice, but with beam-to-beam spacing equal to $2 \times 0.78° = 1.56°$. This permits the feed horns for each MBA to be spaced farther apart then would be the case if a single MBA were used. The greater spacing between feed horns permits use of larger-aperture feed horns, thereby minimizing spillover losses. This results in approximately 3-dB greater gain than could be obtained with a single MBA.

The gain of an MBA beam can be expressed as

$$G_m = \eta(\pi D/\lambda)^2 [8(J_2(u)/u^2)]^2 \qquad (4\text{-}28)$$

where D is the MBA lens diameter, η is approximately 0.6, and

$$u = (\pi D/\lambda)\sin\theta \qquad (4\text{-}29)$$

The angle θ is measured from the beam peak to the observation point.

The lens diameter, D, is chosen to maximize the gain at the edge of

Figure 4-8. Beam Interlacing with Four-aperture Antenna System
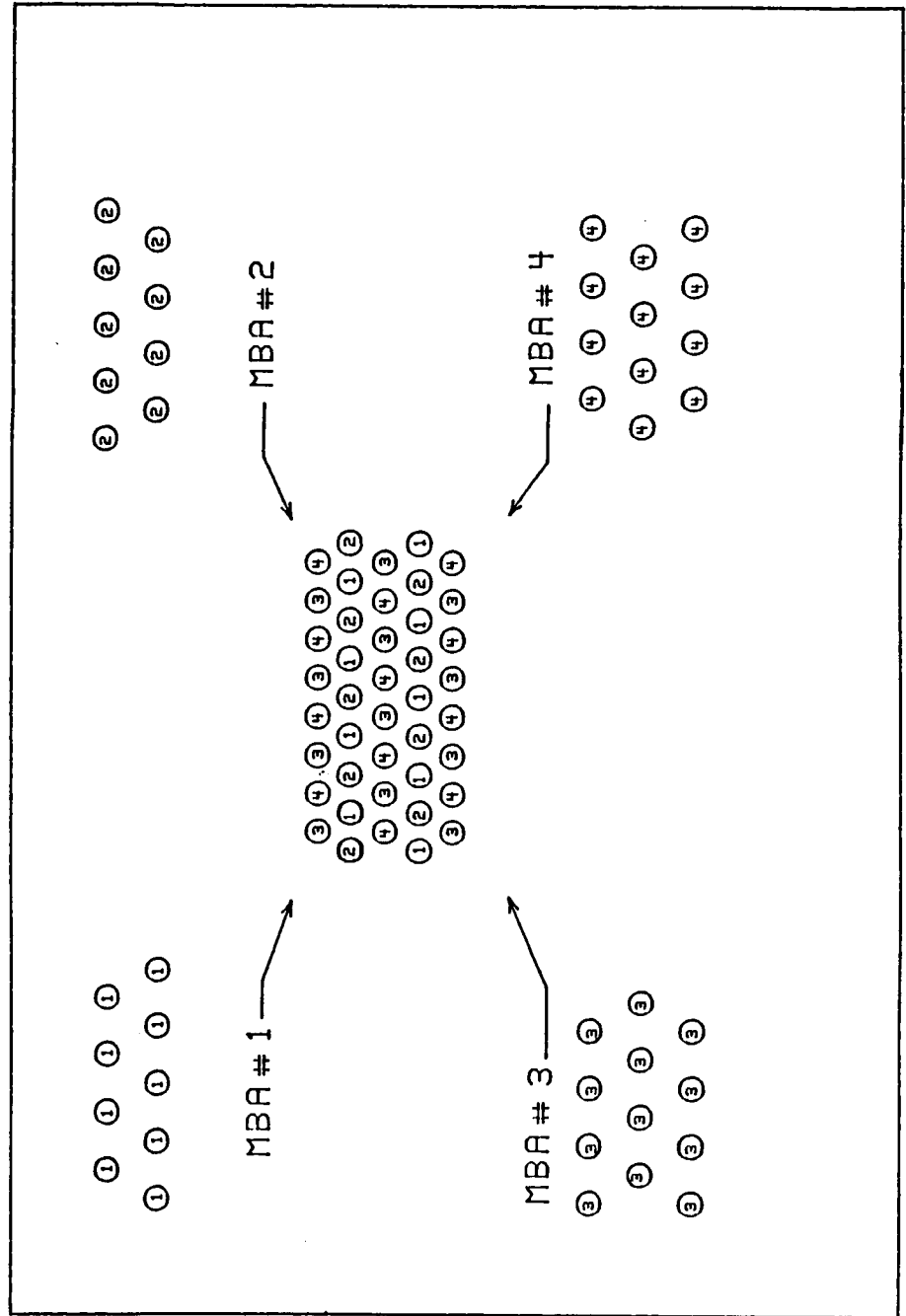
the beam coverage area (i.e., θ = 0.45°). As with the previously discussed antennas, the 4.3-dB beamwidth is 0.9°. The lens diameter is then determined by taking the ratio of the gain at the beam peak to the gain at θ = 0.45°:

$$10 \log [G_m(0°)/G_m(.45°)] = 10 \log [8(J_2(u_{.45°})/u^2_{.45°})]^{-2}$$
$$= 4.3 \text{ dB} \qquad (4\text{-}30)$$

where $u_{.45°}$ is the value of u at θ = 0.45°. Solving this equation for $u_{.45°}$ results in

$$u_{.45°} = (\pi D/\lambda)\sin (.45°) = 2.36 \qquad (4\text{-}31)$$

Finally, D is determined to be 56.6 in. and the gain at the edge of the coverage area is 43.0 dBi.

Assuming a loss of 1.5 dB in the RF switch network between the transmitter and the MBA feed horns, a transmitter output power of 100W will produce an EIRP $\geq$ 61.5 dB over a beam coverage area 0.9° in diameter.

Switch Network. The switching design considered for use both in the MBA beam-selection circuits and the TWTA 8x4 redundancy switch is a ferrite circulator switch configuration. This type of switch has been space-qualified for satellite applications in the 20-GHz downlink band. These switches have demonstrated low insertion loss and the ability to handle relatively high (~100W) levels of RF power. The switching speed

depends on the amplitude of the voltage pulse applied to the circulator's ferrite-core drive wire within the switch. For a given ferrite switch, doubling the applied voltage will approximately halve the switching time. Other parameters governing switch speed are the coercive force, hysteresis properties, and the mass of the ferrite used in the switch.

A switch operating in the 20-GHz band requires about 7.54 μjoule for switching. To switch in 100 ns, a 75-volt drive pulse is required. The switch driver that produces this pulse can be expected to operate at about 15-percent efficiency, so the switching energy required is about 50 μjoule per switch per switching event. Thus a single switch, switching at 20K events/sec, requires about one watt of driver power.

The 8x4 redundancy switch shown in Figure 4-6 requires 52 ferrite switches, with a maximum of 5 switches in series between any TWTA and the input to any MBA beam-selection switch network. The beam selection networks require a total of 38 switches, with a maximum of 4 switches in series between the input and any MBA feed horn. With 0.1 dB insertion loss per switch, and assuming 0.5 dB for the net loss of the interconnecting waveguide, the total switch network loss is 1.4 dB, as previously suggested.

Although the total number of switches required is 94, it can be asasumed that the switches making up the 8x4 redundancy switch are rarely, if ever, switched. In addition, to switch beams in the beam-selection networks, a maximum of four switches in any network

need be switched. A four-beam system will therefore require that no more than 16, and usually only about eight, switches be switched to shift all four beams. Thus, the maximum beam switching power for shifting four beams at a 20K/sec switching rate is about 16W.

4.4. Comparison of Antenna Configurations

To achieve a specified performance level, the active-aperture phased array and the array-fed dual reflector antenna require a similar number of radiating elements. The former has the advantage of not suffering scan loss. It also has better polarization purity in a dual-polarized system. However, the direct-radiating array has a linear dimension that is larger than the array dimension in a dual-reflector system by nearly the magnification factor, M. Typically, M=3. Thus, the dual-reflector system has the advantage of more convenient array packaging and perhaps more conventional deployment. The two systems have comparable weight and power requirements.

The MBA, on the other hand, requires considerably less power than either of the other two configurations, because of the higher efficiency of TWTAs as compared with SSPAs. It is estimated that this power ratio is in the range of 50 to 60 percent. Aside from the need to develop a 100W TWTA at 20 GHz, however, the MBA approach suffers from the vulnerability of the system to TWTA or beam-switching network failures. While TWTA redundancy can ameliorate this vulnerability, reliable data on TWTA lifetime is difficult to obtain. By comparison, both phased-array approaches can tolerate a number of SSPA failures before system

performance is noticeably affected. This graceful degradation greatly enchances the attractiveness of the phased array configurations.

The MBA configuration also suffers from an *a priori* partitioning of geographic coverage, as illustrated by the feed-horn assignments in Figure 4-8. If the traffic should not divide evenly among the four composite geographic areas, saturation of a single downlink beam would lead to degraded service at a total throughput which is less than the nominal satellite capacity.

Because of the large number of elements involved, realization of either phased array configuration at reasonable cost depends on advances in monolithic microwave integrated circuit (MMIC) technology. The desirable degree of integration (e.g., combined vs. separate modules for each phase-shifter/amplifier pair) remains to be determined.

5. BULK DEMODULATOR TECHNOLOGY

The bulk demodulator units provide FDM/PSK-to-TDM digital conversion and measure both signal amplitude and phase on over 100 individual tone slots. The signal phase is differentially detected to form the user data stream, while the signal amplitude is used during acquisition for timing alignment. Both analog (SAW) and digital (FFT) bulk demodulator techniques are examined, together with digital data detection and post processing requirements.

Uplink symbol transitions for each FDM/PSK channel are synchronized to the onboard bulk demodulator timing. This allows a factor-of-3 reduction in the number of Fourier transforms required and eliminates the need for data interpolation. If the terminals were allowed to be nonsynchronous with the demodulators, many of the symbol start/stop times would overlap transform boundaries and cause intersymbol interference, as well as a loss in detected energy due to a time mismatch in the detection filter. This time synchronization requirement is much less stringent than for TDMA systems such as ACTS, where the terminals must meet 25-ns accuracy. The accuracy requirement for the present system is about 1 μs.

Intermodulation and adjacent-channel components are also a concern with the FDM/PSK multiple-carrier format. With the SAW demodulator, sufficient dynamic range must be provided to avoid nonlinear mixing effects. In the FFT, the A/D and arithmetic quantization must be fine enough to ensure accurate reconstruction of the signal, while the range

must be wide enough to ensure that arithmetic overflow does not occur. Since the transmit levels of the terminals in any uplink spot beam will be approximately the same, the dynamic range can be limited to the number of terminals multiplied by the signal-to-noise ratio for a single terminal. With 100 channels and a received E_b/N_0 of 15 dB, the quantization range must be at least 35 dB. This requirement is easily met with an 8- to 10-bit A/D converter.

5.1. SAW Demodulators

One form of FDM/PSK demodulation uses surface acoustic wave (SAW) devices to implement an analog spectrum analyzer known as a chirp Fourier transform. Use of SAW demodulation for spaceborne communications was first investigated by MIT Lincoln Laboratory for the FEP EHF package on FLTSATs 7 and 8. Development of the SAW demodulator at TRW has further refined the technology to meet the additional capability and reliability required for MILSTAR. This effort has demonstrated the ability to manufacture large numbers of these SAW devices, as well as mechanical mounting and digital temperature compensation techniques for both normal and stressed spacecraft environments. The SAW demodulator typically requires from one-third to one-fourth the power required by conventional LSI-based digital FFT processors.

The SAW demodulator examined in this study consists of three basic components: the Fourier transformer, a digital section, and a common LO section (Figure 5-1). In this particular implementation, there are eight Fourier transformer and eight digital sections for each common LO section.

Figure 5-1. SAW Demodulator
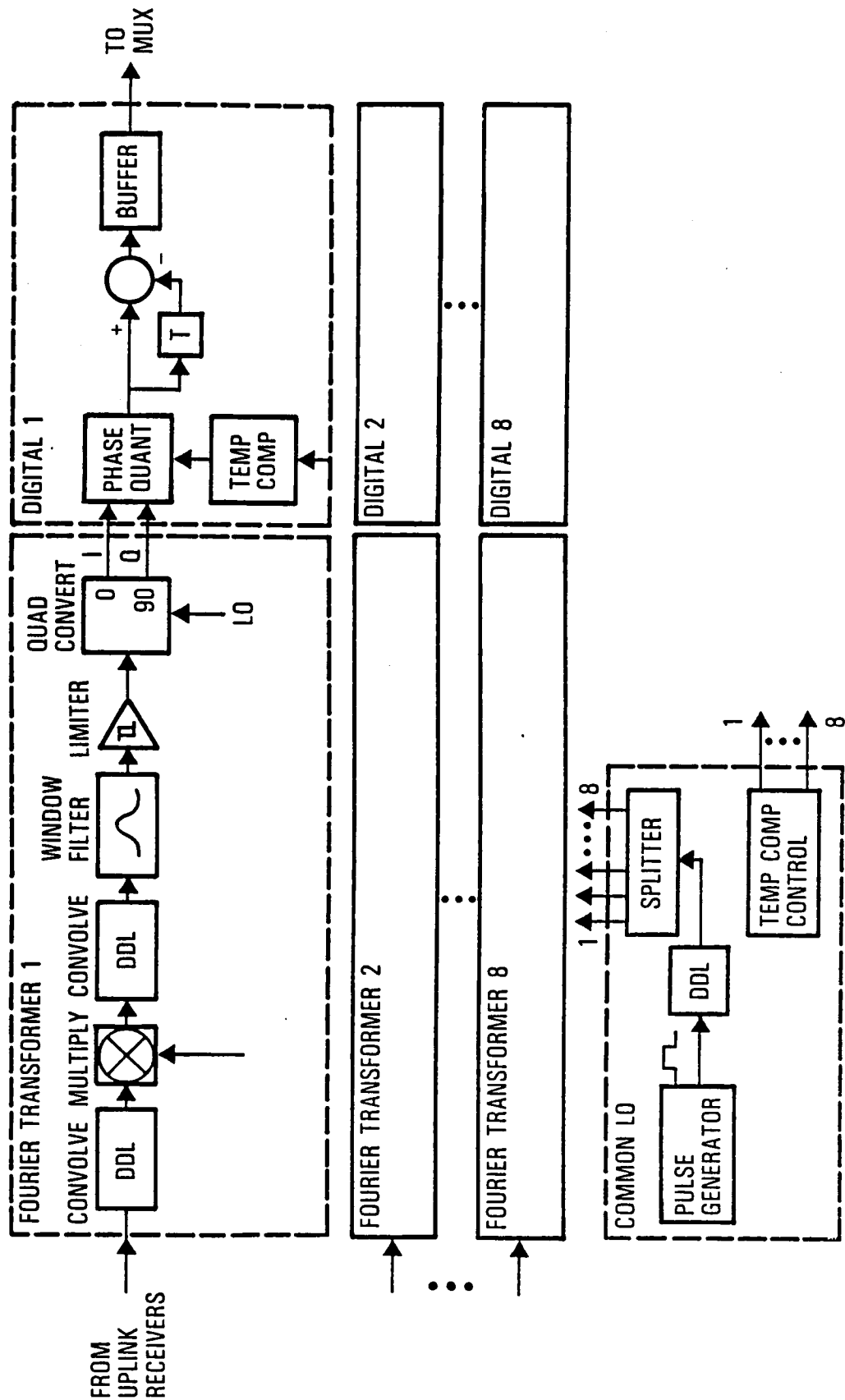
Each demodulator path is responsible for demodulating 100 uplink user channels, while the common LO section supplies a chirp LO and digital timing signals to each path. This LO sharing greatly reduces the overall parts count and power, but still allows for graceful degradation in the event of common LO failure. These components will be described in greater detail in the following sections.

The Fourier transformer can be implemented in two generic forms: convolve-multiply-convolve (CMC) and multiply-convolve-multiply (MCM). These two transforms are mathematical duals of each other and, in theory, produce the same results. The CMC transform, pictured in Figure 5-1, provides additional input filtering and uses a single chirp LO generator, thereby eliminating some of the temperature-controlled timing alignment required in the MCM approach to hold phase stability.

SAW Fourier Transformer. A SAW Fourier transformer block diagram is shown in Figure 5-2. The Fourier transform sections use devices known as reflective array compressors (RAC), shown in Figure 5-3, to implement dispersive time delay functions. The dispersive delays cause low frequencies in their bandwidths to be delayed longer than high-frequency signals. Through use of RAC devices, linear FM chirps can be compressed to a single pulse.

The Fourier transform section first passes the input signals through a dispersive delay to offset their time positions and then mixes them with a linear FM chirp from the common LO section. The mixing is done in a bilinear mixer, which is implemented as a high-frequency analog

Figure 5-2. Compressive Receiver Block Diagram
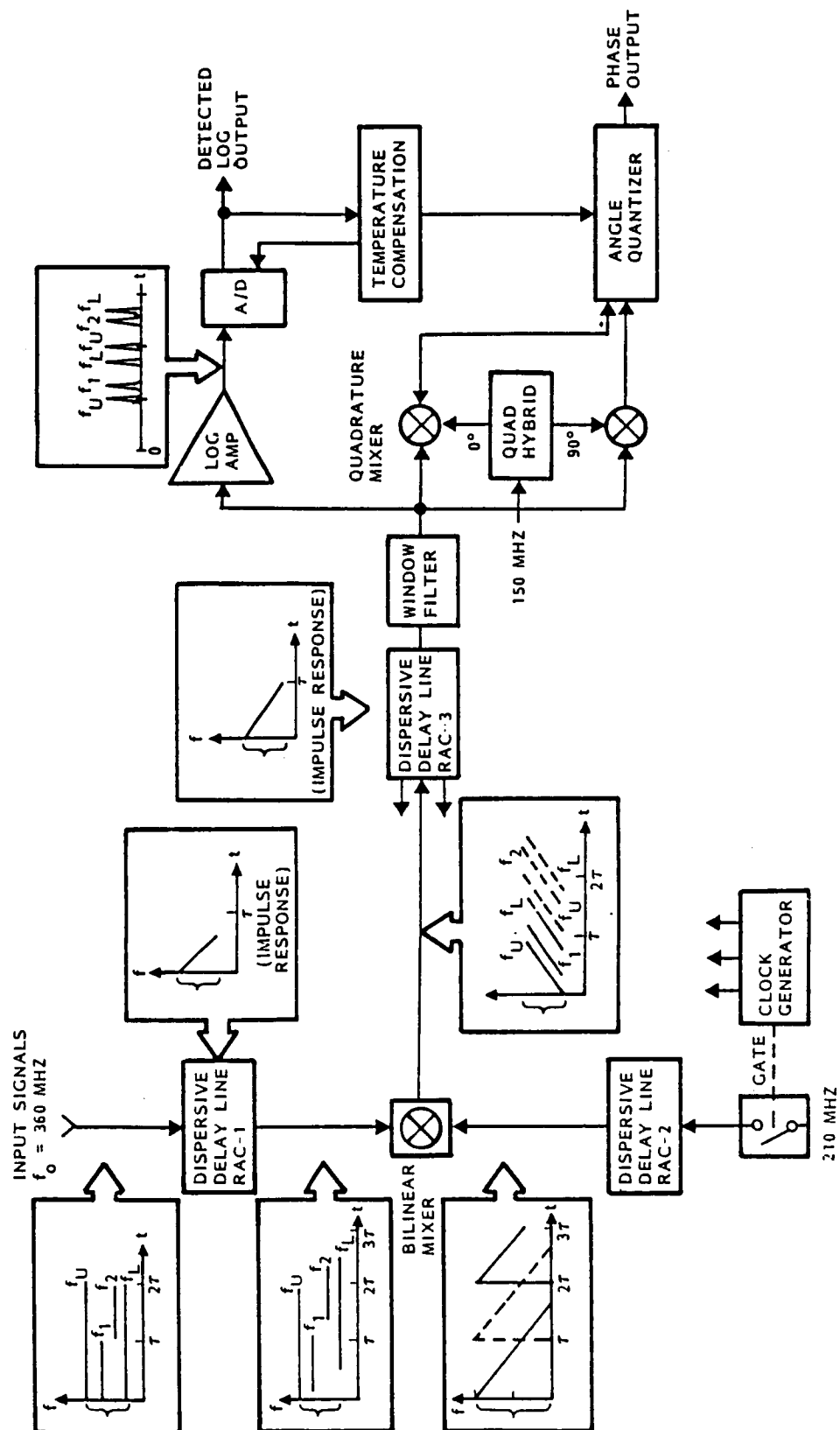
Figure 5-3. Reflexive Array Compressor (RAC) Operation
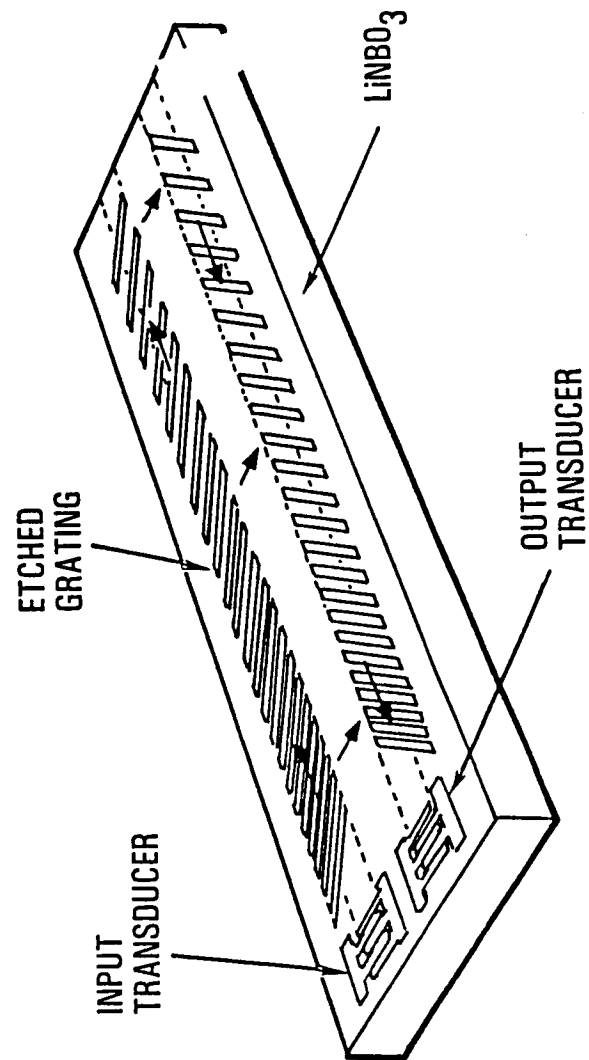
multiplier to avoid intermodulation products. The result is a series of FM chirps, one for each input signal, which cover the same sweep range but overlap in time. Another RAC device, used as a chirp compressor, converts these time-overlapped chirps into discrete time pulses, each corresponding to a different input signal. The amplitude of each pulse envelope and the phase of the carrier under the envelope depend on the input signal amplitude and phase. The time position of each pulse is proportional to the input signal frequency. Figure 5-4 shows the accuracy of the reconstructed signal phase.

The output pulses from the Fourier transform section are routed to the digital section through a SAW bandpass windowing filter. Since the SAW demodulator is a true Fourier transformer, input frequency is translated to output time, and input time is translated to output frequency. In particular, input-time offsets due to terminal timing misalignment result in changes in carrier frequency under the pulse envelope. Providing a filter characteristic in the frequency domain at the output of the SAW Fourier transformer is equivalent, therefore, to time windowing at the demodulator input. Windowing is desirable for reduction of sidelobes caused by close adjacent-channel spacing.

The windowed pulses are passed through a limiter and a quadrature phase detector. This removes any amplitude variations and produces inphase and quadrature phase components which can be sampled and processed by the subsequent digital circuitry. In addition, a linear power detector is used to extract a measure of signal power for use in terminal acquisition and temperature compensation.

Figure 5-4. High Degree of Correlation Between Model and Hardware

ACTUAL COMPRESSED PULSE

COMPUTER SIMULATION

20 nsec/DIV
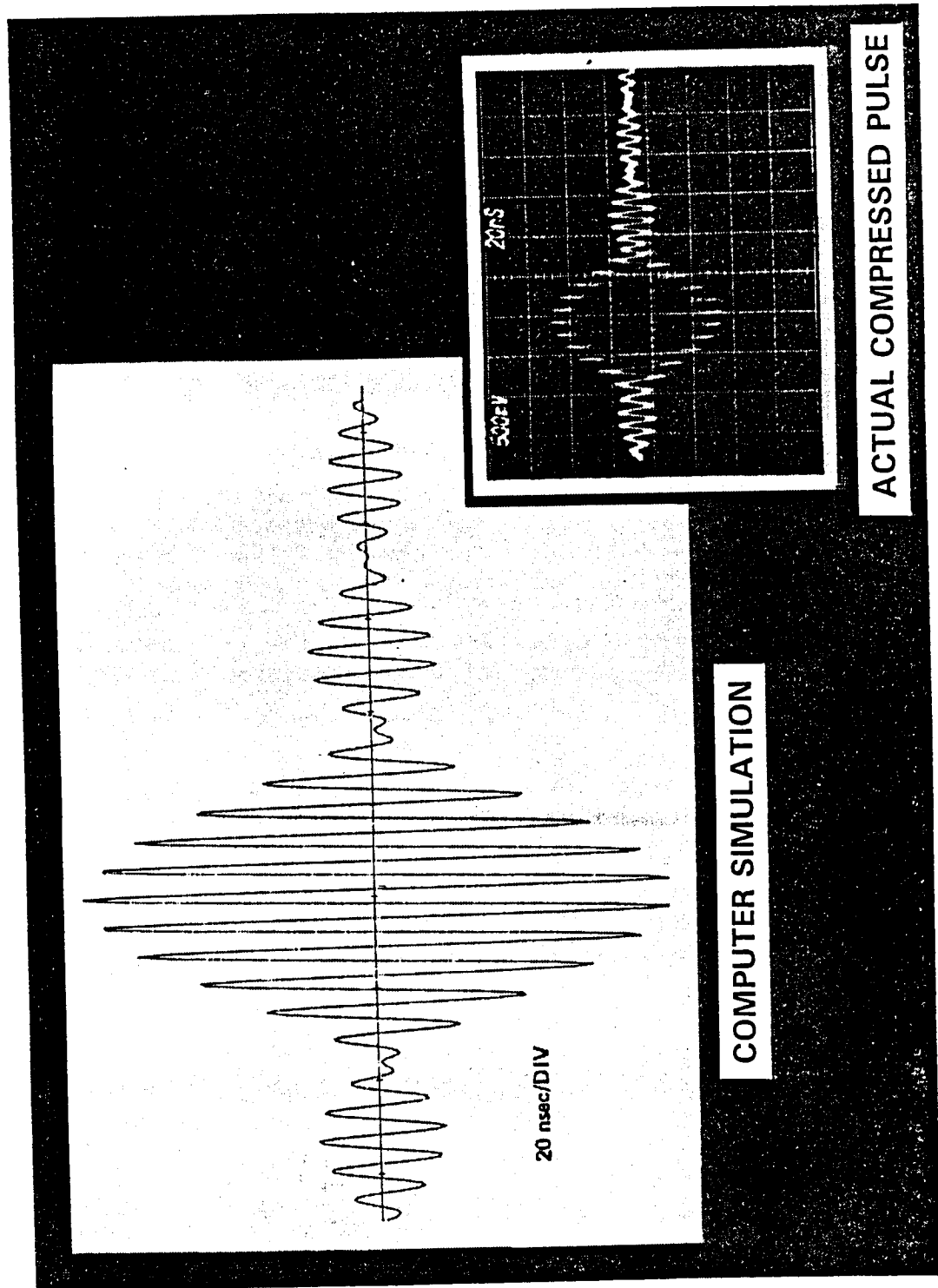
SAW Common LO. The common LO section provides the linear FM chirp signal to each of the Fourier transform sections. The chirps are generated by RAC devices which are sourced by an RF pulse generator. The pulses, which consist of a few cycles of a high frequency LO (typically 200 MHz), can be thought of as wideband (sin x)/x shaped bursts in the frequency domain, with the sinc center at the LO frequency. The RAC devices delay the low-frequency components of this signal by a greater amount than the high-frequency components. This results in a chirp signal that shifts from high to low frequency for each pulse input. The time positions of the input signals at the Fourier transform mixer requires the generation of chirps at a rate of one per input symbol and with a duration of almost two symbols. This means that there are, in general, two different chirps simultaneously present at the output of the chirp generator. The existence of two chirps in the mixer LO port is the driving factor in the selection of a bilinear mixer. Use of a conventional double-balanced RF mixer would result in intolerably large intermodulation products.

Also located in the common LO section are the calibration tones and the temperature compensation loop controller, which are used in correcting demodulator temperature variations. The controller can be shared among the eight Fourier transform sections and is described further in the digital section.

Digital Section. The digital section input consists of a phase quantizer, which performs quantizations based on a ratiometric comparison of the I and Q inputs, and a sample/hold amplifier followed by a low-speed, high-accuracy A/D converter, which can quantize the power

detector output for selected channels. The clock signals for the quantizers are generated by a digital temperature tracking loop.

Temperature compensation is necessary in SAW demodulators because the surface wave propagation velocity in the RAC devices changes as a function of temperature. This causes the output pulses to vary position in an accordian-like fashion, getting closer together or farther apart. Careful design of the SAW demodulator transform relationships ensures that this variation never causes one transformed time output to overlap another.

Accurate sampling of a particular set of frequencies, however, requires a tracking loop that follows any changes in output time position and corrects the quantizer sampling frequency and phase accordingly. The tracking loop required in this application is quite similar to the loop developed for MILSTAR. Calibration tones are injected by the common LO section into each Fourier transformer, one at a time. The calibration tone frequencies are well outside the portion of the input bandwidth used for communications and are injected at the bilinear mixer. This produces an output pulse that provides a reference time position for the band. Switching between the lower and upper band edges allows the temperature compensation loop to track the time-offset and scale-factor variations caused by temperature. A numerically controlled oscillator (NCO) in each digital section provides a sampling which can be adjusted in both phase and frequency to match that demodulator's characteristics.

The remainder of the digital section is devoted to data detection.

QPSK data detection is performed by subtracting the phase measurements of two adjacent symbols and comparing the result to one of four possible 90-degree phase shifts. The closest match is selected as the received symbol and is passed to the downlink multiplexer. This differential detection scheme provides carrier frequency independence at the expense of a doubling in BER. The resulting simplification in the terminal and satellite hardware is considerable since no carrier phase coherence is required.

SAW Bulk Demodulator Technology. SAW demodulators are currently being manufactured for the MILSTAR program. These units have a slightly different LO sparing arrangement, but use the same technologies. Technologies developed at this point include: SAW RAC devices and mounting techniques for 6-inch crystals, wideband bilinear mixers, SAW window filters, log amplifiers, and a high-speed phase quantizer. The temperature compensation hardware uses custom integrated circuits for implementing the digital tracking loop and control functions.

Most of this technology is usable in its present form. However, new RAC devices are required for a different application. In addition, a new temperature control IC and microprocessor control algorithm are required. Total power consumption for a current-generation unit is about 15W per demodulation path, or 1500W for 100 demodulators. Significant reductions in RF power required for the SAWs and the bilinear mixer are not expected, but further reductions in sampler and control hardware power may reduce the power per demodulator to 10W. The weight per demodulator is estimated to be 5 lb.

5.2. FFT Demodulators

The FFT is an efficient implementation of the discrete Fourier transform (DFT) in cases where a large number of orthogonally spaced channels must be separated. The FFT is an all-digital implementation and thus can be much lower in manufacturing cost than SAW techniques. In addition, immunity to temperature and aging effects make the FFT desirable if low-power operation can be obtained. In this case, a 128-point FFT with 2:1 presumming is used to separate 100 channels at approximately 100-kHz spacing. The remaining 28 transform slots fall into the roll-off of the input filter, which is used to prevent aliased components of other channels from entering the desired 100-channel group.

An N-point FFT requires $(N/2) \log_2 N$ complex multiplications. For a 128-point FFT, this results in 448 complex multiplications. Since the baud rate is roughly 50 kHz, with one FFT required per baud, the computational requirement is 22.4 million complex operations per second (22.4 MCOPS). Two different architectures can be used to perform these operations, a recursive FFT and a pipelined FFT.

Recursive FFT. The recursive FFT, as its name implies, performs FFTs using a single arithmetic element by recursively performing the algorithm. Since the FFT algorithm is regular in structure, it can be separated into $\log_2 N$ passes of length N/2. An example of a chip set which currently implements such a recursive FFT is the VHSIC Phase 1 FFT chip set, shown in Figure 5-5. This TRW-developed chip set, which performs FFTs of

C-2

variable length at rates up to 8.2 MCOPS, consists of a arithmetic unit, a control unit, and several four-port memories. By the previously determined sizing, three such sets would be required to perform the transform in the required time. Actually, introduction of presumming and trigonometric recombination functions (described later) make the need for a fourth chip set probable.

Two members of the chip set have completed fabrication and initial test. Current estimates are that the complete set will be available in 1987 and will consume approximately 2.5W of power. The total power requirement for just the FFT portion is thus about 10W. Addition of the A/D converter, buffering and control circuitry puts the total power at approximately 12.5W.

Current-generation VHSIC Phase 1 FFT chips are radiation hardened only to about 10^4 rad/Si, which is insufficient for most geosynchronous requirements. Future generations of these chips, built in the radiation hardened 2-μm CMOS process used for MILSTAR, should have radiation hardening to 3×10^5 rad/Si and should also require less power. The projected total power requirement for a CMOS recursive FFT design is about 9.5 W. The corresponding weight is estimated to be 3.5 lb.

Pipelined FFT. The pipelined FFT performs the same algorithm as the recursive FFT, but it uses a cascade of high-speed stages to perform successive passes of the algorithm in separate arithmetic units. This procedure allows the input of the FFT to operate synchronously with

Figure 5-5. Recursive FFT Using VHSIC I Chips
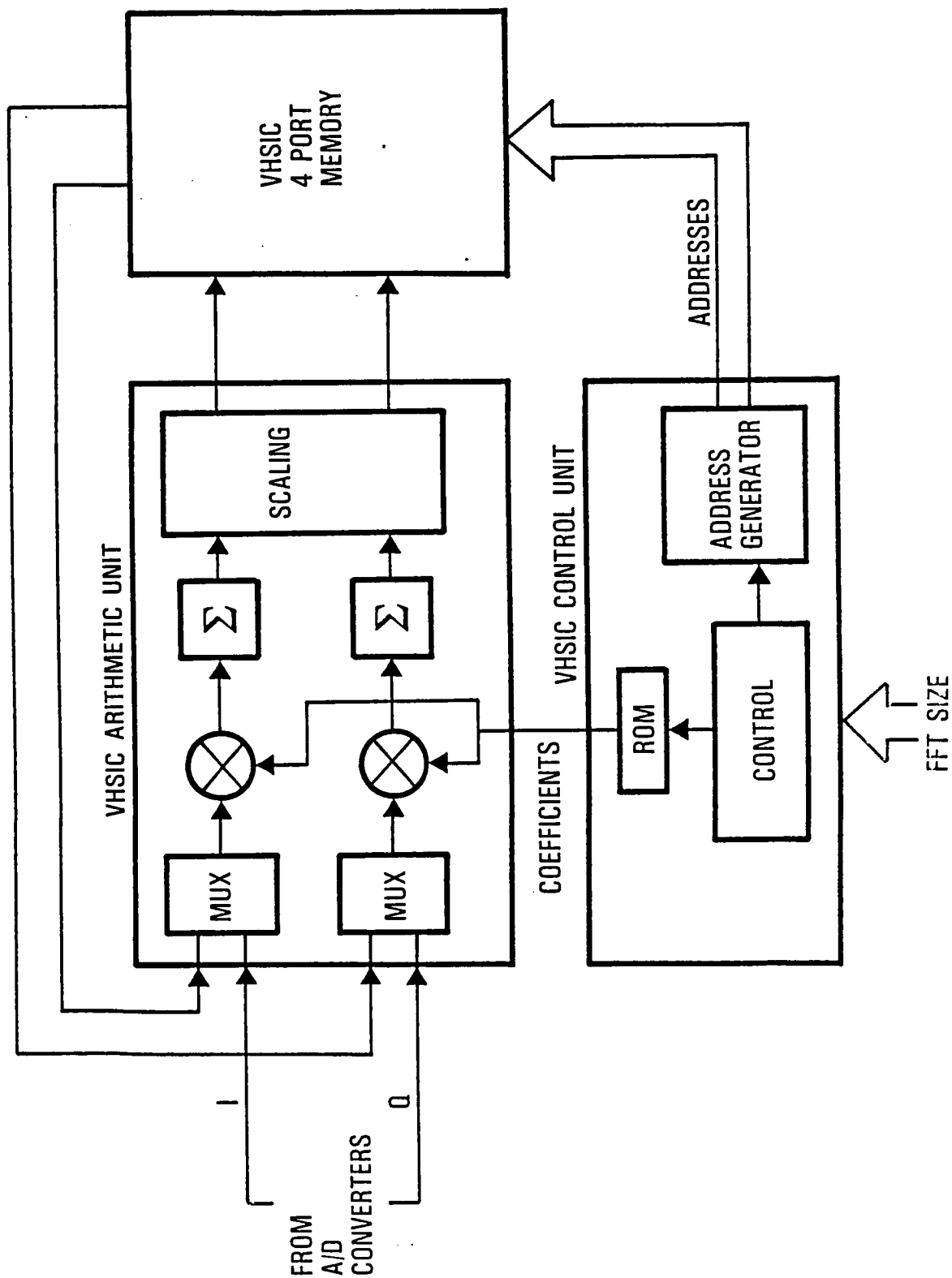
the A/D sampling, thereby eliminating multirate clock difficulties often encountered in recursive algorithms. In addition, the parallel (rather than serial) processing eliminates the need to switch between processors at each baud.

Figure 5-6 shows the architecture of a pipelined FFT developed at TRW. The architecture is based on a complex multiplier, a radix-8 DFT element, and a 64-sample intermediate memory. Each set of these components can perform the equivalent of 15 MCOPS. Three sets are required to perform the necessary calculations for a radix-128 FFT (radix-8 x radix-8 x radix-2). These three sets can readily perform the 22.4 MCOPS previously established as the FFT requirement. These chips require approximately 1.8W per set. They are currently manufactured in the 2-μm CMOS process, with some amount of additional processing needed to produce radiation hardened devices. Total power for a pipeline design is about 8.5W. Each unit weighs about 3.2 lb.

Real vs. Complex Sampling. Another issue for FFT-based demodulators is the question of real versus complex sampling. In most textbooks, FFTs are shown with complex input samples and complex results. This arrangement eases understanding of the algorithms, but it often is not practical to implement. For the present application, which involves spectrum analysis, a high degree of phase and amplitude matching between the quadrature input samples is required to eliminate introduction of in-band aliasing.

As depicted in Figure 5-7, the complex-sample FFT relies on accurate

Figure 5-6.   Pipelined FFT Block Diagram
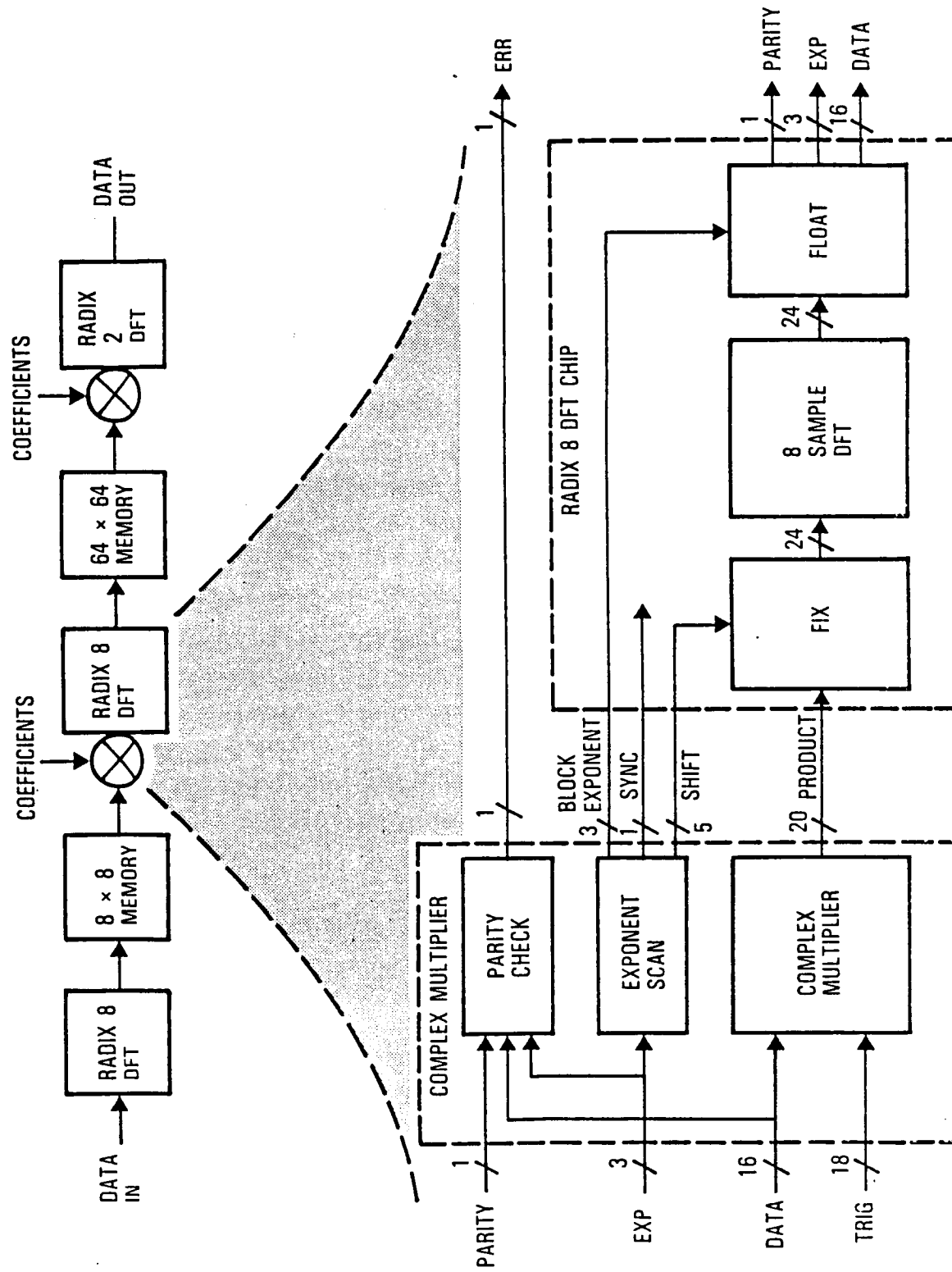
Figure 5-7. Image Signals Due to Phase and Amplitude Mismatch
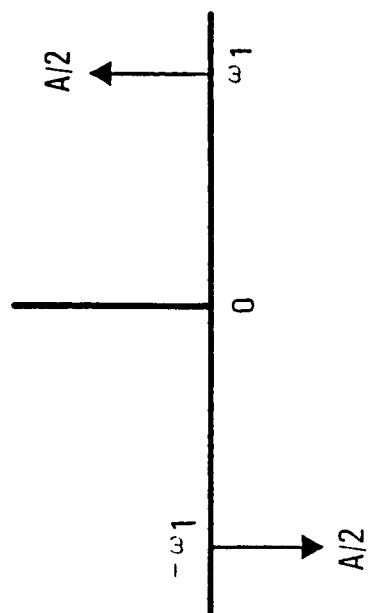
IMAGE DUE TO IMPERFECT CANCELLATION

IN-PHASE COMPONENT

QUADRATURE COMPONENT
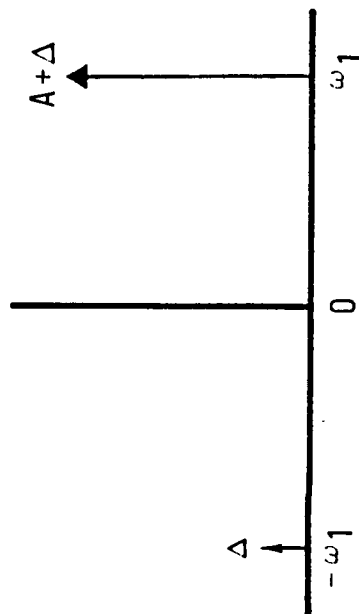
cancellation of image frequency components. If the quadrature downconversion process is unbalanced, these image components leak through. This effect is especially degrading where the dynamic range between users is high, since the image of a strong user can completely mask a smaller user signal. A plot of image strength versus phase and amplitude offset is shown in Figure 5-8. In this case, accuracies of better than 0.5 dB and 2 degrees are required for adequate performance. These tolerances , which are extremely difficult to maintain over temperature and satellite aging, result in high design, component and assembly costs.

One technique for eliminating the effect of quadrature sampling imbalance is to use real sampling. This requires that the input be downconverted to a (low) frequency offset from baseband. The input is then sampled by a single A/D converter operating at a rate equal to twice the input bandwidth. Although the A/D speed is twice that of the complex-sample case, only one converter is required. In addition, since there is only one path, there is no concern for amplitude or phase matching with this design.

Real sampling requires that input samples be fed only to the real-component input of the FFT. With the same number of samples per baud as complex sampling (half the number of samplers at twice the rate), real sampling normally requires an FFT which is twice the size used for complex sampling. In the present case, a 256-point FFT would be required. This is feasible with both implementation approaches, but requires additional hardware in the recursive design. The pipeline design shown has sufficient speed capability to handle a 256-point FFT with the same

Figure 5-8. Effect of Amplitude and Phase Mismatch
on Signal-to-Image Ratio (SIR)
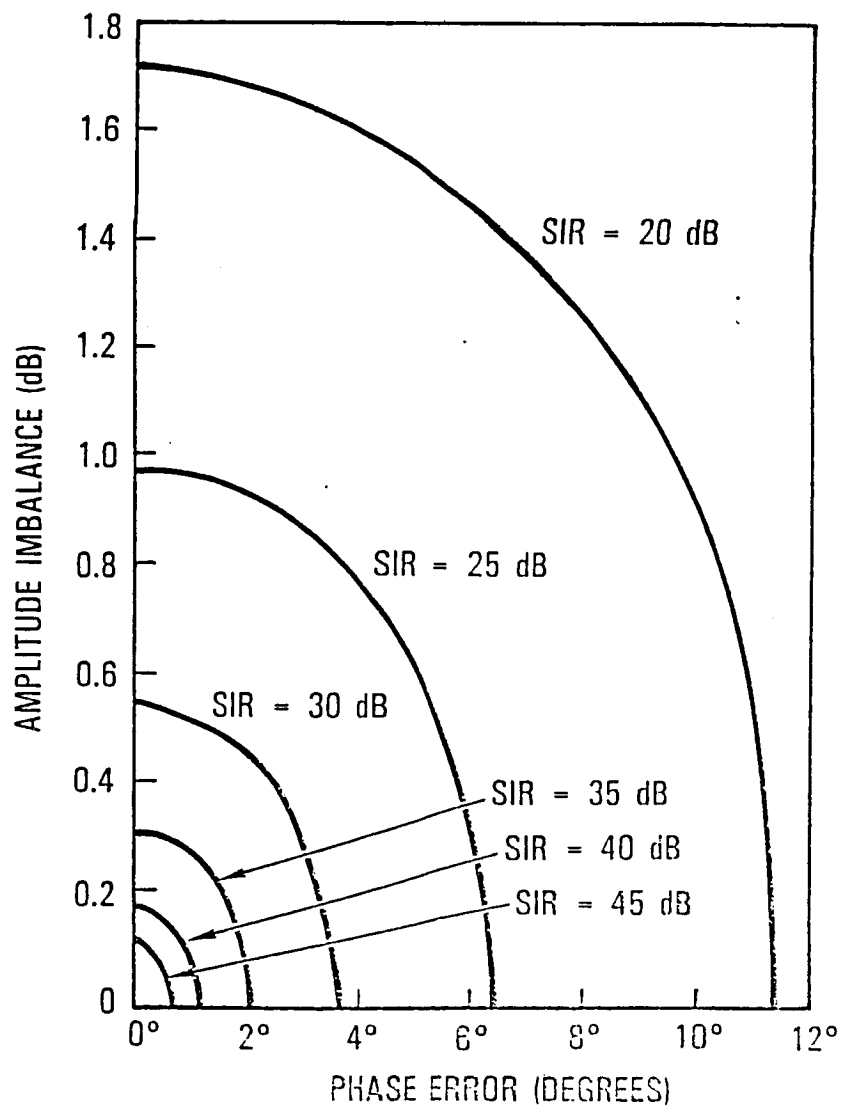
hardware. The memory size must be increased, however, to accommodate the larger number of transform points.

To avoid a factor-of-two growth in the recursive FFT architecture, a technique called the trigonometric recombination algorithm was developed. This algorithm allows every other sample of a real-sample input to be placed in the I and Q inputs of the FFT. The in-phase and quadrature components are transformed and, because of their orthogonal input relationship, can be recovered at the output. An additional algorithmic pass is required to combine image frequency components to produce the desired result. Besides slowing the input rate seen by the FFT by a factor of two, this procedure allows the computations (and thus the hardware) required to be reduced by a factor of two as well. The total computational effort is approximately 14 percent greater than that associated with a complex-input FFT.

Presumming. Since the FFT provides output samples at orthogonal spacing (in this case about 50 kHz), while bi-orthogonal carrier spacing (100 kHz) is used on the uplink, there are twice as many output values as needed. This computational inefficiency can be reduced through a process known as presumming. Figure 5-9 shows an 8-point FFT example.

If only the even-numbered channels are required at the output, approximately one-half the computations can be eliminated by performing only the additions (multiplication by W_0) in the first FFT pass and then implementing a 4-point FFT for the remaining passes. In the present case, only 128 of 256 orthogonal positions are needed. Instead of implementing

Figure 5-9. Presumming Calculations
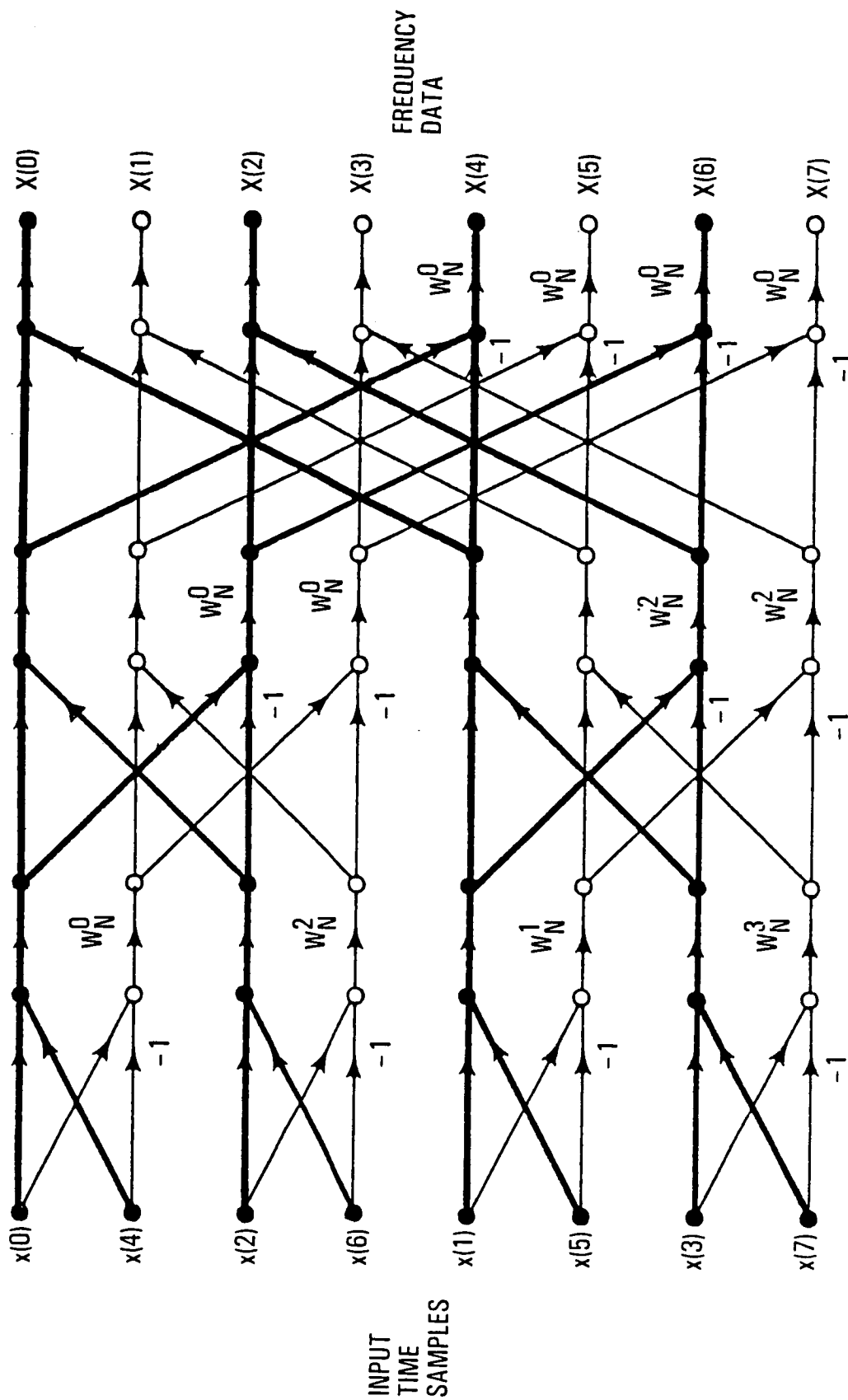
a 256-point transform, a 128-point transform with 2:1 presumming is performed.

The presumming consists of storing the first ·128 sample points (complex) and then adding them one-by-one to the remaining 128 sample points. This produces the 128 complex points which are the even components of the first pass of a 256-point transform. A 128-point FFT is then performed to yield the required results. This technique is mathematically identical to the 256-point FFT and can be used to reduce both the effective input sample rate and the FFT size required.

5.3. Conclusions

In terms of current technology, the SAW demodulator represents the only technique which is both radiation hardened and currently undergoing space qualification. Compared to current qualified discrete LSI techniques, the SAW demodulator holds a favorable position for wideband, low-power Fourier transforms. However, evolution of digital FFT algorithms and LSI processes makes it quite likely that the eventual choice for this application will be an FFT. Insensitivity to temperature effects, constant high precision, lower power and reduced manufacturing costs make FFTs an attractive alternative to SAW demodulators for future applications.

6. BASEBAND MULTIPLEXER TECHNOLOGY

The baseband multiplexer is responsible for assigning uplink frequency channels to downlink time slots in a fashion which allows programmable interconnection of terminals and efficient use of both uplink spectrum and downlink data fields. A large number of serial streams (representing the bulk demodulator outputs) must be multiplexed into a small number of high-rate downlink streams with selectable paths corresponding to particular downlink-beam dwells.

The requirements governing the multiplexer implementation trades are summarized in Table 6-1. The number of multiplexer inputs corresponds to the complement of 100 demodulators, each of 10-MHz bandwidth. A nominal 100-kHz channel spacing has been selected for the multiplexer analysis; consequently, there are 100 channels per demodulator. The channel data rate of $4/3 \times 64 = 85.3$ kbps (which includes the effect of rate-3/4 coding) has been rounded up to 100 kbps. Consequently, the multiplexer input data rate is 10 Mbps per demodulator. The corresponding multiplexer throughput is 1 Gbps. (Note that, when rate-3/4 coding is applied to the satellite throughput of 720 Mbps, a coded data rate of 960 Mbps results.)

It is assumed for descriptive purposes that the multiplexer must simultaneously process one quadriphase symbol per channel for each of 10,000 channels. (It was pointed out in Section 2 that multiple symbols

Table 6-1. Typical Multiplexer Requirements

▲ Number of inputs	100
▲ Input data rate (per demodulator)	10 Mbps
▲ Total throughput	1 Gbps
▲ Number of channels per input	100
▲ Number of bits per channel symbol	2
▲ Number of outputs	6
▲ Number of slots per output	1666
▲ Output data rate	166 Mbps
▲ Desired connectivity	Random interconnect

per channel must be processed jointly to limit the scan rate of the downlink beams.) Six downlink beams are assumed for purposes of this analysis. (The baseline system has four downlink beams.) There are therefore 10,000/6 = 1666 time slots per scan for each beam, under the simplifying assumption that the two bits in each quadriphase symbol have a common destination. The output data rate per beam has been rounded up from 166 Mbps to 180 Mbps to account for the effects of overhead and beam-switching intervals.

Three different multiplexing techniques were evaluated. Each was selected based on its particular merits in one or more categories: size, power, interconnection flexibility, and terminal constraints.

6.1. High-Speed Serial Time-Domain Multiplexers

A logical first step in any multiplexer study is to consider the use of standard, serial multiplexing techniques. Because of their serial nature, these multiplexers are often small and easily understood. In this application, however, serial multiplexers are at a disadvantage. The high rate of information flow, 1 Gbps, limits the ability of serial multiplexers by requiring high-speed IC technologies which currently do not support a high degree of integration. In addition, these multiplexers are often best designed for single output applications where significant time rearrangement is not necessary. In this application, not only must signals be switched among several outputs, but they must also be rearranged in time sequence to allow connection of any uplink frequency slot to any downlink dwell.

The speed issue can be ameliorated by using a separate multiplexer for each downlink. This lowers the maximum speed to about 170 Mbps and eliminates many of the elastic buffering requirements which might appear with several downlinks vying for the same multiplexer output. To facilitate time reordering of symbols between bulk demodulator and downlink beam, each demodulator is provided with a 200-bit buffer memory (one quadriphase symbol for each of 100 channels) which is written in a random order and then read sequentially for downlink transmission. The configuration of random write and sequential read (rather than the reverse) is chosen to minimize speed requirements during downlink readout, where successive reads may be spaced by as little as 6 ns. (Interleaving addresses on smaller memories could reduce the speed requirements further, but at the expense of large numbers of extremely small memories.)

With a single 200-bit buffer assigned to each demodulator, the possibility exists that two or more downlinks may require symbols to be read from a common buffer memory for transmission during the same time slot. This memory contention problem can be avoided by providing a separate buffer memory for each demodulator/downlink pair. The most logical configuration would be a set of six addressable shift registers, as shown in Figure 6-1. These could be integrated on the same chip and fabricated in a high-speed bipolar process.

Figure 6-1. Bulk Demodulator and Buffer for Time-Domain Multiplexer
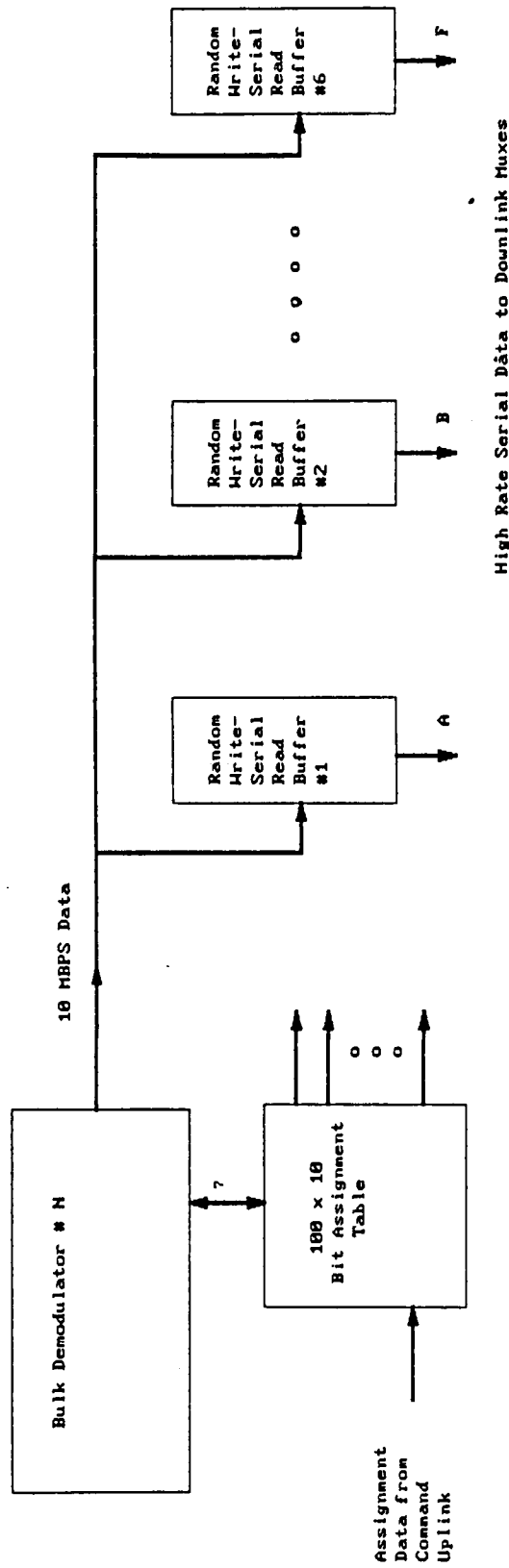
Combining of demodulator outputs can be done in either a serial chip interconnection scheme, shown in Figure 6-2, or a parallel multiplexing scheme, as shown in Figure 6-3. The serial scheme requires fewer interconnections, but requires relay cross-strapping of the serial chain at regular intervals to avoid single-point failures.

6.2. Frequency-Domain Multiplexers

A simple technique for reducing on-board multiplexing requirements is to arrange the uplink frequency slots in a manner that allows simple and efficient direction to the downlink. Reassignment of multiplexed interconnections is performed by reassignment of uplink frequencies and downlink time slots. This results in minimum on-board processing, but it puts some limitations on interconnection flexibility.

Figure 6-4 shows an uplink frequency assignment plan for an approximately 80-MHz segment (one-sixth) of the 500-MHz uplink band. The plan is designed for a satellite system with six independent downlink scanning beams (labeled A through F). This frequency plan is arranged so that each sixth frequency slot is assigned to the same downlink beam. This allows simple uplink spectrum reorganization by downlink beam. It also helps reduce multiplexer speed requirements, since similarly lettered bits from each demodulator can be passed in parallel to a common buffer and converted to serial form for high-rate downlink transmission.

Furthermore, adjacent 80-MHz uplink segments have their A to F downlink beam assignments rotated by one position, thereby ensuring that

Figure 6-2. Time-Domain Multiplexer Serial Interconnection
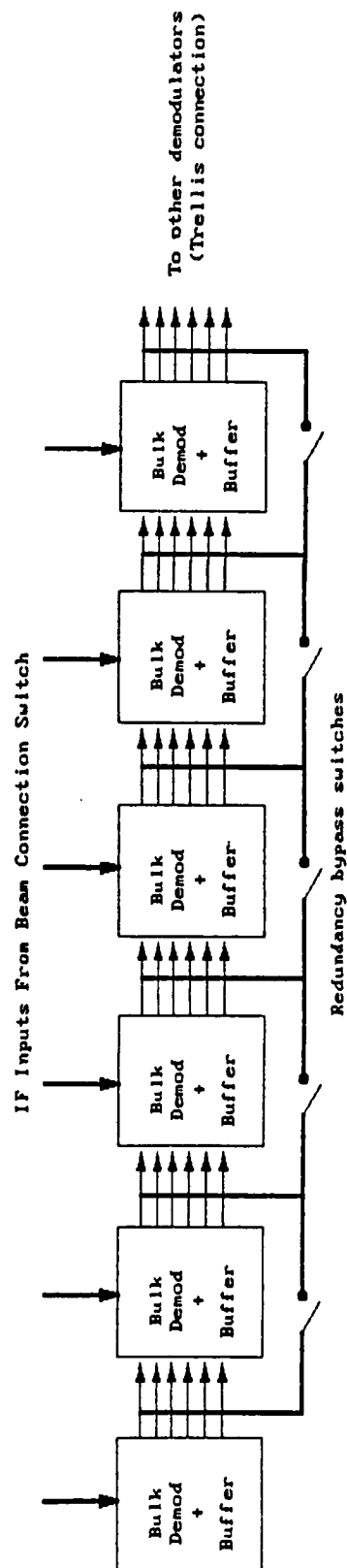
Figure 6-3. Time-Domain Multiplexer Parallel Interconnection
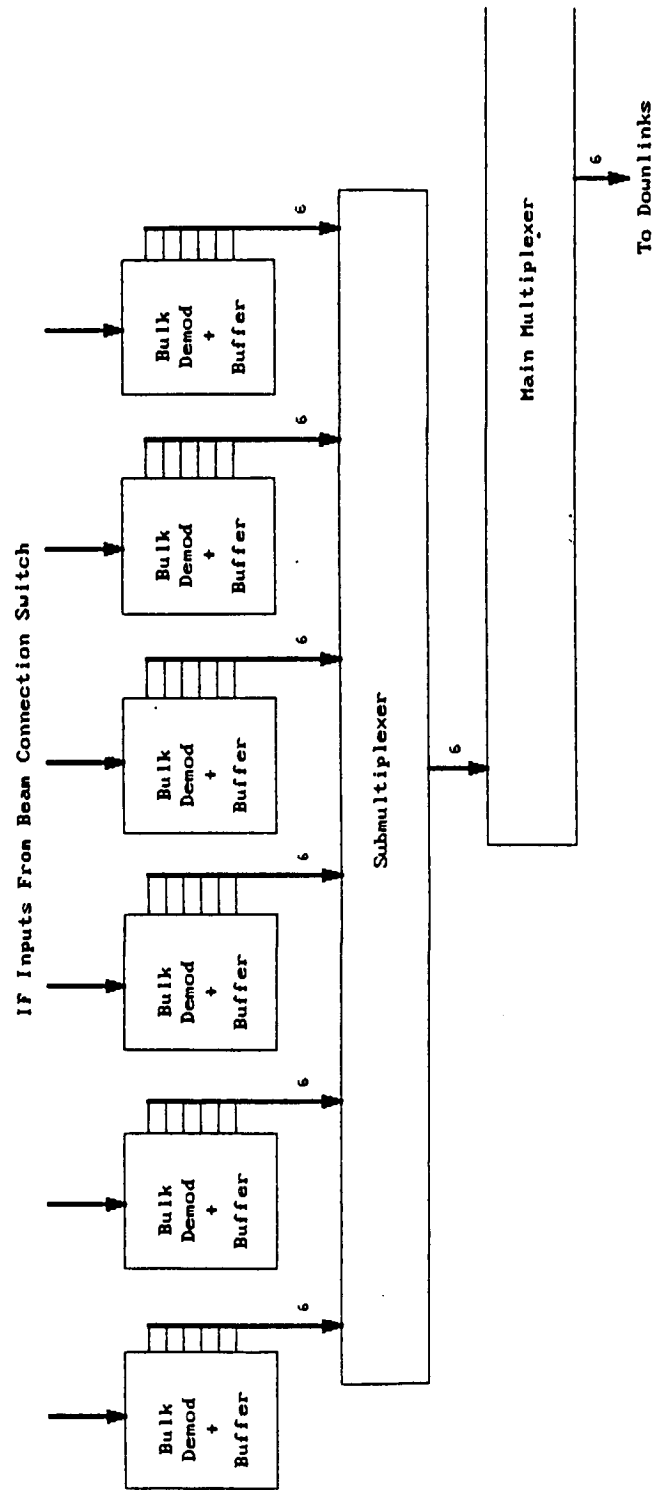
Figure 6-4. Frequency-Domain Multiplexer
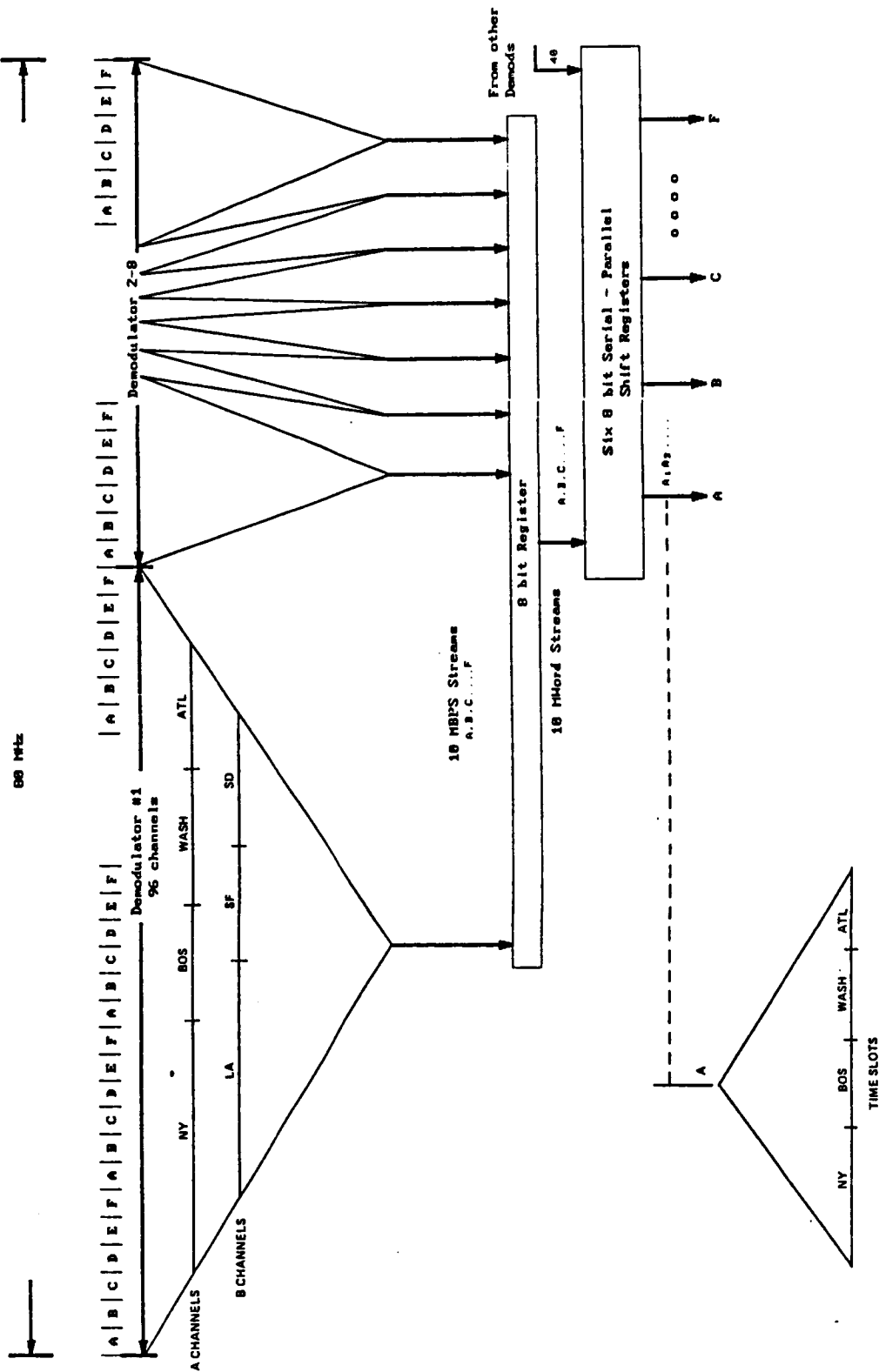
symbols transmitted simultaneously on the six beams are drawn from different 80-MHz segments. A particular downlink beam, say A, is fed data from the lowest 80-MHz segment (on both polarizations) during the first uplink symbol interval. It is fed data from the second segment during the next uplink symbol interval, and so on until all six segments have been read. At this point, the downlink multiplexer returns to the first 80-MHz segment and the sequence is repeated.

Approximately 16 demodulators are read in each position, eight from each uplink polarization. As the A multiplexer moves to the demodulators that correspond to the second 80-MHz segment, the B multiplexer moves to the first 80-MHz segment to receive symbols from the B-designated frequency slots. In this manner, a continuous flow of data is maintained and the word transfer rate does not exceed 10 MHz, allowing CMOS technology to be used for low power consumption.

The description thus far has focused on the association of uplink frequency channels with particular downlink beams. The nature of the traffic matrix supported by such a multiplexing scheme is also illustrated in Figure 6-4. On the uplink, a specific set of demodulators supports each regional beam. One-sixth of the composite capacity of these demodulators is directed at each downlink. Within any frequency subset (corresponding, for example, to letter A), the fractional number of channels allocated to (say) New York-directed traffic must correspond to the percentage of time the downlink beam dwells on New York. This is true for every uplink region.

Whether this constraint on the allocation of satellite capacity significantly decreases the traffic throughput depends largely on the number of uplink regions. The effect on throughput will be relatively small if the number of uplink regions is small. (Note that there are eight uplink regions in the baseline system.) However, if a single metropolitan area (such as New York) dominates a region, the percentage of traffic from that region to the metropolitan area may be significantly less than the percentage of traffic from other regions to that metropolitan area. In this case, the corresponding satellite capacity will be underutilized.

A further shortcoming of this multiplexing scheme is that continuous transmission on some channels may have to be interrupted for short intervals during reallocation of satellite capacity. This is a drawback when compared to a truly random assignment multiplexer, but it is not a severe constraint if only short-duration data/voice connections are required.

6.3. Memory-Based Multiplexers

Memory-based multiplexing techniques are gaining increasing favor because of the tremendous flexibility that they offer (random interconnect). Memory technology is also a rapidly developing area, with increased size, faster speed, and lower-power units being introduced at a quickening pace. Current concerns with spaceborne memory devices center on radiation hardness and single event upset (SEU). Many current CMOS memory devices are showing satisfactory hardness (1E5 rad/Si) for space environments, but they are limited to about 100-ns access times.

SEU-induced bit flips do not represent a significant problem for this application, because they show up as random bit errors which are corrected by the end-to-end coding. SEU latchup remains a critical concern in device selection. Current generation, hardened memories are designed to be latchup-immune through use of dielectric isolation, epitaxial processes, or similar techniques.

Memory-based multiplexers range in size and complexity from simple address-pointer techniques to time-space-time techniques similar to those found in telephone switching systems. The address-pointer technique is shown in Figure 6-5. This is a modification of the serial multiplexing technique. However, in this case each demodulator has a memory which can hold up to 2×10^4 bits of data. This memory capacity represents one data symbol for each downlink-beam/time-slot transmission that takes place during a particular uplink symbol interval. Each demodulator also has a 100 x 14 bit RAM which acts as a map to place each bit from the bulk demodulator in a particular memory position. Broadcast capability can be implemented by placing individual uplink bits into more than one buffer location. The buffer RAMs are then read in 60-bit-wide words which are wire-ORed together in a trellis network to derive six sets of 10-bit words at a 17-MHz rate. These are then serialized for transmission at the downlink rate. The wire-OR function serves to passively multiplex the uplink bits together and can be designed to be single-point error immune. Active selection of necessary bits from the bulk demodulator memories was also considered, but was ruled out based on the high speeds required in the memory read.

Figure 6-5. Address-Pointer Memory-Based Multiplexer (Wire-OR Version)
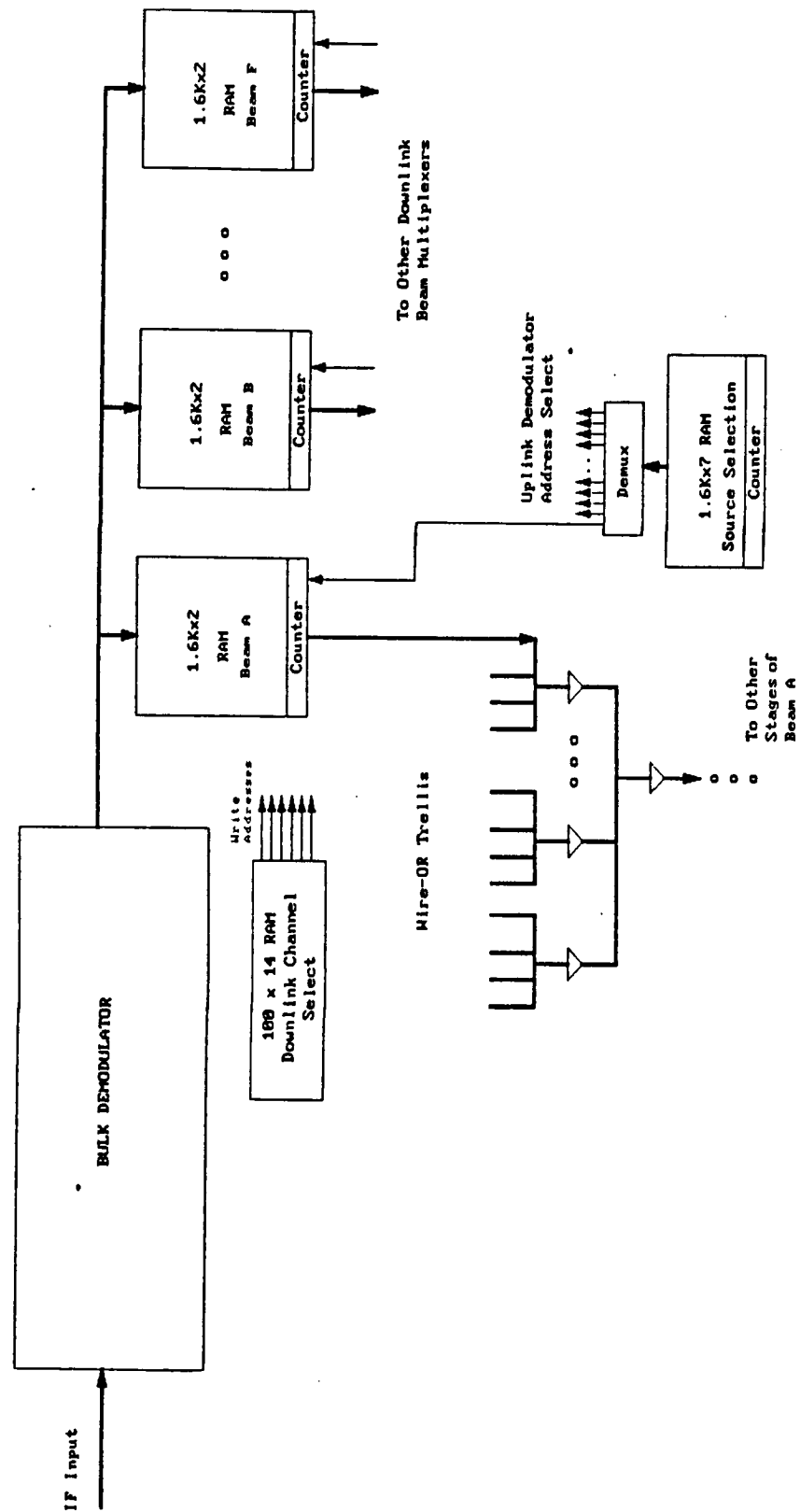
An alternate, and very useful, technique involves serial read-out memories which can be read at rates much higher than the write speed (by performing internal parallel-to-serial conversion). The techniques for producing such memories have been developed commercially to satisfy the need for high-rate raster-scanned computer displays and could be applied to the multiplexer example directly through incorporation of bit-addressable inputs and fabrication in radiation-hardened processes. This greatly reduces the number of external OR operations required and makes serial "daisy-chaining" of chips possible, if reliability concerns can be alleviated through cross-connect switches. A diagram is shown in Figure 6-6.

These memory-based schemes have drawbacks in terms of the efficiency of on-board memory utilization, which is approximately one percent. The total memory required is about 2 Mbits. However, the low cost and versatility of memory-based structures makes such techniques attractive.

Several conclusions can be drawn from examination of the various multiplexing techniques. If on-board simplicity is most desired, the frequency-based assignment technique involves minimum on-board processing and no on-board reconfiguration other than dwell times. If random interconnect, broadcast capability, and lack of outages are most important, the memory-based scheme would seem to have considerable merit. Since the latter properties are most desirable in a thin-route network, the memory-based structure is the preferred configuration.

Figure 6-6. Raster Output Memory-Based Multiplexer
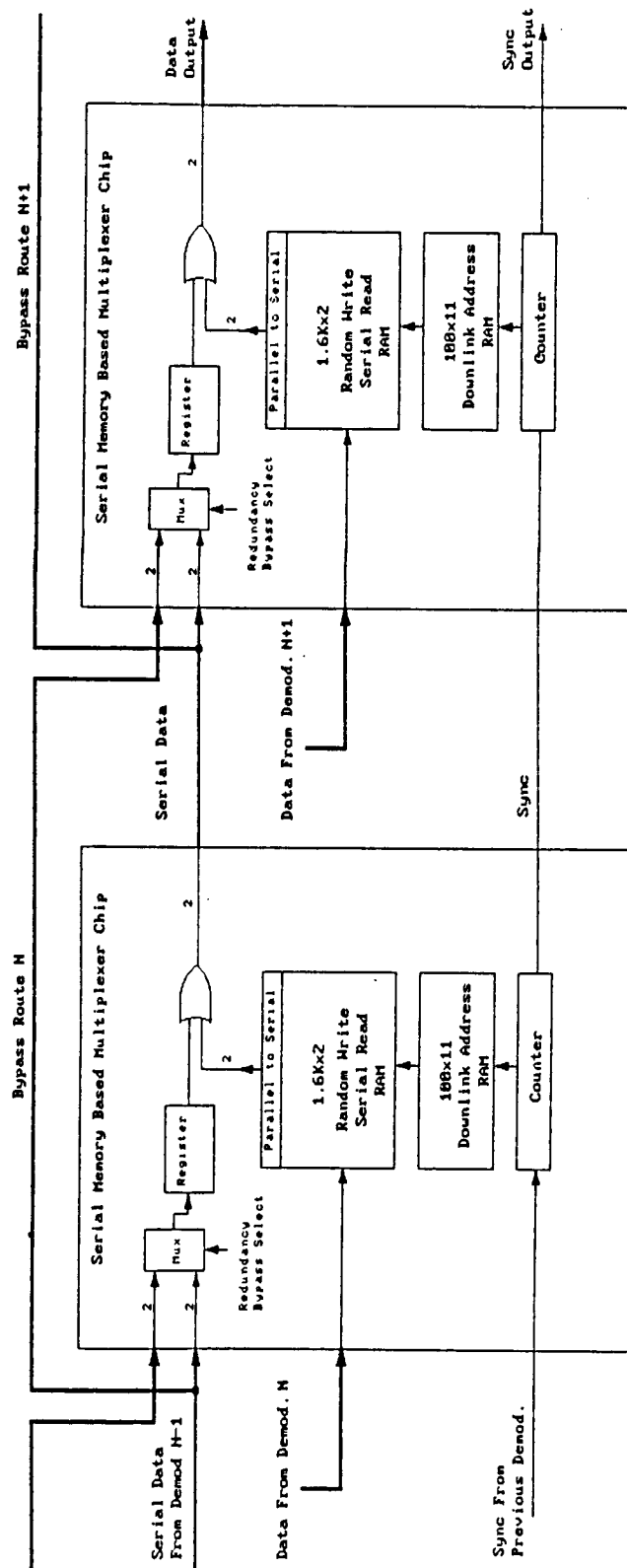
7. TRANSMITTER AND RECEIVER TECHNOLOGY

Design of the satellite uplink and downlink are heavily dependent on achievable performance in the areas of high-power amplifiers and low-noise receivers, at both 30 and 20 GHz. This section provides an assessment of current technology in these areas, as well as projections of performance in the 1990 and 1995 time periods. Only solid-state devices have been considered for the present application.

In assessing 20-GHz power amplifier performance, the quantities normally of interest, power rating and DC/RF conversion efficiency, are discussed. However, it should be pointed out that in the baseline satellite design, each transmit antenna is an array-fed reflector configuration involving 331 elements. Each element has associated with it a final amplifier that produces 300 mW of RF power. Therefore, 20-GHz high-power devices are not especially important to the baseline design. By contrast, high DC/RF conversion efficiency is most important.

Amplifying device power levels are shown in Figure 7-1 for both 20 and 30 GHz. Corresponding device efficiencies are shown in Figure 7-2. In addition to indicating currently achieved performance, various vendors provided performance projections for 1990 and 1995. Except where indicated otherwise, all devices are GaAs FETs. In 1990, single-device power levels of 4W can be expected at 20 GHz, and 1.5W to 3W at 30 GHz. Corresponding collector (i.e., DC/RF) efficiencies are 35 percent at 20 GHz and 25 percent at 30 GHz.

Figure 7-1. Device Power Level Projections

● GaAs FETs Except as Indicated.

Legend:
- ■ 1986 POWER
- ▦ 1990 POWER
- ⊠ 1995 POWER

20 GHZ DEVICES

30 GHZ DEVICES

IMPATT DIODE

HEMT

POWER W

RAYTH   VAR   NEC   FUJ   NEC   GOLD   FUJ
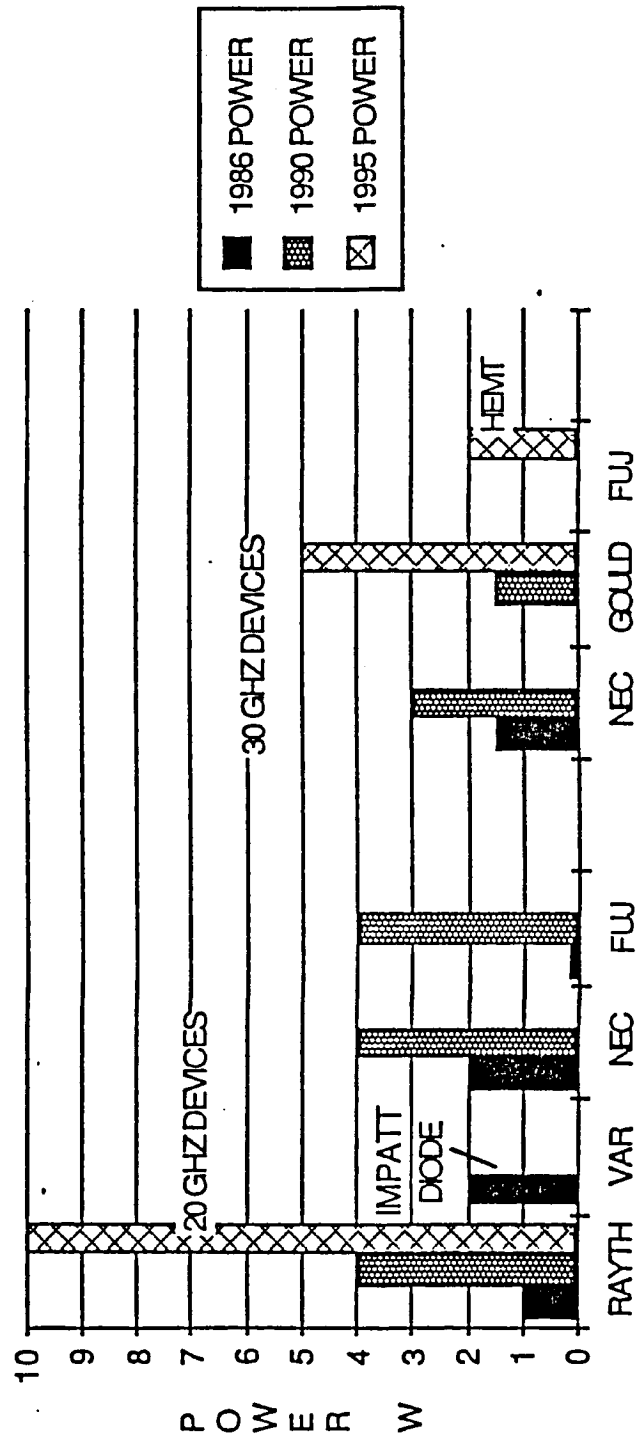
Figure 7-2. Device Efficiency Projections

● GaAs FETs Except as Indicated
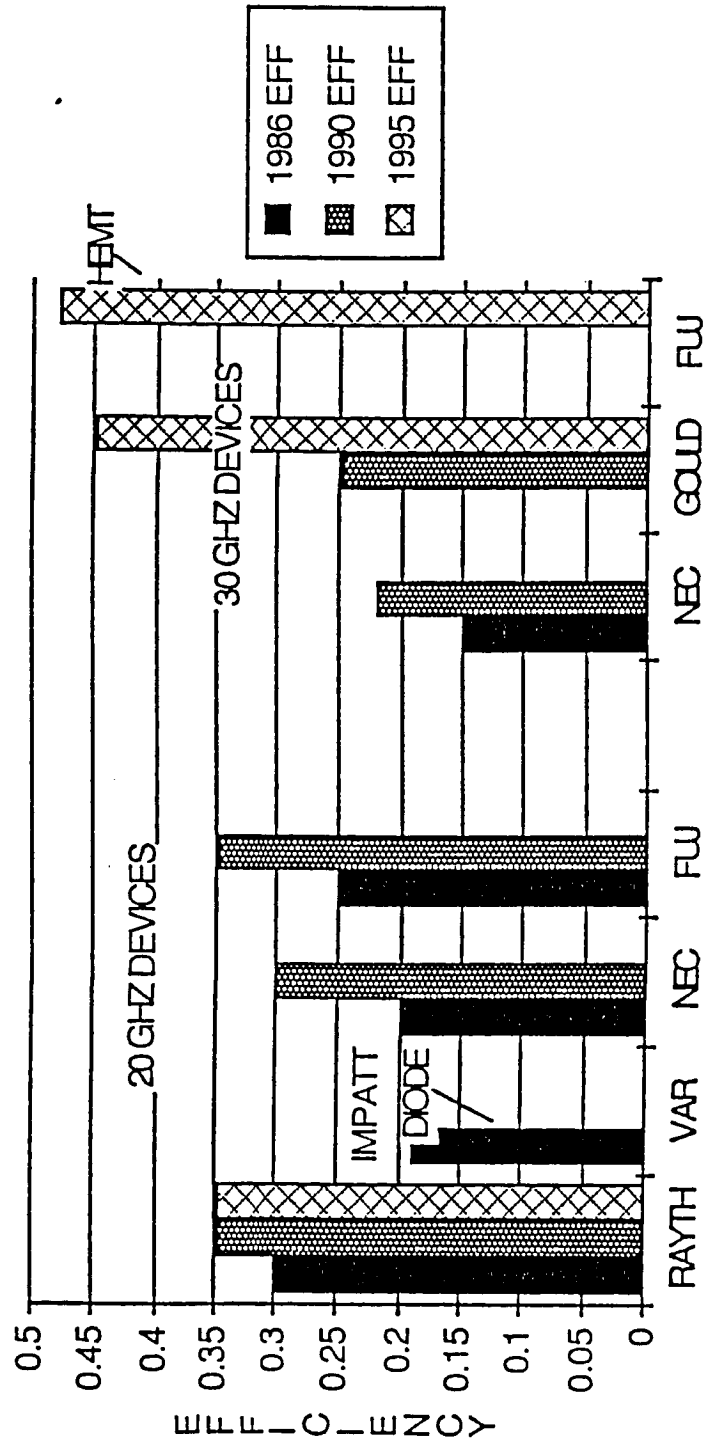
IMPATT diodes are the only devices that today can provide 2W of power at 30 GHz. With similar power levels anticipated for GaAs FETs by 1990 or shortly thereafter, the latter will become the technology of choice for low-power applications. FETs, being three-terminal devices, are inherently more stable than IMPATT diodes. In addition, they are capable of higher efficiency. Finally, they offer the potential for monolithic manufacture, which can lead to greatly reduced cost.

The potential exists for substantial increases in device efficiency by 1995. HEMT and GaAs FET device efficiencies of 45 percent have been projected by different vendors. Of the two technologies, GaAs FETs should have the greater power capability.

Translation of the device efficiency of Figure 7-2 into amplifier efficiency depends on the required amplifier gain. Two examples are given in Figure 7-3, using the Raytheon 20-GHz device projections for 1990. If the 6-dB gain available from a single stage suffices, the DC/RF efficiency is identical to that cited in Figure 7-2 at the device level. The power-added efficiency is only 26.2 percent, however. In the second case, a three-stage gain of 15 dB is required. Because of losses introduced in the first two stages, the DC/RF efficiency is reduced to 24.8 percent. However, the power-added efficiency of 24.0 percent is only slightly below that of the first case.

DC power levels computed from the above amplifier efficiencies must be multiplied by a factor of 1.25 to account for an 80-percent power conversion efficiency.

Figure 7-3. Solid State Amplifier Design Example

Single-Stage Design

▲ Assumption: Raytheon 20 GHz device (1990)

6 dB GAIN
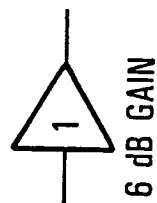
> GAIN: 6 dB
> OUTPUT POWER: 4 W
> COLLECTOR EFFICIENCY: 35%
> POWER ADDED EFFICIENCY: 26.2%

Three-Stage Design

> GAIN: 15 dB (ASSUME MATCHING/1 dB COMP LOSSES)
> OUTPUT POWER: 4 W
> COLLECTOR EFFICIENCY: 24.8%
> POWER ADDED EFFICIENCY: 24.1%

▲ Power (dc) = 0.4 W/0.35 + 1.25 W/0.35 + 4 W/0.35 = 16.1 W
　　　　　　 (1st)　　　　　 (2nd)　　　　　 (3rd)

▲ Collector efficiency (3-stage) = P_{out}/P_{dc} = (4 /16.1) × 100 = 24.8%

▲ Power added efficiency = $(P_{out} - P_{in})/P_{dc}$ = (4 − 0.12)/16.1 × 100 = 24.1%

Vendor projections of LNA device performance are given in Figures 7-4 and 7-5. All devices are GaAs FETs, except where HEMT devices are indicated. By 1990, noise figures on the order of 1.5 dB are widely predicted at 30 GHz, with slightly lower figures at 20 GHz. Device gain values of 10 dB should be achievable at both frequencies by 1990.

Longer-range HEMT performance projections by TRW are considerably more optimistic than long-range vendor projections for GaAs FETs. By 1995, GaInAs HEMT noise figures as low as 0.5 dB are foreseen at both 20 and 30 GHz (Figure 7-6). The anticipated gain of these devices is relatively low, however.

The noise figure for a complete amplifier depends on the number of stages that are combined and the per-stage gain. Based on achieved (1986) TRW HEMT performance, a two-stage amplifier would have a noise figure of 1.4 dB (Figure 7-7). Because of the relatively high per-stage gain of 12 dB, the overall noise figure is only 0.1 dB higher than that of a single stage.

Figure 7-4. Device Noise Figure Projections

● GaAs FETs Except as Indicated
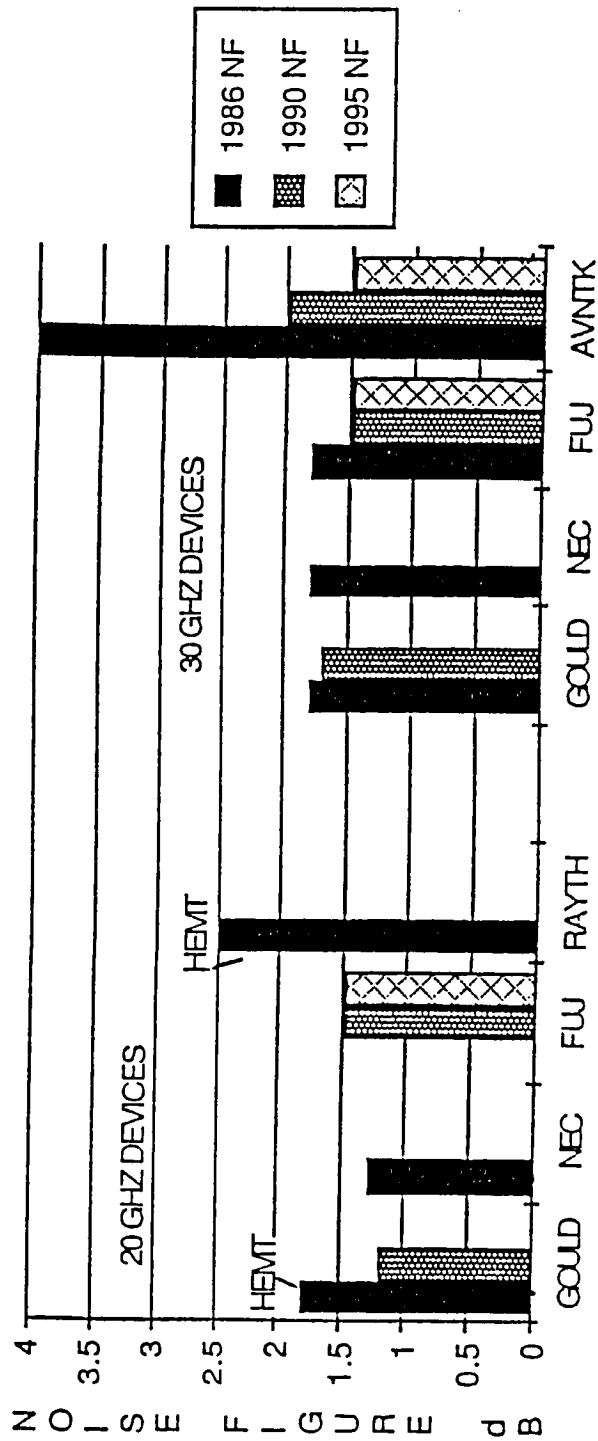
Figure 7-5. Device Gain Projections

- **GaAs FETs Except as Indicated**

Legend:
- 1986 GAIN
- 1990 GAIN
- 1995 GAIN
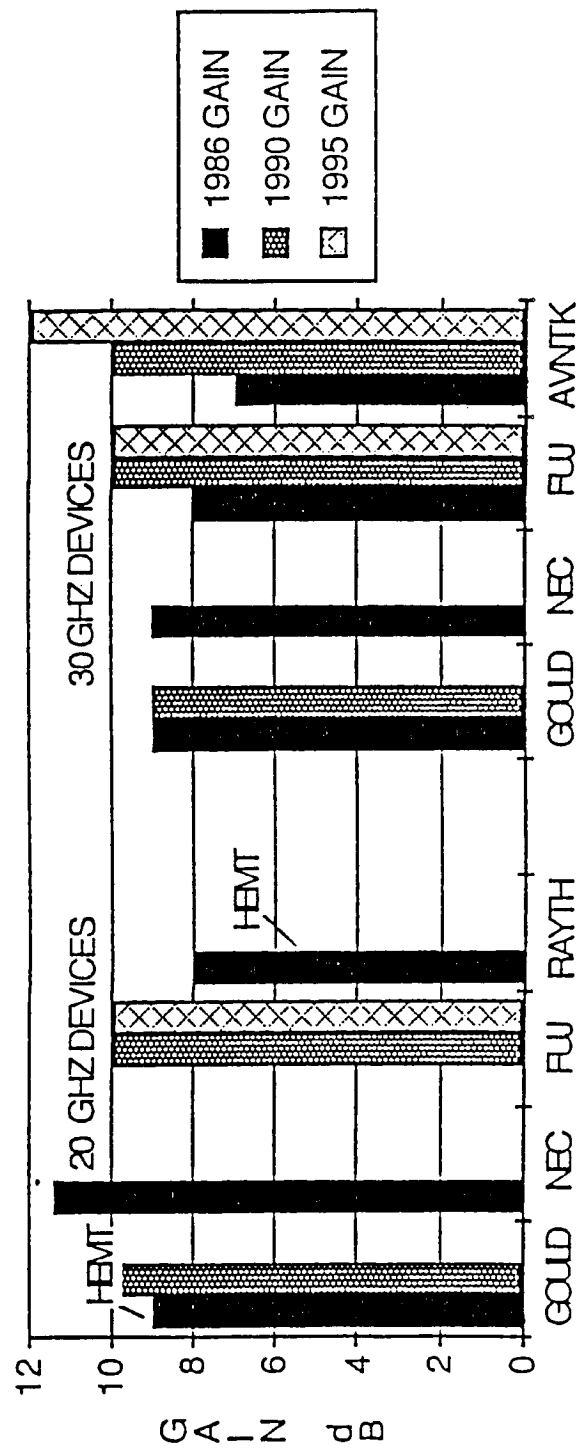
Figure 7-6. TRW HEMT Performance Projections
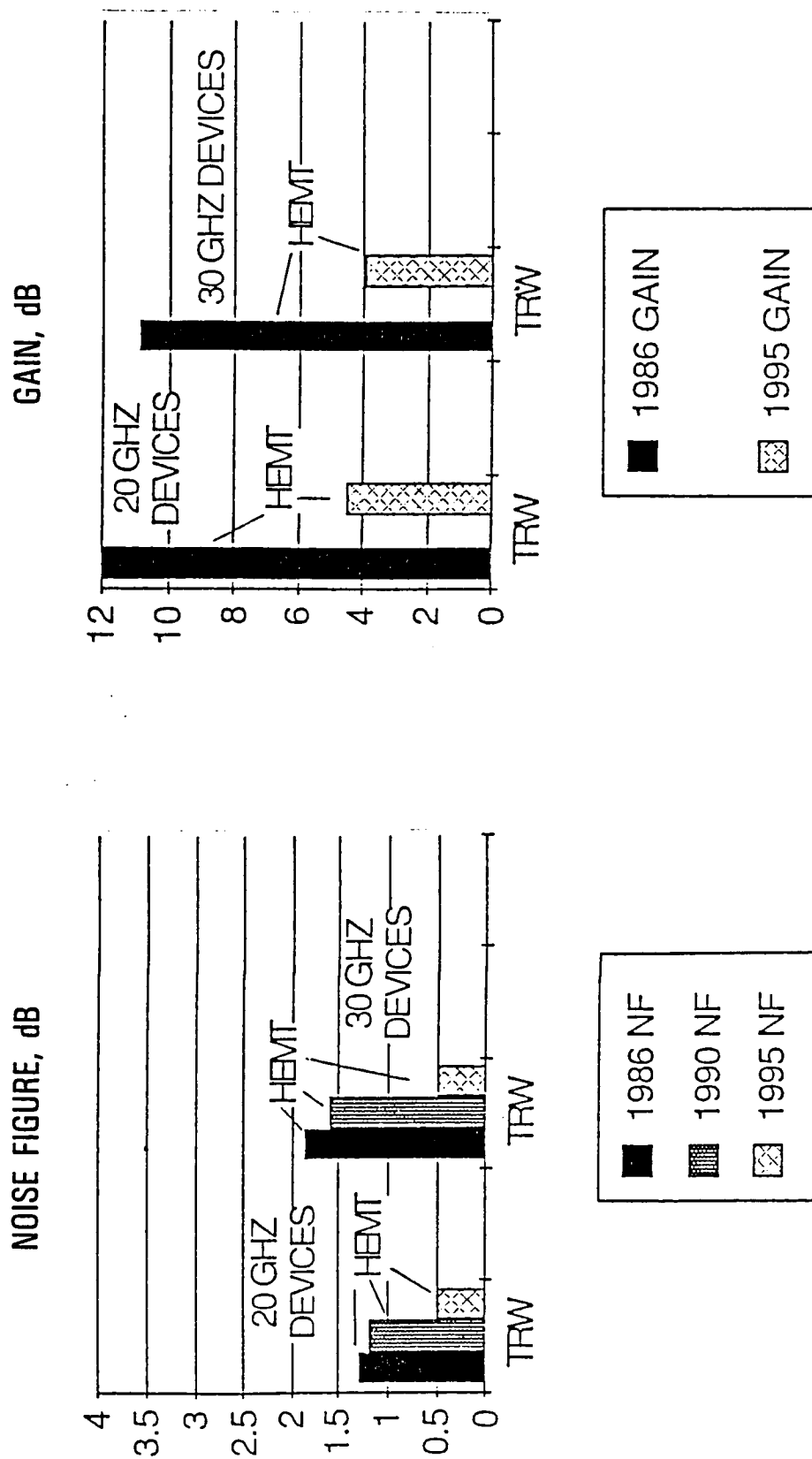
Figure 7-7. Low Noise Amplifier Design Example

▲ Assumption: TRW 20 GHz device (1986)

● 12 dB gain, 1.3 dB noise figure

● Two-stage design results in 24 dB gain (less matching networks)

● Noise figure calculations

```
      ┌─────────────────┐
      │ 2-STAGE AMPLIFIER │
      │   GAIN: 24 dB     │
      │   NF: 1.4 dB      │
      └─────────────────┘
```



```
      /1\            /2\
     /___\          /___\

12 dB GAIN      12 dB GAIN
1.3 dB NF       1.3 dB NF
```
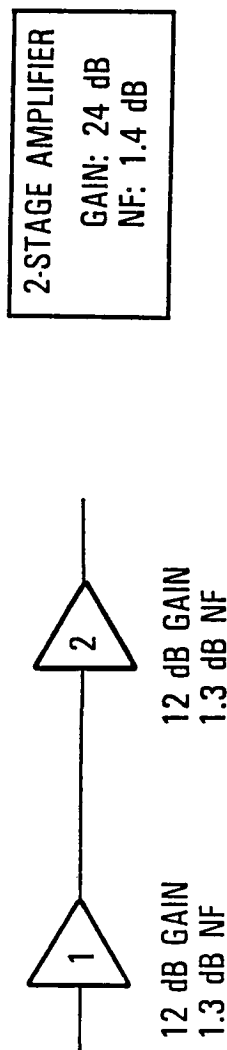
Per device:

NF: 1.3 dB,   1.35 (linear)

Gain: 12 dB, 15.8 (linear)

$$NF = 1.35 + (1.35 - 1)/15.8 + (1.35 - 1)/15.8^2 = 1.37$$

Note: 1st stage should be tuned for low noise figure

8. SATELLITE WEIGHT AND COST

Prior to cost estimation, weight and power estimates are obtained for each satellite subsystem. For certain major payload elements (e.g., receiver/demultiplexer section), a unit weight and power breakdown is provided. For the demodulators and the multiplexer, the chip complement is examined to obtain a power, and thereby a weight, estimate.

8.1. Payload Weight

For purposes of weight and power estimation, the payload is subdivided by major function as shown in Figure 8-1. Accordingly, estimates are provided for: receiver/demultiplexer section, demodulators, baseband processor (i.e., multiplexer), modulator, and transmit arrays. A weight and power summary for the payload is given in Table 8-1. Details of these estimates are provided below.

Receivers/Demultiplexers. The receiver/demultiplexer section of the satellite repeater accepts user transmissions from each of the eight CONUS regions, downconverts the received signals to baseband, and routes the signals to the appropriate bulk demodulators. A functional block diagram of this section of the repeater is shown in Figure 8-2. Only the portion corresponding to a single polarization is shown.

An individual demodulator accepts a composite signal bandwidth of 10 MHz. Each of the 50 demodulators associated with a particular polarization must be connected to the uplink beam to which its 10-MHz

Figure 8-1. Satellite Payload Functional Block Diagram
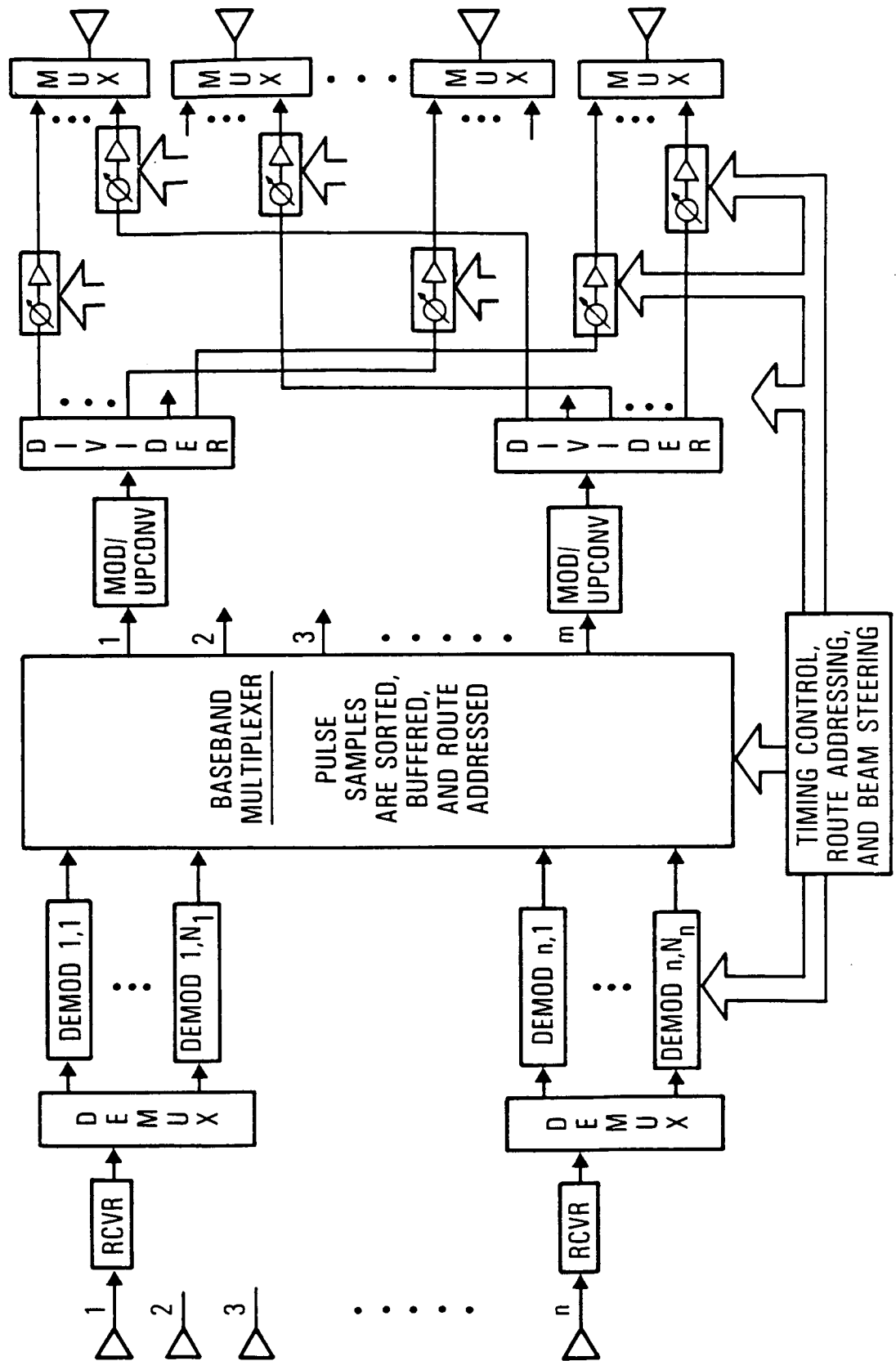
Table 8-1. Payload Weight and Power Summary

Item	Weight (lb)	Power (W)
Receiver antennas	10	—
Receiver/demultiplexer	310	755
Bulk demodulators	300	1020
Baseband multiplexer	40	150
Modulators	15	50
Transmit arrays	300	2980
Total	975	4955

Figure 8-2. Receiver/Demultiplexer Block Diagram
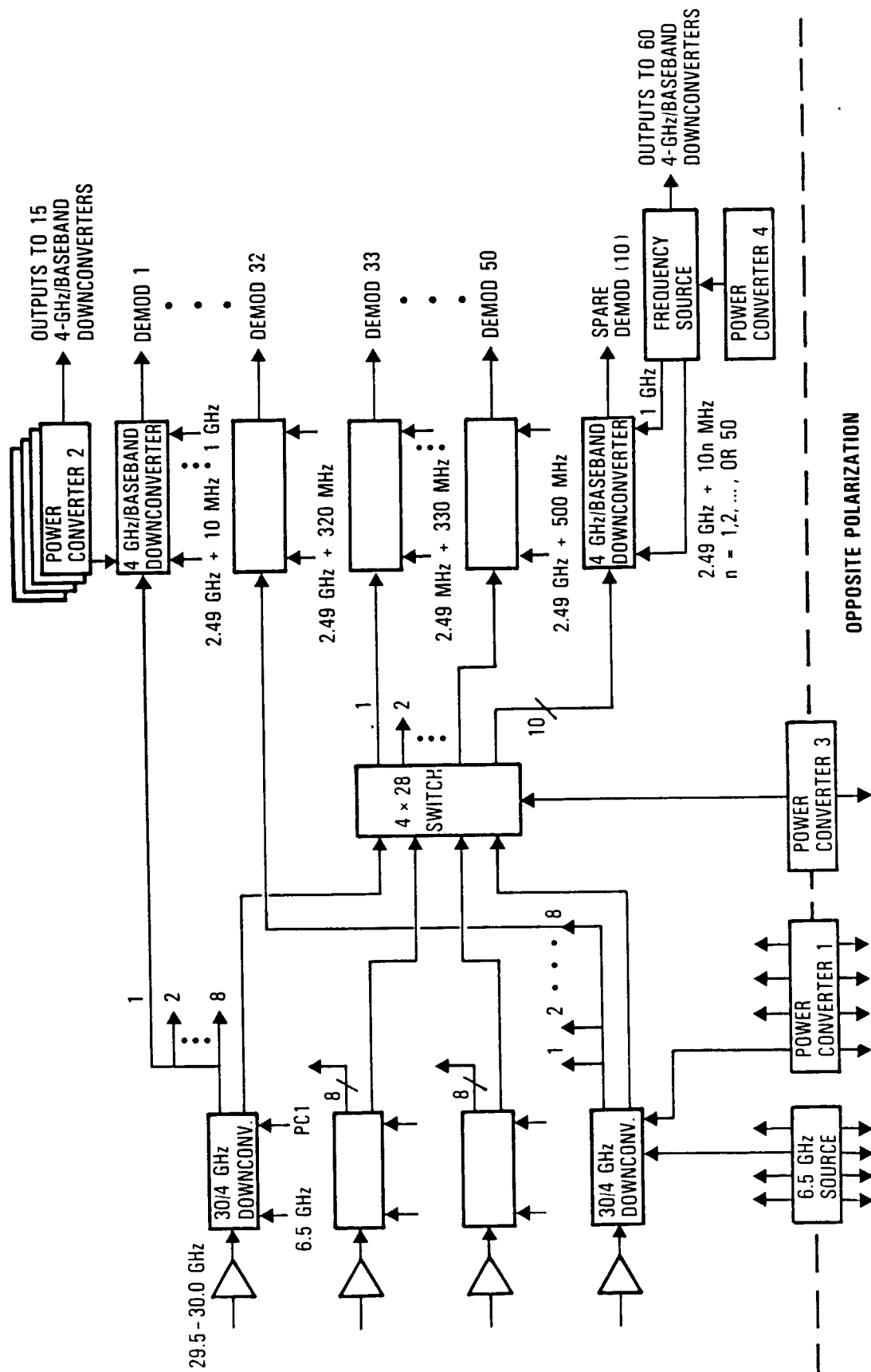
segment has been assigned. It must also be provided with a downconversion chain that translates the 10-MHz segment to baseband (i.e., 1-11 MHz). It is assumed that, of the fifty 10-MHz segments on each polarization, 32 are permanently assigned to particular uplink beams. For simplicity, these 32 segments are shown in Figure 8-2 as distributed uniformly among the four uplink beams and assigned to demodulators 1 to 32. The remaining 18 10-MHz segments (i.e., demodulators 33 to 50) can be assigned to any of the four uplink beams by means of the 4 x 28 switch. The connections are chosen to match the time-varying geographic traffic division among the four beams.

In addition to the first 50 demodulators, which are given fixed RF frequency assignments, 10 spare demodulators are provided for each polarization. The downconverters preceding these demodulators have variable LO frequencies. The spare demodulators also serve to avoid reduced channel utilization due to a division of the uplink-beam traffic which does not correspond to an integer multiple of 10 MHz in each beam. For example, to divide a given 10-MHz segment between two beams, each beam output would be connected to a demodulator assigned to that 10-MHz segment. One of these demodulators would be selected from the "spare" complement. At the demodulator outputs, only those samples corresponding to occupied channels would be fed to the downlink beams.

Weight and power estimates for the units in Figure 8-2 are given in Table 8-2. The only nonredundant units are the 4-GHz/baseband down-converters, inasmuch as spare units are explicitly provided. Units that support half the demodulator complement or less have been made singly

Table 8-2. Receiver/Demultiplexer Weight and Power Estimate

UNIT	UNIT WEIGHT (LBS)	UNIT POWER (WATTS)	QTY	TOTAL WEIGHT (LBS)	TOTAL POWER (WATTS)
6.5 GHz FREQUENCY SOURCE (DOUBLE-REDUND)	8.7	4.4	1	8.7	4.4
30/4 GHz D/C (REDUNDANT)	4.2	7.0	8	33.6	56.0
4 GHz/BASEBAND D/C (NONREDUNDANT)	0.3	2.0	120	36.0	200.0
FREQUENCY SOURCE (REDUNDANT)	64.0	141.0	2	128.0	282.0
4 × 28 SWITCH (REDUNDANT)	36.0	26.0	2	72.0	52.0
POWER CONVERTER 1 (DOUBLE-REDUND)	3.6	15.0	1	3.6	15.0
POWER CONVERTER 2 (REDUNDANT)	1.6	7.5	8	12.8	60.0
POWER CONVERTER 3 (DOUBLE-REDUND)	3.6	15.0	1	3.6	15.0
POWER CONVERTER 4 (REDUNDANT)	6.4	36.0	2	12.8	72.0
TOTAL				311.1	756.4

redundant. Those units supporting both polarizations (i.e., the 6.5-GHz frequency source and power converters 1 and 3) have been made doubly redundant.

In a number of cases, unit sizing is based on existing designs. For example, the 30/4-GHz downconverter is similar to the corresponding ACTS downconverter. The power converters are based on second-generation MILSTAR designs.

The weight and power of the receiver/demultiplexer section are dominated by the two frequency sources (one for each polarization). These units contribute 41 percent of the total weight and 37 percent of the total power. The technology involved in the frequency sources is not expected to change radically in the future, so significant weight and power reductions are not expected. In addition, the 120 4-GHz/baseband downconverters account for 26 percent of the required power. Significant reduction in this value is also not anticipated.

Demodulators. Demodulator weight and power estimates are provided for a pipelined FFT configuration (see Section 5.2) using 1-μm CMOS VLSI technology. Sizing is based on 1991 technology estimates for LSI density and power consumption.

The requirements for a 128-point FFT with real sampling, as established in Section 5.2, are:

- 24.6-MHz sampling rate (real samples)

- 128 points with windowing and trigonometric recombination
- 10-μs computation time

These requirements translate into $(N/2T)(\log_2 N + 2)$ equivalent complex operations per second (COPS), or 57.6 MCOPS per demodulator.

As a basis for estimate, two current FFT technologies were examined: the TRW VHSIC I FFT chip set and a TRW pipelined FFT chip set. The VHSIC chip set comprises a 1-μm CMOS control chip, a 1.25-μm CMOS four-port memory, and a 1.25-μm CMOS arithmetic unit chip. This chip set is capable of 8.192 MCOPS at a power dissipation of 2.2W. Improvements expected in 1987-88 are expected to reduce this value to about 1.8W. The equivalent power per MCOPS is 220 mW.

The pipelined chip set uses 2-μm CMOS technology and consists of four chip types: a complex multiplier, an 8-point discrete Fourier transform (DFT), a control-chip, and a 674-word memory. This chip set is capable of 15 MCOPS and dissipates approximately 2.5W. Future conversion to 1-μm CMOS is expected to reduce power consumption to 1.5W, or 100 mW per MCOP. Future advances in areas such as submicron wafer-scale integration (WSI) are expected to reduce power consumption to values below 100 mW per MCOPs in the 1992 time frame.

Based on the power requirements of a pipelined chip set using 1-μm CMOS technology, the power needed for a 128-point FFT is 5.8W. Additional input/output memory for the FFT requires about 500 mW, based on 4K bits of storage at 25 MHz and a 1-μm CMOS estimate of 0.1 mW/bit

for hardened static RAM. Among other demodulator elements, the 25-Msps 8-bit A/D converter currently requires 1.2W; however, improvements in CMOS processing should reduce the power level to 600 mW. Post-processing data detection, accomplished by a semicustom 1-µm CMOS chip, consumes about 250 mW. Finally, control and logic overhead and interfaces require about 1W. Thus, the total power needed for a single demodulator is 8.15W.

A complement of 100 active demodulators would therefore require 815W of secondary DC power. Assuming 80-percent-efficient power converters, the primary DC power required by the demodulators is 1020W.

The demodulator weight is based on a rule-of-thumb coefficient of 3.3 W/lb for CMOS satellite hardware. For purposes of weight estimation, the spare demodulator units must be included; therefore, the appropriate secondary power is 1.2 x 815 = 978W. The equivalent demodulator weight is about 300 lb.

Multiplexer. The multiplexer is based on a three-level memory multiplexing technique with an equivalent of three chips per demodulator. These chips have high-speed interfaces with each other and with the demodulators. In addition, bipolar, high-speed formatter chips are required for each downlink.

Each memory chip consists of a number of serial inputs and outputs, together with a multiport internal-registered data memory and a separate control table memory. These chips are constructed in 1-µm CMOS and

consume 350 mW. The output formatters require 3 to 4 chips per downlink, at approximately 1W per chip. Onboard computer control is expected to require 10W. With 100 active demodulators and four downlinks, the multiplexer requires about 130W of secondary DC power. The power requirement on the primary side of the power converters is 165W.

The multiplexer weight is computed from the secondary DC power that would be required for 120 active demodulators, which is 152W. At 3.3 W/lb, this power level translates into 46 lb. Because of the bipolar components, which have a higher power/unit-weight ratio than CMOS, the multiplexer weight may be taken as 40 lb.

Modulators. The modulator section of the repeater is shown in Figure 8-3. The four BPSK modulators have as inputs the appropriate data streams for the four downlink beams and a 5-GHz tone. The latter undergoes a x4 multiplication in the modulator to provide a 20-GHz carrier. The 20-GHz solid-state amplifier raises the carrier level to the required input for the initial amplifier in the HPA chain. The latter successively divides and amplifies the modulated carrier until the required number of signals (331 in this case) are provided to the radiating elements at the appropriate power level (0.3W). The modulator weight and power estimate is detailed by unit in Table 8-3.

Transmit Arrays. There are two identical transmit arrays, each supporting two of the four downlink beams. The elements of each array, together with weight and power estimates, are itemized in Table 8-4. The

Figure 8-3. Modulator Block Diagram

OUTPUTS TO TOTAL OF FOUR
20 GHz BPSK MODULATORS
AND 20 GHz SOLID-STATE AMPLIFIERS

POWER
CONVERTER 5

DATA →

20 GHz BPSK
MODULATOR

20 GHz SOLID
STATE AMP

5 GHz FREQUENCY
SOURCE

D/L BEAM 1

D/L BEAM 2

D/L BEAM 3

D/L BEAM 4
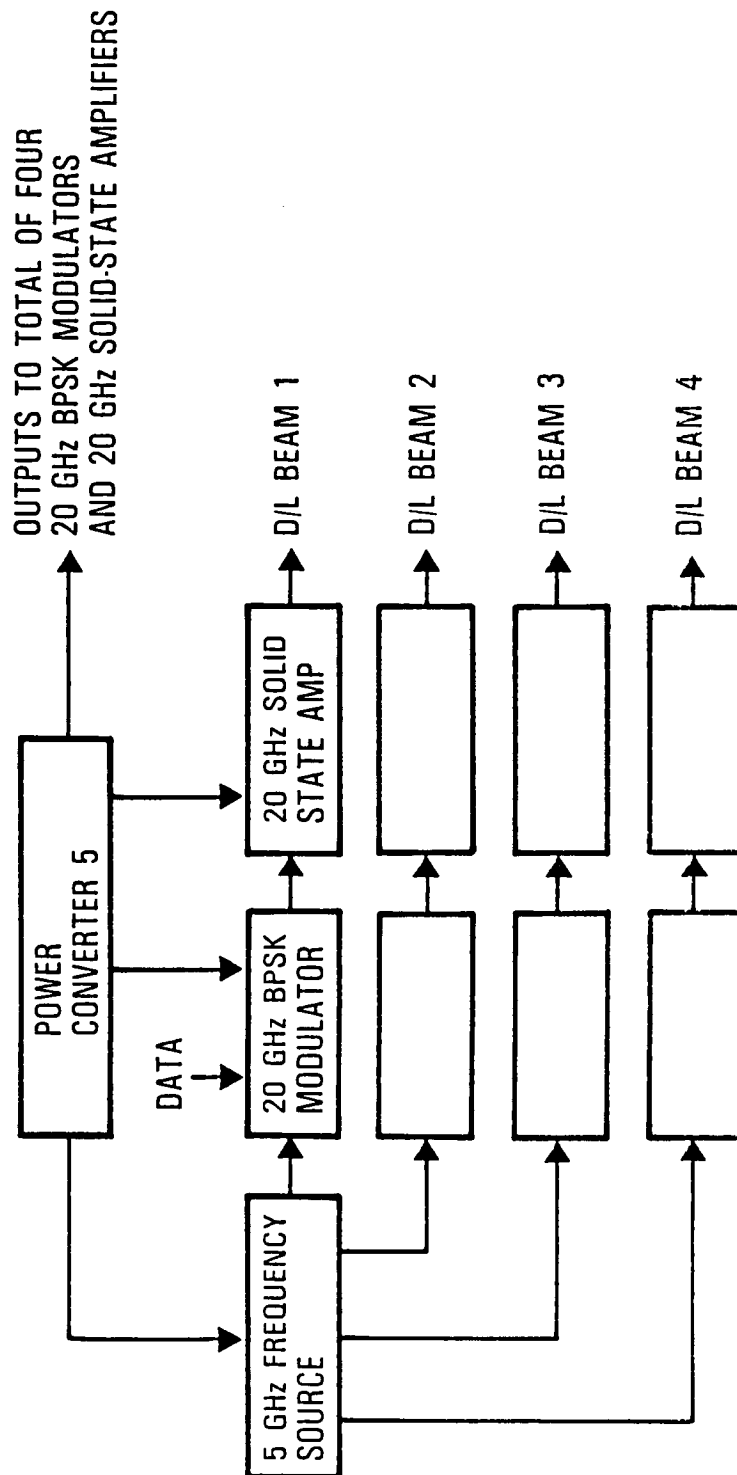
Table 8-3. Modulator Weight and Power Estimates

Unit	Unit Weight (lb)	Unit Power (W)	Quantity	Total Weight (lb)	Total Power (W)
5 GHz frequency source (doubly-redundant)	7.2	7.2	1	7.2	7.2
20-GHz BPSK modulator (redundant)	0.8	5.7	4	3.2	22.8
20-GHz SSPA (redundant)	0.7	2.4	4	2.8	9.6
Power converter 5 (doubly redundant)	2.4	10.0	1	2.4	10
Total				15.6	49.6

Table 8-4. Array-Fed Dual Reflector Antenna Weight and Power Estimates

Item	Quantity*	Weight (lb)	Power (W)
Feed horns	331	5	—
Phase shifters	662	10	165
Phase-shifter controllers	2	10	100
HPAs	772**	20	925
Transmission line and cabling		20	—
Power converters		15	300
Structure		30	—
Reflectors	2	40	—
Total		150	1490

*For one of two identical antennas

**Includes amplifiers in power-divider network

baseline array design has 331 radiating elements. Since a separate set of phase shifters is needed for each beam, there are 662 phase shifters in each array. There is a like number of final amplifiers; however, an additional 100 or so amplifiers are needed for the divide-and-amplify HPA chain.

The DC power requirements for the HPAs are based on an assumed 25-percent efficiency and a radiated power per element of 0.3W. Phase shifters for a phased array at 20 GHz do not presently exist; consequently, estimates of required power are subject to sizable errors. Based on discussions with workers in this field, it is felt that the estimate of 0.25W per phase shifter used in Table 8-4 is realistic, and may in fact prove conservative. The phase-shifter controller power estimate is based on use of PROM look-up tables for each element. This approach is made feasible by a time-tagged power strobe technique, in which each PROM is powered only when it is being read. This process requires less than 1 μs.

8.2. Satellite Weight

As shown in Table 8-1, the baseline payload configuration weighs 975 lb and consumes 4955 of power. The satellite power requirements are detailed in Table 8-5. It is assumed that 25 percent of the full communications capability is maintained during eclipse. This choice results from the tradeoff of satellite weight vs. eclipse capability displayed in Table 8-6.

Table 8-5. Satellite Power Requirements

Subsystem	Power During Normal Operation (W)	Power During Eclipse (W)
Payload	4955	1240
Mechanical	100	20
Thermal Control	75	200
Data Management	250	250
TT&C	200	200
Propulsion	100	100
Guidance, Navigation, and Control	400	400
EPS	770	260
Total	6850	2670

Table 8-6. Satellite Weight vs. Eclipse Capability

Eclipse Capability (%)	Satellite Weight (lb)
10	5310
25	5603
50	6093
100	7073

The power consumed by the payload and supporting subsystems, as seen at the interface with the electrical power subsystem (EPS), is 6080W. When power distribution losses and the need to recharge the batteries during normal operation are taken into account, the power requirement increases to 6850W. The corresponding EPS weight is 1800 lb. In computing the battery charging requirements, an eclipse period of 1.2 hrs is assumed. The battery sizing is based on (1) specific weight of 140 lb/kW for NiH_2 batteries, and (2) 75 percent depth of discharge.

A satellite weight budget is given in Table 8-7. The payload and EPS weights have already been accounted for. The thermal control subsystem weight is explained in Table 8-8. All heat-generating units other than the transmit arrays are presumed to require cold plates and a heat transport mechanism, in addition to radiators. Only radiators are required by the phased arrays. The 2235W dissipated by the pair of phased arrays accounts for the difference in load presented to the thermal subsystem elements.

Table 8-7. Satellite Weight Budget

Subsystem	Weight (lb)
Payload	975
EPS	1800
Thermal Control	580
Propulsion	780
Data Management	150
TT&C	150
GNC	200
Subtotal	4635
Structure @ 10%	465
Margin @ 10%	510
Total	5610

Table 8-8. Thermal Control Subsystem Weight

Item	Specific Weight (lb/kW)	Net Load (W)	Weight (lb)
Cold Plates	38	3095	118
Heat Transport	19	3095	59
Radiators	75	5330	400
Total			577

The propulsion subsystem weight is based on the need for 50 lb of propellant per year for orbit maintenance over a period of 10 years. In addition, 150 lb of propellant is provided for insertion/initialization, and 50 lb for emergency disposal. The structural weight of the propulsion subsystem is taken as 11 percent of the propellant weight.

Examination of Table 8-7 reveals that the satellite weight is largely attributable to the payload power requirements. It is tempting, therefore, to reduce the power requirements through an increase in the size of the transmit arrays (i.e., an increase in the number of elements with the inter-element spacing held fixed). For example, if the number of elements is doubled, the RF power requirement is halved, and the DC power consumed by the power amplifiers is also halved. However, the DC power associated with the phase shifters is doubled, under the assumption that each amplifier output has an independent phase setting. The net result is that the DC power required by the pair of phased arrays decreases from

2980W to 2230W. The combined array weight, however, increases from 300 lb to 540 lb. Insofar as total satellite weight is concerned, the decreased power and the increased weight of the transmit arrays offset one another; i.e., the two configurations have virtually identical weight.

It is possible, with double the number of radiating elements, for each phase shifter to serve a pair of elements, thereby holding constant the number of phase shifters. (Grating lobe and scan loss properties must be re-examined, however.) This further reduces the DC power consumed by the phased arrays from 2230W to 1810W. However, the satellite weight is only reduced from 5620 to 5460 lb. Moreover, the resulting satellite configuration (as well as the configuration with twice the number of phase shifters) has the disadvantage of significant added complexity in the phased arrays. For these reasons, the satellite configuration based on a pair of 331-element phased arrays is retained as the baseline design.

8.3. Satellite Cost

Engineering estimates of the satellite cost presented below are exclusive of fee. Estimates of nonrecurring and first-unit costs are provided. Three separate assembly phases are assumed: payload, bus, and payload-to-bus. A satellite cost summary is shown in Table 8-9. (Listing of the cost estimates to one decimal place is a computational convenience and is not intended to imply knowledge to that accuracy.) The nonrecurring or development cost is $110 million, while the first-unit cost is $113 million. All costs are in 1987 dollars.

Table 8-9. Satellite Cost Summary

Item	Nonrecurring Cost ($M)	First-Unit Cost ($M)
Payload	54.3	60.8
Spacecraft bus	42.3	36.6
System engineering	4.7	1.8
Program management	2.8	5.4
Product assurance	0.9	0.9
Assembly, integration, and test	4.7	7.3
Total	109.7	112.8

Cost estimates for the payload hardware elements are based on a dollars/pound analogy with space-qualified electronics of known cost. The payload cost is compiled in Table 8-10 by enumerating, in addition to the major hardware sections (e.g., receiver/demultiplexer), the activities required to deliver a fully assembled payload. For those hardware sections involving a large number of similar units (e.g., the bulk demodulator section has 120 distinct demodulators), the term "quantity" refers to the number of hardware "slices" into which the section is divided. For example, the bulk demodulator section comprises 15 slices, each containing eight demodulators and weighing 20 lb. Each of these slices is considered a unit for costing purposes. The first five units are assumed to be prototypes, all of which are produced at identical cost. A 95-percent "learning" curve is assumed to apply to the remaining units.

The nonrecurring cost (NRC) is computed according to

$$NRC = 3(RC) + 0.25 (N-1)(RC)$$

when RC is the recurring cost and N is the number of units produced.

The spacecraft bus cost estimate is given in Table 8-11. Spacecraft subsystem costs represent best estimates based on comparisons of cost estimating relationships (CER) and dollars/pound analysis.

Table 8-10. Payload Cost Summary

Item	Quantity	Nonrecurring Cost ($M)	First-unit Cost ($M)
Receive antenna	1	0.2	0.2
Receiver/demultiplexers	10	9.0	16.1
Bulk demodulators	15	5.2	10.8
Baseband multiplexer	2	2.9	1.8
Modulators	1	0.8	0.5
Transmit arrays	2	14.3	11.5
Contingency		7.8	5.3
Hardware total		40.2	46.9
System engineering		5.2	1.6
Program management		2.2	4.9
Product assurance		1.1	1.2
Assembly, integ, & test		5.6	6.2
Total		54.3	60.8

Table 8-11. Spacecraft Bus Cost Summary

Item	Nonrecurring Cost ($M)	First-Unit Cost ($M)
Propulsion	3.7	1.9
Thermal	3.4	2.6
Attitude control	6.1	5.2
Electrical power	9.0	11.5
Data management	5.3	3.5
TT&C	2.1	2.1
Structure	3.0	1.4
Hardware total	32.6	28.2
System engineering	2.3	0.6
Program management	1.9	2.8
Product assurance	0.6	0.8
Assembly, integration, and test	4.9	4.2
Total	42.3	36.6

9. USER TERMINAL DESIGN AND COST

Based on the system architecture described in Section 2, the user terminals must satisfy the following requirements:

- Transmit a single 64-kbps, QPSK carrier

- Frequency agility over 500 MHz

- Transmit (on command) either right-hand or left-hand circular polarization; receive on opposite sense polarization

- Transmitter power of 2W

- Figure-of-merit, G/T, equal to 18.3 dB/K

- Differentially detect BPSK data bursts on 240-Msps carrier; received carrier may be at either of two frequencies and on either polarization

- Provide voice and/or data capability.

In addition to these technical requirements, the terminal design was influenced by the following factors:

- Minimization of (recurring) cost
- Terminal production in large quantities (e.g., 10,000 units)
- Deployment to begin in early 1990s.

Accordingly, the following guidelines and assumptions were observed in the terminal design procedure:

- Maximum sharing of uplink/downlink resources

- Functional partitioning to minimize environmental control needs

- Minimum number of frequency translation stages

- No built-in test equipment or health status reporting

- Maximum use of automated factory procedures, including automated alignment and testing

- Temperature control optional.

9.1. Terminal Description

The terminal block diagram, shown in Figure 9-1, is partitioned into six subassemblies, which are designated A1 through A6. The downlink signal path is shown in bolder lines than the uplink path. Figure 9-2 depicts the terminal packaging and indicates where the subassemblies reside.

Subassembly A1, which is one of two indoor subassemblies, performs the following functions:

- A/D multiplexing for voice digitizing and data routing, according to the user-selected mode

- Satisfaction of network requirements for coding, frame formatting, and data transition and frame-time slot acquisition under CPU control

- QPSK modulation at 70 MHz

- Provision of high-precision and low-phase-noise 10-MHz reference for uplink and downlink frequency sources

Figure 9-1. User Terminal Block Diagram

FOLDOUT FRAME

Figure 9-2. User Terminal Configuration

► INDOOR ELECTRONICS
  ● UPLINK IF & LO REFERENCE
  ● DOWNLINK BASEBAND PROCESSING
  ● TERMINAL CONTROL

A1,A2

A6

A4,A5

► OUTDOOR ELECTRONICS
  ● INTEGRAL ANTENNA &
    RF ELECTRONICS
  ● DOWNLINK DEMODULATOR &
    BIT SYNC

POWER INPUTS MODE

DATA
VOICE

A3

► FIBER OPTIC INTERFACE
  ● UPLINK IF & LO REFERENCE
  ● DOWNLINK BASEBAND
  ● OUTDOOR ELECTRONICS CONTROL
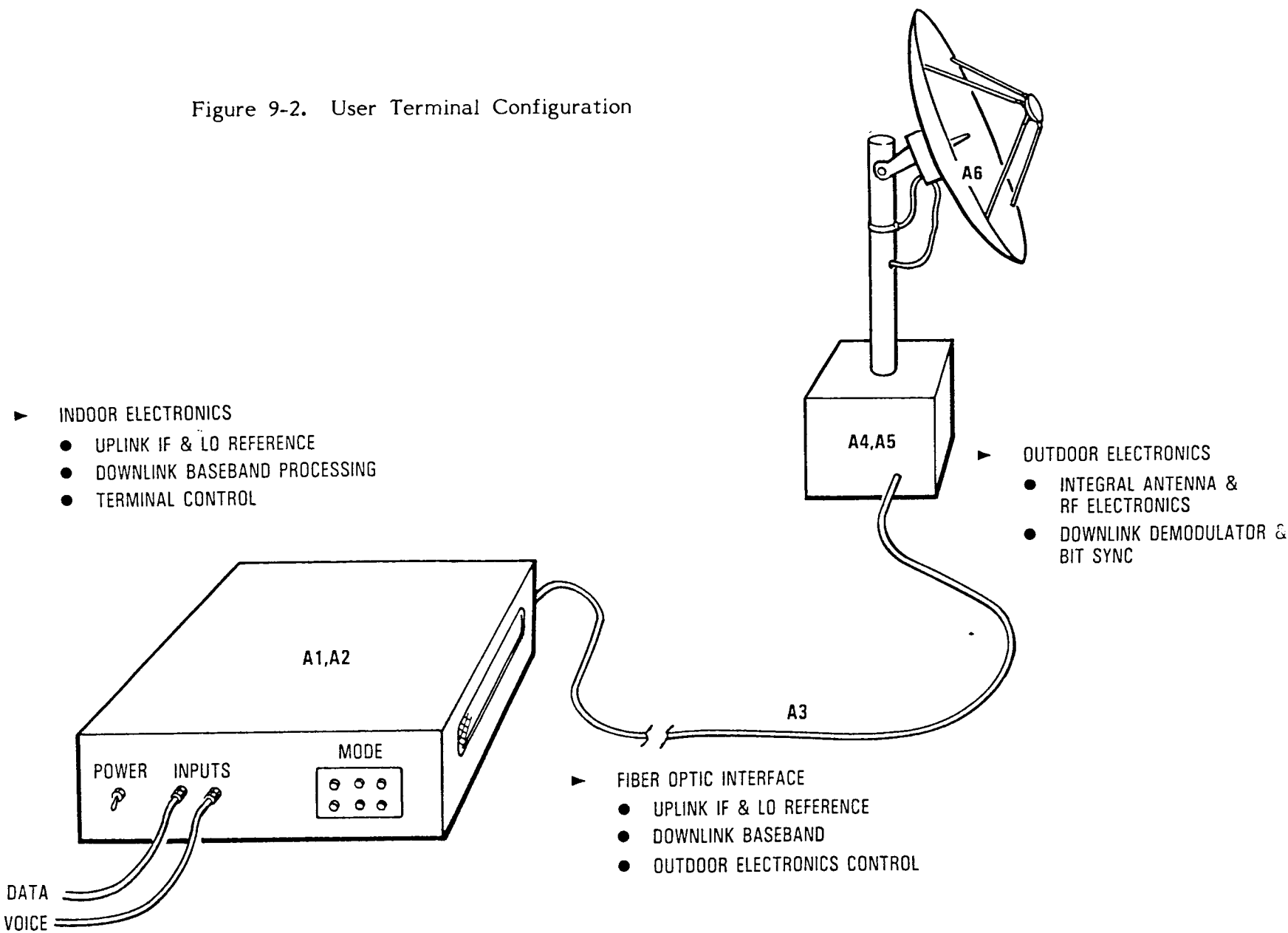
- Provision of electrical-to-optical conversion for both the 10-MHz reference and the 70-MHz QPSK signal.

Data transition times are controlled because it is necessary that these transitions occur simultaneously in all channels accessing a common satellite bulk demodulator. A frame structure is established so that periodic orderwire bits arrive at the satellite simultaneously.

Indirect, rather than direct or RF, modulation was chosen because direct modulation is relatively expensive and is attractive only when size and weight are of paramount importance. A direct modulator would reside in the outdoor package and would impose the need for strict temperature control. Indirect modulation is performed indoors at a common IF frequency.

Costs associated with high frequency stability dictate the use of a single frequency reference, together with a distribution network to all reference sources within the terminal. Reference oscillator costs are very sensitive to temperature range requirements. To reduce this cost driver, the frequency reference is placed in the indoor electronics.

Both copper and optical fiber cabling were considered for the indoor/outdoor interface (Subassembly A3). The costs of the two materials are now comparable. However, fiber has the following virtues, which led to its selection:

- Signal sharing of a relatively small and flexible cable

- Immunity to electrical interference

- Availability of cost-effective LED sources to support the data rate requirements

- Removal of indoor/outdoor distance limitations

- Rapidly dropping electrical/optical and optical/electrical conversion costs.

The uplink IF signal is converted to S-band in Subassembly A4. The final upconversion is accomplished using a harmonic mixer (n=2) and an OEM S-band synthesizer and X6-multiplier second LO. The OEM synthesizer provides the required uplink frequency agility, while selection of a harmonic mixer, with input at 13.8 GHz, eliminates the need to provide costly gain at 26 GHz. Pre- and post-HPA filtering is included to meet FCC spurious emissions requirements. The HPA is a 2W IMPATT amplifier with on/off control via a power gate controlled by the indoor CPU (part of Subassembly A2). The 30-GHz transmitter output from the A4 subassembly (contained in a waterproof housing behind the antenna) drives the transmit feed via a circular polarizer, which is controllable to either RHCP or LHCP.

The received signal is first passed through a low-pass filter, which provides isolation between transmitter and receiver. The filter output is fed to Subassembly A5, which is contained in a weatherproof housing behind the antenna. The LNA and associated filters (for rejection of out-of-band signals) exhibit a noise figure of 2.6 dB. Single conversion to a 4-GHz IF is accomplished by a harmonic mixer (n=2) with an LO input derived from a X4 multiplier fed from the uplink first LO.

The received carrier can be at either of two frequencies. Separate

DBPSK demodulators, with center frequencies of 3.88 and 4.02 GHz, are provided for the two cases. Selection of the appropriate demodulator output is done at baseband. A single demodulator with transfer switching to accommodate the two frequencies could be used instead, at comparable cost. However, hardwired, dedicated demodulators should prove more reliable.

The received signal power variation will be no greater than 10 dB. This variation is small enough to be removed at baseband, thus precluding need for a costly voltage-controlled attenuator at 4 GHz.

Clock recovery is a key issue. Because symbol transitions from burst to burst are spaced by multiples of the baud length, clock recovery during startup can take place over many bursts, with a "flywheeling" technique used to recognize symbol transitions during ongoing communications. The bit synchronizer data and clock outputs are converted to optical signals and transmitted to the indoor electronics via the A3 fiber optic cable.

Health status reporting and other test functions are eliminated from this design. It is necessary, however, to build in certain safeguards. Synthesizer phase-lock failure or any other condition that would cause interference to any service must be detected and the transmitter shut down. Since the clock signal from the bit synchronizer is normally continuous, a simple and cost-effective clock activity monitor in Subassembly A2 could serve as a shut-down alarm.

Subassembly A2 performs the following functions:

- All necessary automatic station control for both the indoor and outdoor assemblies (outdoor control via fiber optic cable)

- Unique word detection, data demultiplexing (selection of low-data-rate traffic for a particular station based on time position with respect to the unique word)

- Decoding of received data stream

- D/A conversion for voice traffic and provision of line drivers for data traffic.

9.2. Key Design Issues

Several aspects of the terminal design deserve special attention in the effort to strike a proper balance between performance and cost. These issues are discussed below.

LNA Configuration. The merits of three different receiver configurations are compared in Table 9-1. The all-discrete approach provides the lowest noise figure and the highest possible gain, but at the highest cost. The completely monolithic approach provides the lowest production cost at the expense of an unacceptably high noise figure. The preferred approach is to realize the first stage of the LNA as a discrete HEMT amplifier yielding 9 dB of gain and resulting in an LNA noise figure of 2.3 dB, with the remaining gain realized by a monolithic gain block having a noise figure of 5 dB. The 9-dB gain of the first stage minimizes the noise figure contribution of the monolithic stages.

Table 9-1   LNA Implementation Tradeoff

Configuration	Development Cost	Production Cost	Noise Figure
All discrete receiver	Lowest	Highest	Lowest
Discrete/MMIC receiver	High	Moderate	Low
All MMIC receiver	High	Lowest	Highest

LNA Filters. Losses contributed by the filter preceding the LNA contribute significantly to the receiver noise figure. To hold the insertion loss to a tolerable level, a two-stage approach was adopted. A three-pole, E-plane waveguide filter with a 0.2 to 0.3 dB insertion loss precedes the LNA, and a five-pole microstrip filter follows the LNA. The latter choice lowers the composite filter cost and, because of its placement after the LNA, does not significantly impact the LNA noise figure. The LNA/bandpass filter combination has a noise figure of 2.6 dB. However, the low-pass filter, polarizer, and waveguide interconnects introduce 1.5 dB of loss, thereby increasing the receiver noise figure, as measured at the antenna terminals, to 4.5 dB.

HPA Configuration. Figure 9-3 shows the IMPATT amplifier design and a recommended power profile. The amplifier requires 22 individual parts. This number is not expected to change dramatically in the next five years. A projected cost for these parts is $2200. Although automated parts placement, wave soldering and automated final checkout are employed for a major portion of the terminal, the HPA remains labor intensive. A labor cost estimate was generated using an aggressive time

Figure 9-3.   IMPATT Amplifier Design
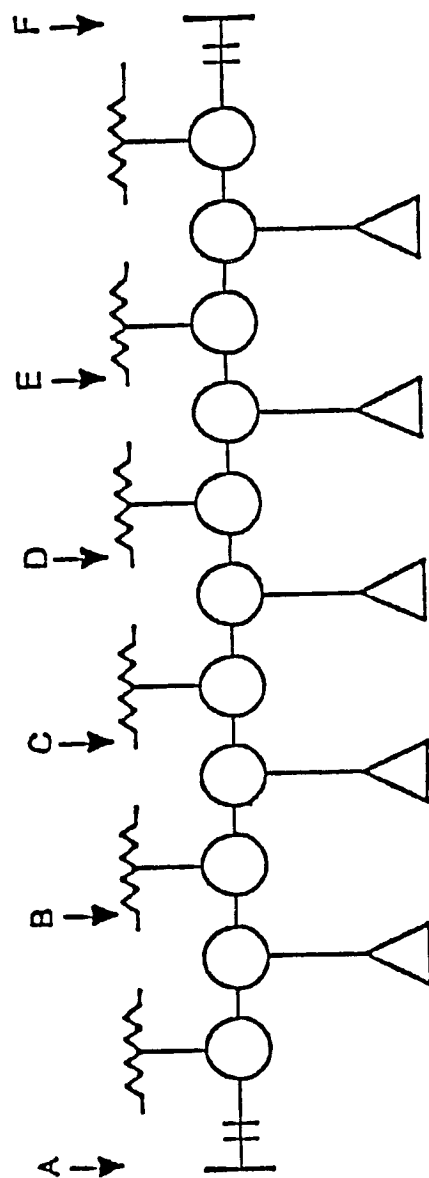
• Impatt Amplifier
•• Termination

Circuit Q=14.22   Circulator loss= 0.2dB
Gain=8.68dB   Waveguide loss= 0.1dB

Power profile location	A	B	C	D	E	F
Power(dBm)	-7.00	0.99	9.07	17.15	25.23	33.0

schedule for each operation and minimum labor grades. This estimate places the labor cost at $1800, yielding a total HPA cost of $4000.

9.3. Terminal Cost

Cost estimates for the units identified in Figure 9-1 are presented in Table 9-2. These unit costs are based on quantities of 10,000. The source of each estimate, either TRW or a vendor, is indicated in a column at the right of the table. The designation ASIC in the Remarks column indicates that development of an application specific integrated circuit has been assumed for the unit in question.

The cost estimates are summarized in Table 9-3, in which a 10 percent profit margin has been added. The total cost per terminal is $24,475.

While the terminal cost is distributed over a large number of units, the HPA and LNA are major cost drivers. The cost of the HPA, in particular, is difficult to project at this time. By contrast, at Ku-band, the combined cost of a 2W HPA and an LNA is about $1500, compared with $6000 as shown in Table 9-2. This disparity is largely a result of the proliferation of small earth terminals at Ku-band, in addition to the lower cost that normally accompanies a reduction in frequency. A similar production history at Ka-band could drive the RF component costs below those indicated in Table 9-2.

Table 9-2. Unit Cost Estimates

Assy No.	Component Description	Cost $	Remarks	Cost Data Source	Assy subtotal
A1	10 MHz Ref.	450	High stab/low noise	Vendor	
A1	A/D Mux	200	ASIC	TRW	
A1	Coder & Frame Form.	300	ASIC	TRW	
A1	Slot Acq.	500	ASIC	TRW	
A1	X7	150		TRW	
A1	QPSK Mod	100		TRW	
A1	E/O (70 MHz)	150		TRW	
A1	E/O (10 MHz)	150		TRW	
A1	PWB	50		TRW	
A1					
A1					
A1					
A1					2050
A2	CPU Control	600	ASIC	TRW	
A2	UW Det/DS/Decoder	250	Discrete/ASIC	TRW	
A2	O/E (data)	100		TRW	
A2	O/E (clock)	100		TRW	
A2	O/E (control)	100		TRW	
A2	PWB	50		TRW	
A2					
A2					1200
A3	Basic Cable (100 M)	100	$1.00/meter	TRW	
A3	5 Fibers (100M)	100	$0.20/meter/fiber	TRW	
A3	Connector Assy	75	Indoor	TRW	
A3	Connector Assy	50	Outdoor	TRW	
A3					
A3					325
A4	O/E (70 MHz)	100		TRW	
A4	O/E (10 MHz)	100		TRW	
A4	Amp (70 MHz)	20	Available IC	TRW	
A4	Amp (10 MHz)	10	Available IC	TRW	
A4	BPF SAW	15		TRW	
A4	Mixer	125		TRW	
A4	X200	600		Vendor	
A4	BPF (2.07 GHz)	65		Vendor	
A4	Amp (2.07 GHz)	90	MMIC	TRW	
A4	OEM S Band Synth	1200		Vendor	
A4	X6	650		Vendor	
A4	Harmonic Mixer	350		TRW	
A4	BPF (29.5-30 GHz)	85		Vendor	
A4	HPA	4000		TRW	
A4	Post HPA BPF	250		Vendor	
A4	Assy structure	100		TRW	
A4					
A4					7760
A5	Pre LNA BPF	250		Vendor	
A5	LNA	2000	Discrete/ MMIC	TRW	
A5	Post LNA BPF	85		Vendor	
A5	Harmonic Mixer	350		TRW	
A5	X4	500		Vendor	
A5	BPF (A)	90		Vendor	
A5	BPF (B)	90		Vendor	
A5	DBPSK Demod (A)	350	Discrete/ MMIC	TRW	
A5	DBPSK Demod (B)	350	Discrete/ MMIC	TRW	
A5	Baseband AGC	120		TRW	
A5	Bit Synch	850	Available MSI	TRW	
A5	E/O (Clock)	150		TRW	
A5	E/O (Data)	150		TRW	
A5	O/E (Control)	100		TRW	
A5	Control Electronics	300		TRW	
A5	Baseband Switch	30		TRW	
A5	Assy structure	100		TRW	
A5					
A5					5865
A6	LPF	250	Provides 30 GHz stop	TRW	
A6	Main reflector	900		TRW	
A6	Subreflector	300		TRW	
A6	Ant Mount	350		TRW	
A6	OMT & CP Control	950		TRW	
A6					2750

Table 9-3.   User Terminal Cost Estimate

Cost Element	Cost ($)
A1	2,050
A2	1,200
A3	325
A4	7,760
A5	5,865
A6	2,750
Housings (indoor/outdoor)	400
Power supplies	400
Integration and test	1,500
Profit	2,225
Total	24,475

10. SUBSCRIBER CHARGE

For purposes of computing the charge imposed on a system subscriber, it is assumed that the user terminals are owned by the system operator. Therefore, the subscriber charge is an all-inclusive charge that covers use of both space and ground segments. In practice, the subscriber charge would have two components: (1) a minimum monthly fee for access to the system, including use of a terminal installed on the customer premises, and (2) a usage charge based on the number of channel-minutes per month the terminal is active. For simplicity, a common terminal activity factor is assumed. Consequently, a uniform service charge, based on the number of minutes of terminal activity per month, is imposed on all subscribers.

The subscriber charge is computed to provide a specified rate of return on invested capital. A 10-year period of operation is assumed. This is preceded by a four-year period for the development, production, and launch of the initial satellite. The remaining useful life of the satellites on-orbit at the conclusion of operations is accounted for by introduction of a satellite salvage value.

By virtue of prior contractual agreements, system traffic at the start of operations is assumed to require 5,000 64-kbps channels, or roughly half the capacity of a single satellite. Furthermore, a 20-percent annual traffic growth is assumed. The number of satellite channels needed to accommodate this traffic at the start of each year of operations is shown in Table 10-1.

Table 10-1. Traffic and User-Terminal Profiles

Start of Year	Active Channels	Satellites on Orbit	Terminals Added
1	5,000	1	5,000 + 1,000
2	6,000	2	1,200
3	7,200	2	1,440
4	8,640	2	1,728
5	10,368	3	2,074
6	12,442	3	2,488
7	14,930	3	2,986
8	17,916	3	3,583
9	21,500	4	4,300
10	25,799	4	5,160

At the start of Year 1, a single satellite is on-orbit. The second satellite, provided at the start of Year 2, serves as a spare satellite until the channel requirement exceeds 11,250. At this point (Year 5), two operational satellites plus a spare are required, so a third satellite is launched. By the start of Year 9, three satellites are needed to handle the offered traffic. At this point a fourth satellite is launched to serve as an on-orbit spare.

As a minimum, the number of terminals installed on customer premises must equal the maximum channel demand. This minimum terminal complement suffices only if two conditions are satisfied: (1) each active terminal is engaged in duplex transmission (i.e., terminals and channels are both paired to form 64-kbps duplex circuits), and (2) at peak satellite loading, all terminals are active. With respect to the first condition, the opposite extreme would be for each pair of terminals to engage in one-way or simplex transmission. This mode of operation would lead to a terminal complement which is twice the maximum number of active channels. The second condition would tend to be satisfied only if the traffic per terminal should comprise a substantial number of independent transmissions (e.g., a T1 carrier). In the present instance, with at most four independent bit streams per terminal (corresponding, for example, to four 16-kbps voice channels), a significant number of terminals will be idle during the peak traffic period. To allow for the possibilities of simplex transmission and idle terminals, the number of installed terminals (relative to the peak channel demand) is treated parametrically in the subscriber charge calculation.

The minimum number of terminals needed to handle the traffic that builds up by the end of each year is shown in the last column of Table 10-1. The entries indicate the number of terminals that must be added each year. In the case of the first entry, 5,000 terminals are needed at the start of system operations, and 1,000 more are needed to handle the increase in peak channel activity during the first year. Each succeeding entry is 20 percent of the cumulative total to that point, corresponding to the 20 percent annual rate of traffic buildup.

For simplicity, it is assumed that all terminals needed during the course of a year are installed by the first of the year. This conservative assumption is offset by the optmistic assumption that the first 6,000 terminals can be manufactured and installed in the year preceding the start of operations.

The subscriber charge is determined from the revenue stream needed to produce a specified internal rate of return (IRR) to the system operator. The revenue realized during each year of system operation is proportional to the total channel activity (i.e., number of channel-minutes of service provided) during the year. The channel activity profile in Table 10-1, on the other hand, represents the peak channel usage, since it has been used to compute both the number of operational satellites and the (minimum) number of terminals needed to support the indicated level of channel activity. It will be assumed that the total annual channel activity is proportional to the peak channel usage. It follows that the revenue profile for the ten-year program is proportional to the channel activity profile given in Table 10-1. Only the level of the revenue profile remains to be

determined. (In computing the required annual revenue, the channel activity in a given year is taken as the average of the start-of-year and end-of-year values.)

The required annual revenue is divided by the peak channel demand to obtain the required revenue on a per-channel basis. The corresponding charge per channel-minute of actual usage is derived from the assumption that channel usage averages 9000 minutes per month, which is equivalent to slightly more than seven hours per business day.

A number of additional assumptions are required to perform the service charge calculation. These are listed in Table 10-2. As indicated in Table 10-1, a maximum of four on-orbit satellites (including a spare) are required to handle the peak system traffic. In lieu of an expenditure for insurance covering launch and in-orbit operations (the cost and, in fact, the availability of which are highly uncertain at this time), the system operator is assumed to incur the cost of manufacturing a fifth satellite. In the most optimistic scenario, no launch or on-orbit failure occurs and the fifth satellite is never launched. The most pessimistic scenario considered involves a launch or on-orbit failure in Year 2, necessitating that a replacement satellite be on-station at the start of Year 3. An earlier failure, occurring before an on-orbit spare is available, would result in a loss of revenue and is not considered. Neither is the possibility of a second satellite failure, which would leave the system without an on-orbit spare.

The schedule for satellite development and manufacture is shown in

Table 10-2. Assumptions for Service Charge Calculation

- $120M launch cost per satellite

- No insurance for launch or on-orbit failure

- Ground spare manufactured in lieu of insurance

- $110M nonrecurring satellite cost (to manufacturer)

- $113M first-unit satellite cost (to manufacturer)

- 90 percent learning curve for satellite manufacture

- 12 percent profit to satellite manufacturer

- $25K terminal cost

Figure 10-1. The development period has a duration of 2-1/2 years. The manufacture of each satellite requires 18 months; however, successive satellites are completed one year apart. Th minimum launch interval, therefore, is also one year. For simplicity, the indicated launch dates are chosen to coincide with the initial service dates for the various satellites. All launch dates are predetermined with the exception of the one accompanied by an asterisk. This launch takes place only if there has been a previous failure.

Program expenditures are tabulated by year in Table 10-3. The cost of each satellite launch is spread over three years, according to the payment schedule required by NASA. The case shown corresponds to the "no-failure" scenario; consequently, no launch costs are associated with the ground spare. Satellite storage costs (two years for the third satellite, five years for the fourth satellite, and six years for the fifth satellite) are ignored here. The control station hardware is purchased and integrated over a two-year period; by contrast, the control station software is developed over a four-year period.

All expenditures except those for O&M represent depreciable capital assets. The depreciation period for all assets is five years. In general, the depreciation period begins with the year an asset is placed in service. For the nonrecurring satellite costs, this is taken as the first year of operations. For each satellite actually launched, depreciation of both the satellite and its launch vehicle begins in the year of launch. For the scenario in Table 10-3, the ground spare is never launched; its entire cost is assumed to be recovered at the end of the program (i.e., after ten years

Figure 10-1. Satellite Development and Manufacturing Schedule
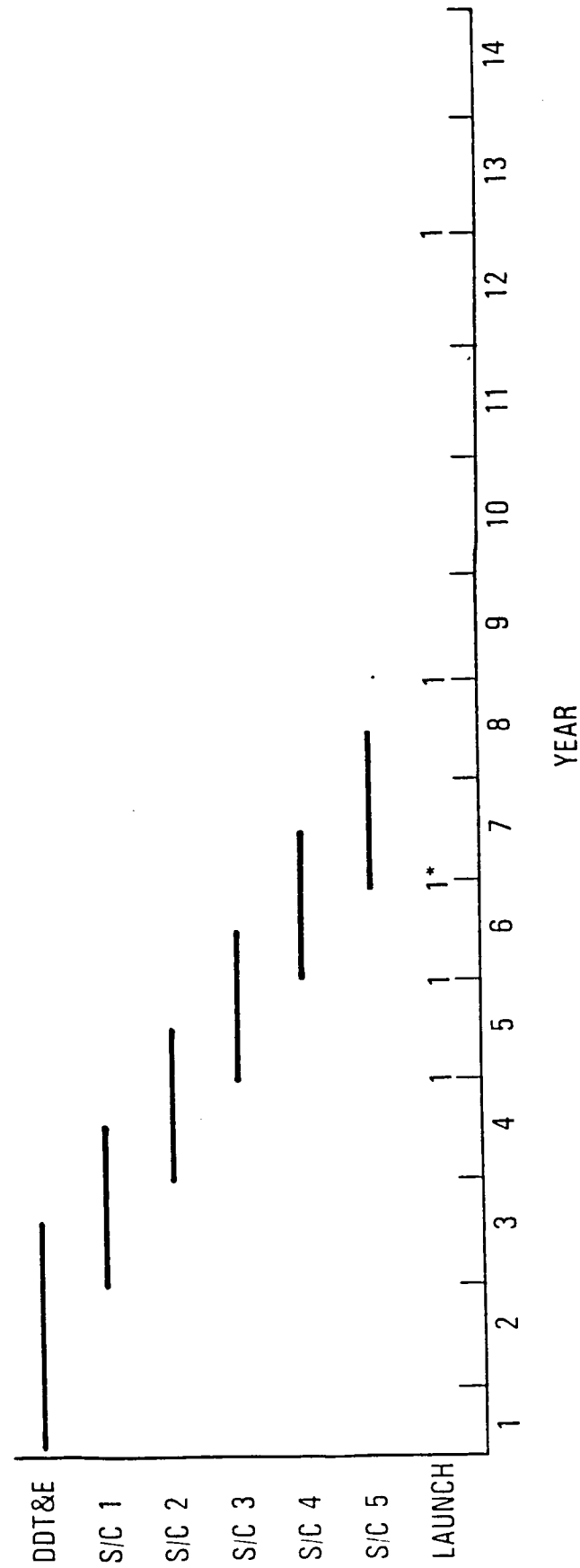
*FAILURE SCENARIO

Table 10-3. Program Expenditure Profile for
Minimum Number of Terminals

YEAR	1	2	3	4	5	6	7	8	9	10	11	12	13	14	TOTAL
SATELLITE (NR)	49.2	49.2	24.5	–	–	–	–	–	–	–	–	–	–	–	122.9
SATELLITE (R) #1	–	–	84.2	42.1	–	–	–	–	–	–	–	–	–	–	126.3
#2	–	–	–	67.3	33.7	–	–	–	–	–	–	–	–	–	101.0
#3	–	–	–	–	62.3	31.2	–	–	–	–	–	–	–	–	93.5
#4	–	–	–	–	–	59.0	29.5	–	–	–	–	–	–	–	88.5
#5	–	–	–	–	–	–	56.5	28.2	–	–	–	–	–	–	84.7
LAUNCH 1	–	–	36.0	36.0	48.0	–	–	–	–	–	–	–	–	–	120.0
LAUNCH 2	–	–	–	36.0	36.0	48.0	–	–	–	–	–	–	–	–	120.0
LAUNCH 3	–	–	–	–	–	–	36.0	36.0	48.0	–	–	–	–	–	120.0
LAUNCH 4	–	–	–	–	–	–	–	–	–	–	36.0	36.0	48.0	–	120.0
TERMINALS	–	–	–	150.0	30.0	36.0	43.2	51.9	62.2	74.7	89.6	107.5	129.0	–	774.1
CONTROL STATION	10.0	10.0	25.0	25.0	–	–	–	–	–	–	–	–	–	–	70.0
O&M	–	–	–	–	9.8	9.9	9.9	10.0	10.0	10.1	10.1	10.3	10.5	10.6	101.2
TOTAL	59.2	59.2	169.7	356.4	219.8	184.1	175.1	126.1	120.2	84.8	135.7	153.8	187.5	10.6	2,042.2

of operations). In a similar vein, the fourth satellite launched is assumed to have a salvage value equal to its book value after two years of depreciation. The first three satellites are fully depreciated by program end and therefore have zero salvage value.

Program expenditures in each category of Table 10-3 are shown as a percentage of the total program cost in the "pie" chart of Figure 10-2. Approximately 54 percent of the program cost is associated with the space segment and 46 percent with the ground segment. (O&M costs, which for the most part involve control station personnel, are associated with the ground segment.) Figure 10-2 corresponds to the minimum number of user terminals. Expenditure distributions corresponding to double or triple the minimum number of terminals are shown in Figures 10-3 and 10-4.

The annual revenue that must be derived from each active channel is shown in Table 10-4 for several values of IRR and for terminal profiles equal to one, two, and three times the minimum set of values. The equivalent per-minute charge, assuming 9000 channel-minutes of use per month, is shown in Table 10-5.

It is instructive to compare the per-minute charge in Table 10-5 for a 64-kbps channel with the corresponding charge for switched 56-kbps service now offered terrestrially (Reference 1). The latter service is presently offered by three vendors: AT&T, MCI/SBS, and Argo, at a per-minute usage charge ranging from $0.30 to $0.70 for a <u>duplex</u> circuit, plus a monthly port charge. For monthly terminal usage ranging between

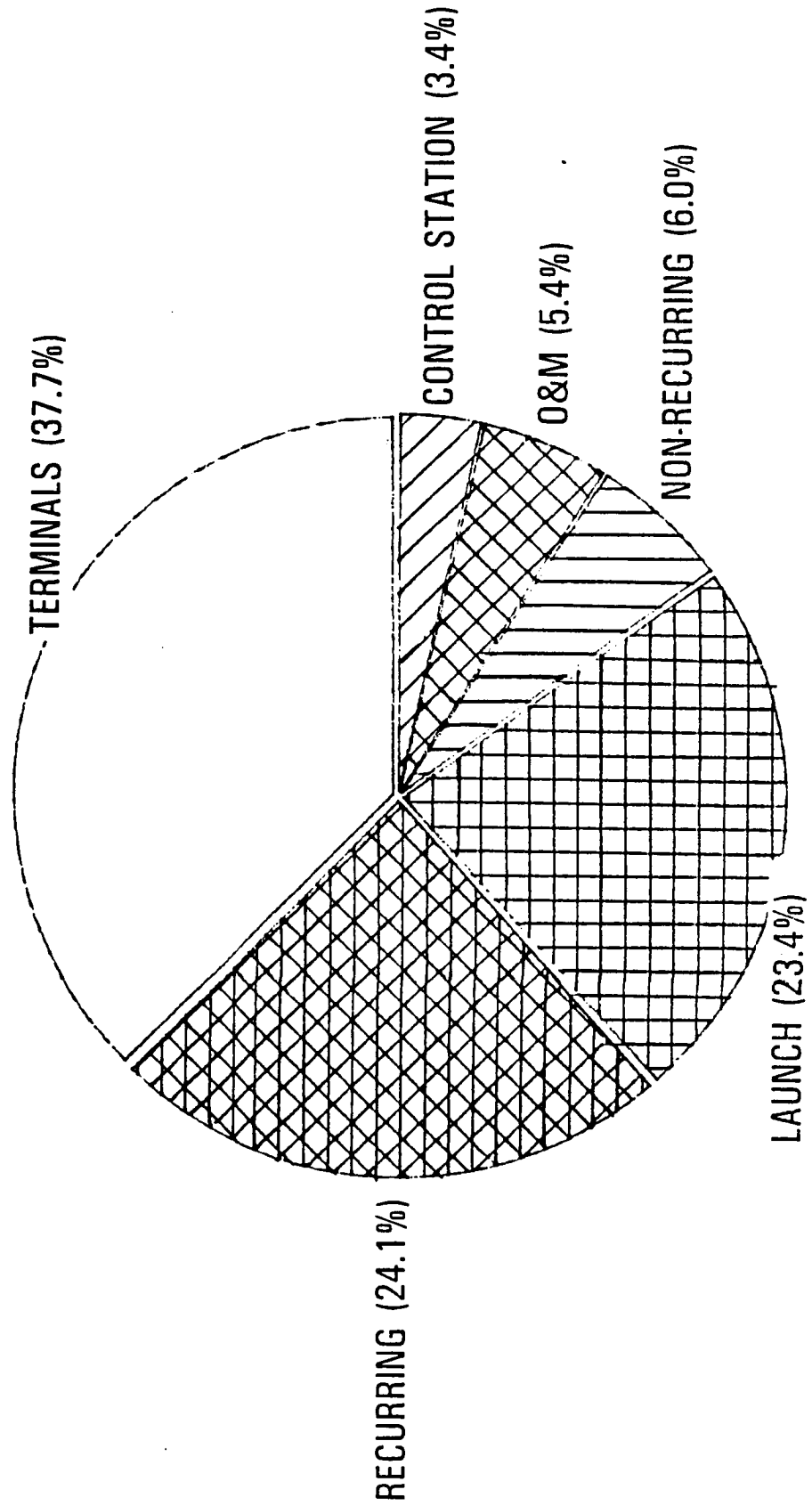Figure 10-2. Program Expenditures for Minimum Number of Terminals

TERMINALS (37.7%)

CONTROL STATION (3.4%)

O&M (5.4%)

NON-RECURRING (6.0%)

LAUNCH (23.4%)

RECURRING (24.1%)

Figure 10-3. Program Expenditures for Twice Minimum Number of Terminals

TERMINALS (54.7%)

CONTROL STATION (2.5%)

O&M (4.1%)

NON-RECURRING (4.3%)

LAUNCH (17.0%)

RECURRING (17.5%)
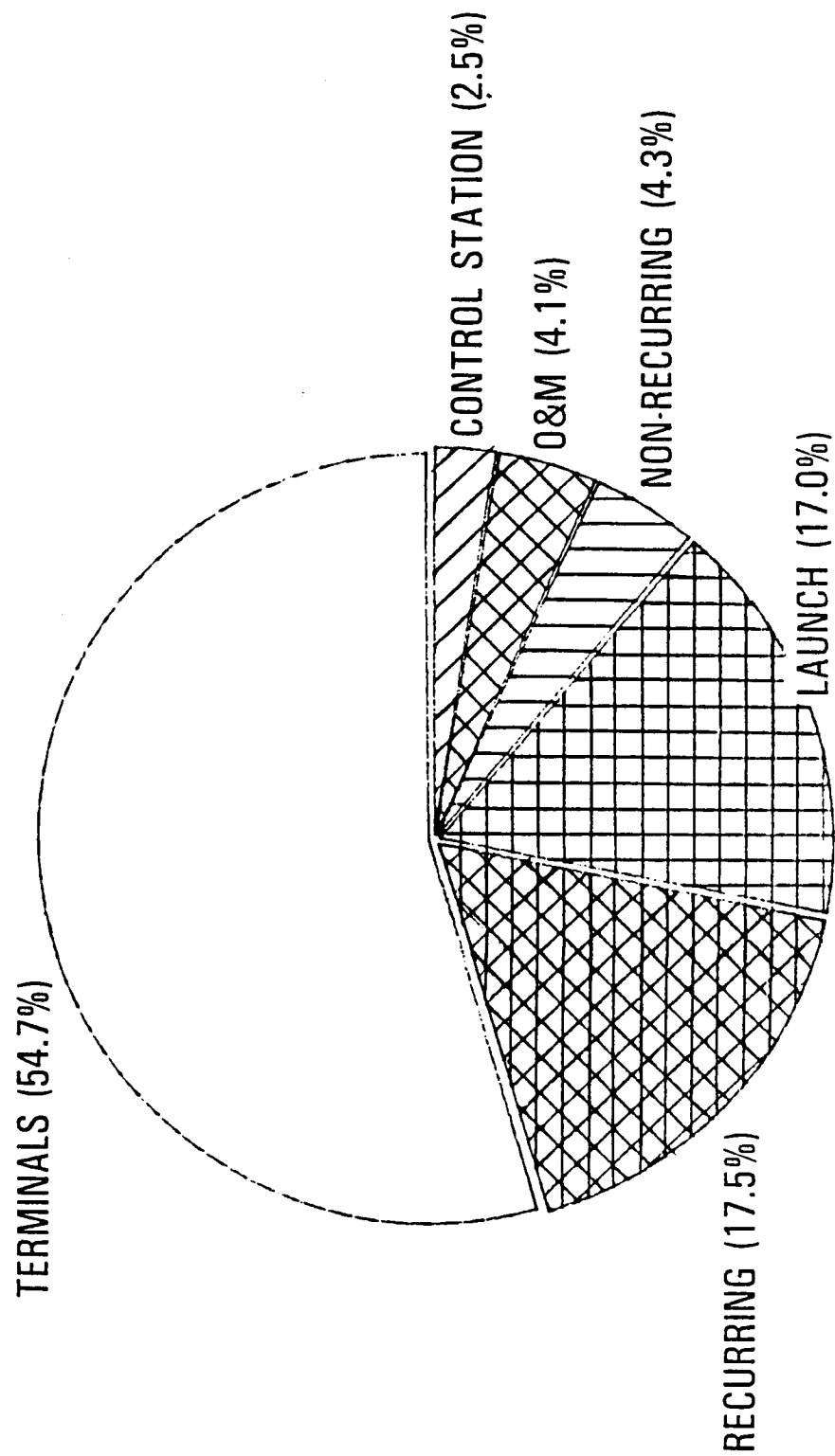
Figure 10-4. Program Expenditures for
Three Times Minimum Number of Terminals

CONTROL STATION (1.9%)

O&M (3.3%)

NON-RECURRING (3.4%)

LAUNCH (13.7%)

RECURRING (13.3%)
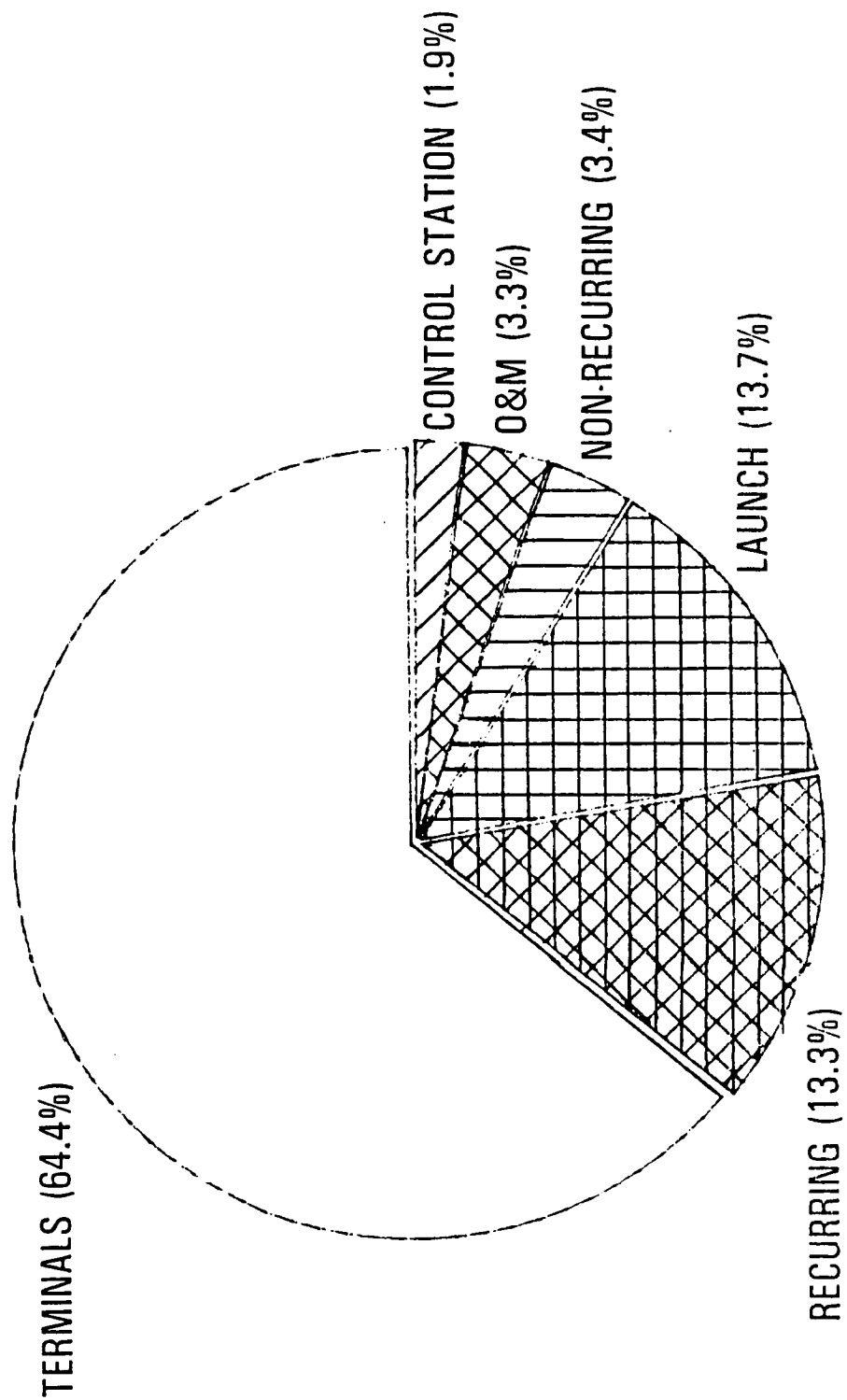
TERMINALS (64.4%)

Table 10-4. Required Revenue ($000 per Channel-Year)

Rate of Return (Percent)	Relative Number of Terminals		
	x1	x2	x3
20	37.1	46.5	55.8
25	44.9	56.6	67.4
30	55.8	68.1	80.3

Table 10-5. Subscriber Service Charge
(¢ per Channel-Minute)

▲ Assumption: average channel usage = 9000 min/mo

Rate of Return (Percent)	Relative Number of Terminals		
	x1	x2	x3
20	34.4	43.1	51.7
25	42.5	52.4	62.4
30	51.7	63.1	74.4

1000 and 4000 minutes, the port charge raises the total per-minute charge to between $0.46 and $0.95 for the case where the usage charge is $0.30 per minute (Argo). The corresponding range for a usage charge of $0.70 per minute (AT&T) is $0.84 to $1.25. Although MCI/SBS has a usage charge of only $0.45 per minute, as a result of the highest port charge its total per-minute charge ranges from $0.72 to $1.52.

The service to which the above charges apply is limited to less than a two-mile radius surrounding the long-distance carrier's "point of presence" (POP) in a major city. This radius can be extended by the purchase of Dataphone digital service (DDS), which is presently available in about 50 percent of telephone company central offices. However, DDS is too expensive for most customer premise equipment (CPE) customers. On the other hand, end-to-end delivery will become available with regional Bell operating company (RBOC) offerings of 56-kbps service. Most RBOCs were planning to begin offering this service by the end of 1986.

For comparison with the above charges for terrestrial switched 56-kbps service, the per-minute charge in Table 10-5 must be doubled so that it corresponds to a duplex circuit. When this is done, it is found that the charge for satellite service is comparable to that for terrestrial service. The former, however, would afford considerably greater flexibility in terms of customer location.

Sensitivity of the per-minute charges in Table 10-5 to changes in the major system cost parameters was determined. For this purpose, the baseline case corresponds to the minimum number of user terminals and a
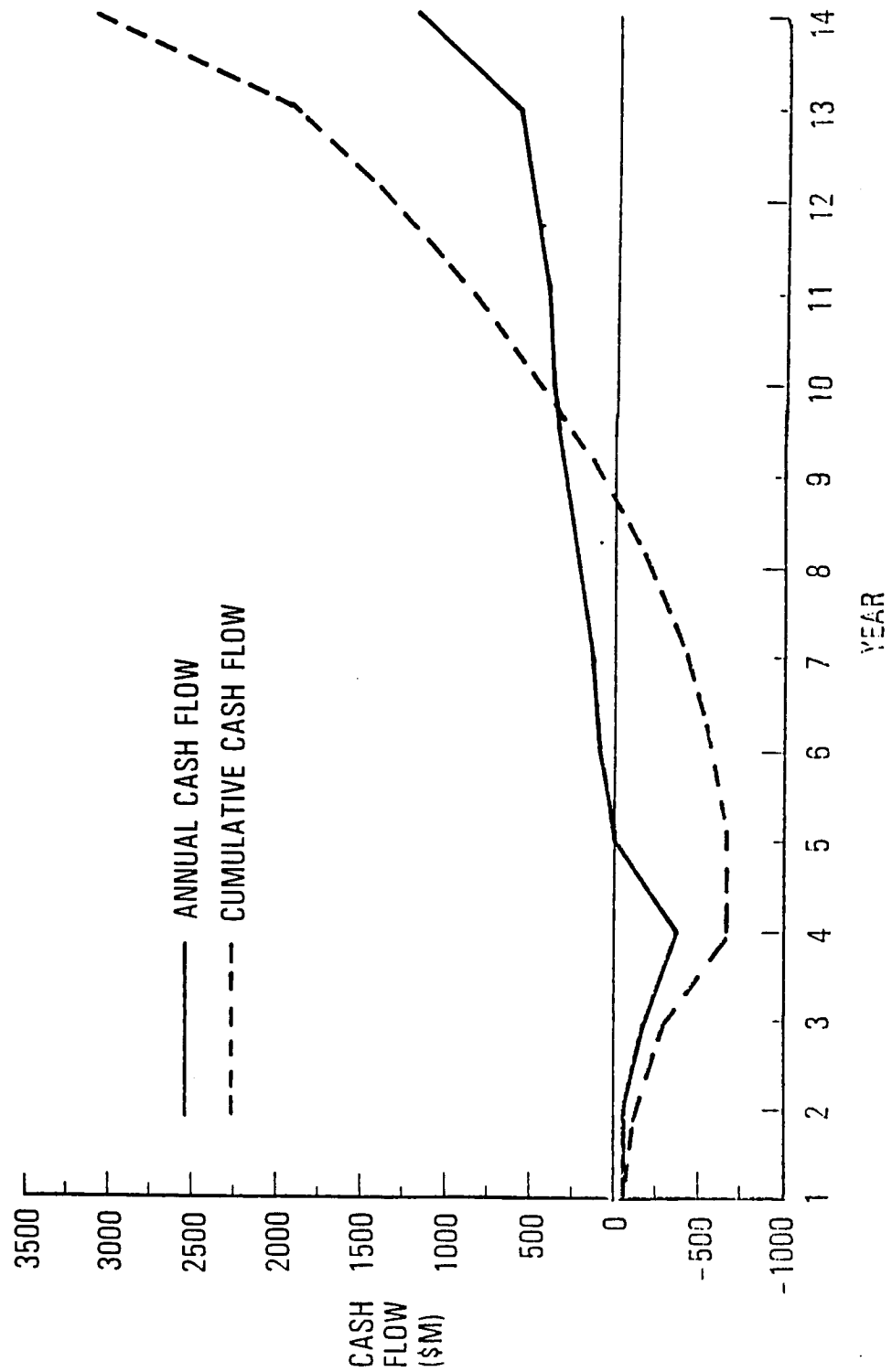
25-percent IRR. A 50-percent increase in nonrecurring satellite costs produces a 7.2-percent increase in service charge. A 20-percent increase in recurring satellite costs results in a 5.4-percent increase in service charge. A virtually identical increase in service charge accompanies a 20-percent increase in launch costs. For the latter comparison, a fifth launch (i.e., of the ground spare) is assumed to be necessary. As a result, there is a one-to-one association of launch vehicles and satellites. Since launch costs and recurring satellite costs are comparable, similar service charge sensitivity to increased costs in either area can be expected.

A nondiscounted cash flow profile for the baseline case (25-percent IRR) is shown in Figure 10-5. The solid curve shows the annual cash flow, while the dashed curve depicts the cumulative cash flow. A similar pair of curves, representing the discounted cash flows corresponding to a 25-percent IRR, is shown in Figure 10-6. The cumulative discounted cash flow at program end, which by definition is the net present value for the program, is necessarily equal to zero.
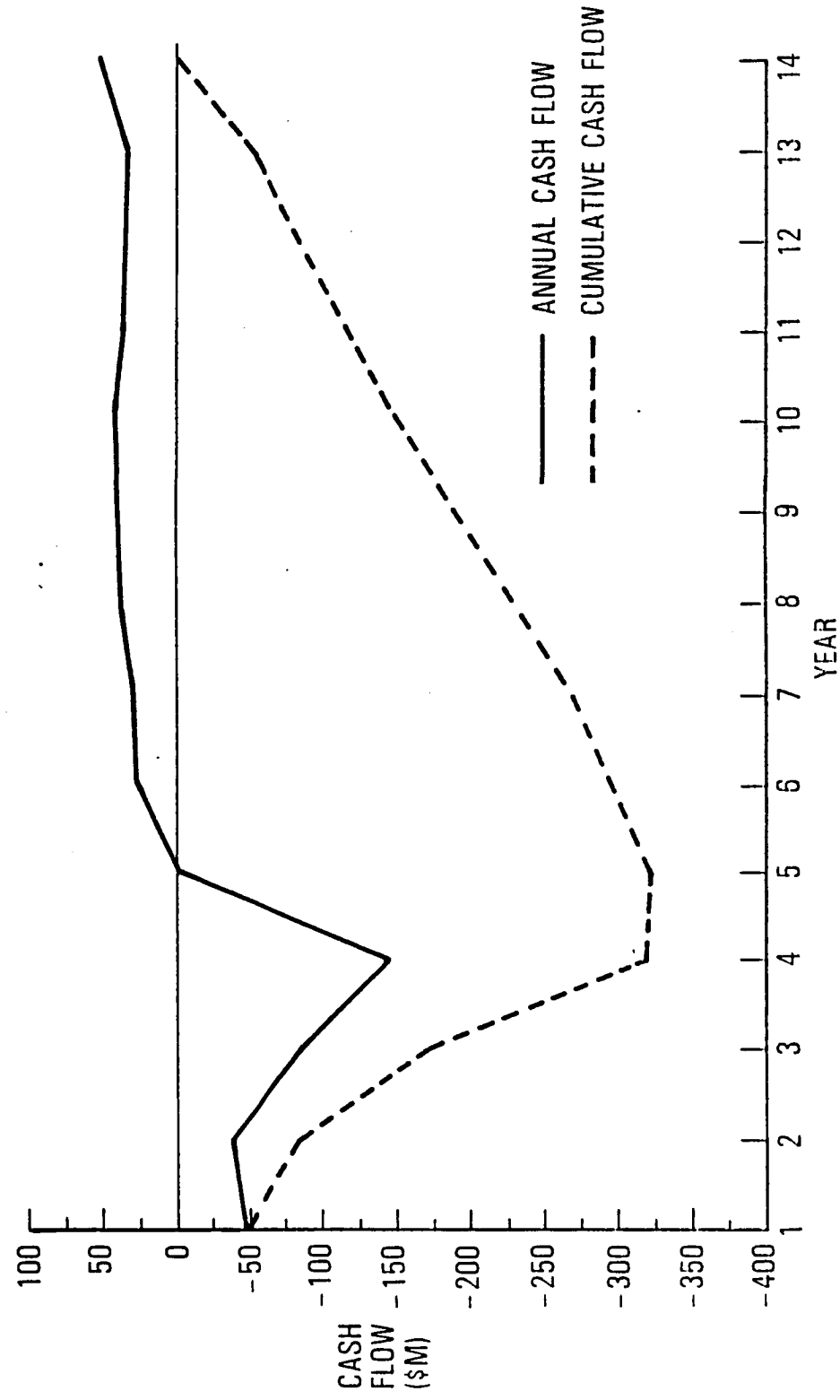
Reference:

10-1.   "The How and Where of Switched 56-kbit/s Service", Data Communications, August 1986, pp. 119-133

Figure 10-5. Nondiscounted Cash-Flow Profile for Minimum Number of Terminals

ANNUAL CASH FLOW
CUMULATIVE CASH FLOW

CASH FLOW ($M)

3500
3000
2500
2000
1500
1000
500
0
-500
-1000

1 2 3 4 5 6 7 8 9 10 11 12 13 14

YEAR

Figure 10-6. Discounted Cash-Flow Profile for
Minimum Number of Terminals

11. CONCLUSIONS

A satellite system architecture has been developed to provide point-to-point voice and/or data communications among a large number of CPS terminals. The system features narrowband FDMA uplink transmission and wideband TDMA downlink transmission. Payload weight and power are held to manageable levels through use of digital bulk demodulator technology. Anticipation of advances in large-scale memory wafers has led to the choice of a "memory-based" baseband processor to multiplex the demodulator outputs onto the downlink carriers. Rapidly scanning downlink beams are provided by a pair of 20-GHz array-fed dual reflector antennas. Implementation of the feed arrays at reasonable cost depends on MMIC technology developments.

Realization of the above system architecture at Ka-band requires the use of coding for error correction and, in addition, provision of sizable link margins to overcome rain attenuation. Introduction of coding limits the capacity of a single satellite (for a 500-MHz frequency allocation) to approximately 720 Mbps. The link margin requirements restrict the end-to-end link availability in the worst case to 0.99. In addition, the high cost of 30-GHz power amplifiers limits the terminal transmission rate to about 64 kbps.

The traffic scenario adopted for computation of the user service charge begins with a peak demand of 5,000 64-kbps channels and grows at a 20-percent annual rate to nearly 31,000 channels after ten years of operation. Since a single satellite has a capacity of 11,250 channels,

three operational satellites (plus an on-orbit spare) are needed toward the end of the program. In addition, production of a ground spare has been assumed in lieu of insurance to cover launch or on-orbit failures.

The required subscriber charge depends primarily on the desired IRR and the number of terminals in the system. (User terminals are assumed to be owned by the system operator; consequently, terminal costs are reflected in the subscriber charge.) For an IRR of 25 percent, for example, the charge is in the neighborhood of $0.50 per channel-minute, the exact amount depending on the number of terminals. This figure is comparable to the charge for terrestrial 56-kbps switched service offered by long-distance carriers.

The question of how single-hop interconnectivity is to be maintained in a multisatellite environment has not been addressed in this study. For a set of terminals that need to communicate only among themselves, single-hop interconnectivity can be established by assigning the terminals to (i.e., pointing the terminal antennas at) a common satellite. More generally, intersatellite links can be used to establish single-hop interconnectivity.

1. Report No. NASA CR 179592	2. Government Accession No.	3. Recipient's Catalog No.
4. Title and Subtitle Advanced Space Communications Architecture Study Volume 2 - Technical Report		5. Report Date March 1987
		6. Performing Organization Code
7. Author(s) Michael Horstein, Principal Investigator Peter J. Hadinger, Collaborator		8. Performing Organization Report No.
		10. Work Unit No.
9. Performing Organization Name and Address TRW Inc. One Space Park Redondo Beach, CA 90278		11. Contract or Grant No. NAS3-24743
		13. Type of Report and Period Covered Contractor Report Jan 1986 to March 1987
12. Sponsoring Agency Name and Address NASA Lewis Research Center 21000 Brookpark Road Cleveland, OH 44135		14. Sponsoring Agency Code

15. Supplementary Notes

Contract Monitor - Grady H. Stevens
NASA Lewis Research Center
Cleveland, OH 44135
216: 433-3463

16. Abstract

This study investigates the technical feasibility and economic viability of satellite system architectures that' are suitable for customer premise service (CPS) communications. System evaluation is performed at 30/20 GHz (Ka-band); however, the system architectures examined are equally applicable to 14/11 GHz (Ku-band). Emphasis is placed on systems that permit low-cost user terminals. Frequency division multiple access (FDMA) is used on the uplink, with typically 10,000 simultaneous accesses per satellite, each of 64 kbps. Bulk demodulators onboard the satellite, in combination with a baseband multiplexer, convert the many narrowband uplink signals into a small number of wideband data streams for downlink transmission. Single-hop network interconnectivity is accomplished through use of downlink scanning beams.

Each satellite is estimated to weigh 5600 lb and consume 6850W of power; the corresponding payload totals are 1000 lb and 5000W. Nonrecurring satellite cost is estimated at $110 million, with the first-unit cost at $113 million. In large quantities, the user terminal cost estimate is $25,000.

For an assumed traffic profile, the required system revenue has been computed as a function of the internal rate of return (IRR) on invested capital. The equivalent user charge per-minute of 64-kbps channel service has also been determined.

17. Key Words (Suggested by Author(s)) Satellite communications Customer premise service Bulk demodulators Phased-array antennas	18. Distribution Statement Unclassified-Unlimited
19. Security Classif. (of this report) Unclassified	20. Security Classif. (of this page) Unclassified	21. No. of pages 186	22. Price*